INTERACTIONS OF COLLOIDAL PARTICLES IN THE PRESENCE OF A PARALLEL APPLIED FIELD

By

FRANKIE KAY WOOD

Bachelor of Science

Central State University

Edmond, Oklahoma

1984

Submitted to the Faculty of the
Graduate College of the
Oklahoma State University
in partial fulfillment of
the requirements for
the Degree of
DOCTOR OF PHILOSOPHY
May, 1989

INTERACTIONS OF COLLOIDAL PARTICLES

IN THE PRESENCE OF A PARALLEL

APPLIED FIELD

Thesis Approved:

Thesis Adviser

Dean of the Graduate College

PREFACE

The experimental method employed in this study is not just limited to the investigation of the interparticle forces presented between the particles. It can be used for aggregation studies, as a model for the interactions that occur in electrorheological fluids, and may be employed a an optical switching device. I encourage the extension of this technique to these other applications as well as investigating the effects of surface chemistry, pH, etc. on the interparticle interactions. I, also, encourage further work on the ferrofluid composite systems. I strongly belive that these systems can be understood and that the information obtained will further our understanding of the interactions present in colloidal systems.

I wish to express my sincere gratitude to my thesis advisor, Dr. B. J. Ackerson, and my thesis committee for their help and understanding during this investigation. The Department of Physics has also been instrumental to the successful completion of this work.

I wish to thank people like Wayne Vincent, Aslam Chowdhury, Eddie Behrens, and Guy Gilland for all of their constructive criticism, advice and useful

suggestions.

I would like to express to my close friends -- Thank you for putting up with me during these hectic and difficult times especially when it seemed that I really was looney. (P.S. I do believe that one day I will write that book.)

TABLE OF CONTENTS

Chapter Page

LIST OF TABLES

LIST OF FIGURES

***

TABLE OF SYMBOLS

α	electronic polarizabilty
A	the Hamaker constant
a_o	the Bohr radius
a_1	sphere radius
a	sphere radius
B	retarded Hamaker constant
Γ	adsorption
c	speed of light
c_i	concentration of ions in solution
γ	parameter defined in diffraction grating theory
∇^2	Laplacian operator
d	center to center separation
ε_o	permittivety of free space
ε	dielectric constant
ε_p	dielectric constant of the particle
ε_w	dielectric constant of water
E	electric field
e	charge of the electron
G	free energy
G	constant in gravity study
H	magnetic field
H	separation (surface to surface)
h	Planck's constant

h'	ring radius
θ	angle
I	Intensity
I_i	ionization potential
κ	Debye-Huckel reciprocal length
k_B	Boltzmann's constant
λ	wavelength
$\mathcal{L}$	Laplace transform
l	length or height of cylinder
l	length of polymer chain
μ_0	magnetic permeability
ω	orbiting frequency
m	order of diffracted maxima
n_p	index of refraction of the plate (particle)
n_m	index of refraction of the medium
q_i	number of molecules per unit volume
R	separation (center to center)
R_i	cylinder radius
r	separation
ρ	surface charge density
T	temperature
u	dipole moment
$V(r)$	interaction energy
V	interaction energy
v	volume
w	frequency of dominant relaxation
Φ	volume fraction

x	dimensionless separation
χ_e	effective suseptibility
ψ	potential
Z	partition function
z	valence

CHAPTER I

INTERMOLECULAR FORCES

Introduction

Physicists and chemists have always been interested in the nature of and the control of intermolecular forces. These intermolecular forces in turn give rise to the interparticle forces stabilizing the colloidal particles in suspension. The stabilization forces between particles are responsible for the overall behavior of colloidal substances.

One example of interparticle forces between colloidal particles producing dramatic results in a colloidal suspension is an electrorhelogical fluid [Stangroom (1983); Brooks, et. al. (1986); Duclos, et. al. (1988)]. These fluids flow normally until an electric field is applied. When the field is applied the fluid changes in character - the fluid's viscosity increases with the applied field - due to the interaction between the suspended particles and the applied field. The interaction between the particles and the field leads to the formation of chains of particles aligned parallel to applied field. Similar behavior has been observed in ferrofluids (the magnetic

counter part of the electrorhelogical fluid). [Jordan (1973); Popplewell, et. al. (1981); Rosensweig (1985); Chikazumi, et. al. (1987); Morozov, et. al. (1987)] In ferrofluid composite systems, a ferrofluid in which monodispersed micron sized polymer spheres have been suspended, it has been observed that the suspended spheres behave as interacting magnetic dipole holes.

It is important for the development of new materials or the modification of present materials to specific applications to identify and to quantify the interactions responsible for phenomena present. Recently, there have been two methods by which the intermolecular forces have been measured. In the more well known experiment, the Israelachvili box, microscopic forces are measured between two macroscopic plates or crossed cylinders. This is a direct force versus separation experiment. However, it uses two macroscopic surfaces: thus, results must be extrapolated to the colloidal regime. The second experiment is semi-microscopic. This work presented by Prieve (1987 and 1989) measures the forces present between a colloidal sized particle and a macroscopic plate. This method must incorporate the effects of thermal motion due to the Brownian movement of the colloidal particles. The study presented here is a method by which interparticle forces can be examined between colloidal particles, thus extending both of the previous works to the microscopic

level.

Particle-Particle Interactions

Particle-particle interactions arise from more commonly known intramolecular and intermolecular forces. The origin of intermolecular forces has its basis in the Hellman-Feynman theorem. The Hellman-Feynman theorem states that once the distributions of the electron clouds have been determined from the solution of the Schrodinger equation, the intermolecular forces may be calculated on the basis of classical electrostatics. [Israelachvili (1985)] More simply stated, intermolecular forces are strictly electrostatic in origin. However, these forces can be classified into major categories which are more easily discussed.

Two bodies interact through a) direct forces of molecular origin - van der Waals; b) solvent forces - liquid structural forces, hydrogen bonding, hydrophobic and hydrophilic interactions; c) electrostatic forces - double-layer forces; and d) others - adhesion, steric forces, etc. [Israelachvili (1981); Ninham (1982); Overbeek (1984)] The distinction between these is strictly artificial and such forces may not always be independent or superimposable.

London-van der Waals Interactions

In 1873, J.D. van der Waals attempted to explain the behavior of imperfect gases by incorporating the finite size of the molecules and the observed attraction between them. [Tabor, et. al. (1969)] Similarly, an attraction has been observed in colloidal suspensions in the form of coagulation and flocculation which has been attributed to the same type of interaction. The work of van der Waals was put on a firmer foundation by London (1930) [Verwey, et. al. (1948); Dzyaloshinskii, et. al. (1961)] who showed that this attraction arose quantum mechanically when second-order perturbation theory was applied to the electrostatic interactions between two dipoles, hence, the reference to the London-van der Waals attraction. This theory has been applied and the forces measured directly, revealing two regions of attraction - normal and retarded. However, in most cases the retarded van der Waals forces are unimportant.

Even though these forces are quantum-mechanical in origin, one may gain an intuitive understanding from the following example:

> Consider a non-polar atom or molecule, i.e. an atom or molecule whose time averaged dipole moment is zero. At any given instant in time a finite dipole moment exists due to the instantaneous positions of the electrons of the system with respect to the protons of the system. This instantaneous dipole moment gives rise to an electric field which in turn polarizes any nearby neutral atom or molecule. This then orients the instantaneous dipole moment of the nearby body, creating an interaction between the two, and this time averaged force is finite. [Israelachvili (1985)]

A simple semiquantitative explanation may also be developed [Israelachvili (1985)]. Consider the interaction between two Bohr atoms. The smallest distance between the electron and the proton is a_o, the Bohr radius. This is the radius at which the coulomb energy is equal to $2\hbar\nu$, or

$$e^2/(4\pi\varepsilon_o a_o) = 2\hbar\nu \qquad \text{I.1}$$

where e is the charge of the electron, $\hbar$ is Planck's constant, and ν is the orbiting frequency of the electron. For a Bohr atom ν is 3.3×10^{15} s^{-1}, with h = 2.2×10^{-18} J gives

$$a_o = 0.053 \text{ nm}.$$

This is the radius at which the energy of the electron is equal to the energy needed to ionize the atom - the first ionization potential I.

The Bohr atom is inherently neutral, it has no permanent dipole moment. However, at any given moment in time, it does have an instantaneous dipole moment given by

$$u = a_o e \qquad \text{I.2}$$

This instantaneous dipole moment has a field which polarizes a nearby neutral atom, giving rise to an attractive interaction that is analogous to the interaction observed between a dipole and an induced dipole.

This interaction has an energy given by

$$V(r) = -(a_o e)^2 \alpha_o / (4\pi\varepsilon_o)^2 r^6 \qquad \text{I.3}$$

where α_o is the electronic polarizability of the second Bohr atom, which may be approximated as

$$\alpha_o \approx 4 \pi \varepsilon_o a_o^3. \qquad \text{I.4}$$

Substituting for α_o in equation I.3, the interaction energy is approximated as

$$V(r) \approx - \alpha_o^2 \hbar\nu / (4 \pi \varepsilon_o)^2 r^6 \qquad \text{I.5}$$

Except for a constant equation I.5 is the same as that first derived by London using the quantum mechanical perturbation theory. London's expression for the interaction energy between two atoms or molecules is

$$V(r) = -3 \alpha_o^2 \hbar\nu / 4 (4 \pi \varepsilon_o)^2 r^6 \qquad \text{I.6}$$

$$= -3 \alpha_o^2 I / 4 (4 \pi \varepsilon_o)^2 r^6$$

This is often expressed as

$$V(r) = - C_{disp} / r^6 \qquad \text{I.7}$$

For two dissimilar atoms London showed that

$$V(r) = - 3 \alpha_{o1} \alpha_{o2} I_1 I_2 / 2 (4\pi\varepsilon_o)^2 r^6 (I_1 + I_2)$$

London's equation has since been superseded by more exact treatments [McLaclan (1963)] but gives fairly accurate results. These results are generally lower than measured values.

These forces are generally referred to as dispersion forces and are only one component of what is collectively termed the London-van der Waals force. The London-van der Waals force is made up of an induction force, an orientation force, and a dispersion force, but all vary with the inverse sixth power of distance. [Israelachvili (1985)]

The induction force corresponds to the permanent moment in one of the molecules polarizing the second molecule and the interaction of the induced moments in the second with the first molecule. [Hirschfelder (1967)] This induction force also arises from a second-order perturbation. The interaction energy may be written as

$$V(r) = - (u_1^2 \alpha_{o2} + u_2^2 \alpha_{o1}) / (4 \pi \varepsilon_o)^2 r^6 \qquad I.8$$

$$= - C_{ind} / r^6$$

Equation I.8 [Israelachvili (1985)] takes into account the interaction of the permanent dipole of molecule 1 with the polarization of the molecule 2 and the interaction of the permanent dipole of molecule 2 with the polarization of the molecule 1.

The orientation force results from the definite orientational dependence of the dipole moments (induced or permanent). The Boltzmann distribution can be used to determine the orientational distribution of the molecules. The angle averaged dipole-dipole interaction energy for the orientation force may be written as [Israelachvili (1985)]

$$V(r) = - u_1^2 u_2^2 / 3 (4 \pi \varepsilon_o)^2 k_B T r^6 \qquad I.9$$

$$= - C_{orient} / r^6$$

This orientation interaction is also referred to the as the Keesom interaction.

The dispersion-London forces generally exceed the dipole-dependent induction and the orientation forces.

(See Table 1) Therefore, for practical purposes one need only consider the dispersion-London term.

TABLE 1

INDUCTION, ORIENTATION, AND DISPERSION ENERGY CONTRIBUTIONS TO THE TOTAL VAN DER WAALS ENERGY IN A VACUUM FOR PAIRS OF MOLECULES AT 273 K. C IN 10^{-79} J m^6.

Molecules	C_{ind}	C_{orient}	C_{disp}
Ne-Ne	0	0	4
CH_4-CH_4	0	0	102
HCl-HCl	6	11	106
HI-HI	2	0.2	370
H_2O-H_2O	10	96	33
HCl-HI	7	1	197
H_2O-CH_4	9	0	58

[From Table X in Israelachvili (1985)]

For macroscopic bodies, such as colloidal particles, the interparticle separation is generally greater than the interatomic distances within the particle. Thus, interacting particles are insensitive to atomic detail and one can treat the particle as a macroscopic continuum [Parsegian, et. al. (1971)]. Using this approach Hamaker in 1936 and 1937 derived equations for the attractive forces between two

particles [Overbeek (1977)]. Hamaker's formulation only incorporated the normal London-van der Waals interactions.

Hamaker derived his results by dividing the interaction into two parts - a part attributed to the interactions of the atoms that comprise the particle and the part referring to the geometries of the particles. The portion related to the material has been reduced to a constant. The constant A (or B for retarded cases), the Hamaker constant, is dependent only on the interactions of the atoms or molecules of the material. Note: for most practical applications in the study of colloidal stability only the nonretarded van der Waals forces are important [Overbeek (1977)]. To understand this relationship (the separation of the geometric part from the constant part); consider again the interaction energy between atoms or molecules,

$$V(r) = - C / r^6$$

The pair energies are additive in the first approximation. Thus, the energy of attraction, $V(r)_{att}$, between two macroscopic objects of V_1 and V_2 can be written as (see Figure 1)

$$V(r)_{att} = - \int_{V_1} \int_{V_2} q_1 \, q_2 \, C / r^6 \quad dV_1 \, dV_2 \qquad I.10$$

where q_1 and q_2 are the number of molecules per unit volume in particles 1 and 2 respectively [Overbeek (1984)]. Since the differential volumes of particles 1

and 2 are proportional to the cube of the linear scale, $V(r)_{mtt}$ is independent of the scale.

Equation I.10 has been evaluated for a number of geometries: [Overbeek, (1984)] Figure 2.

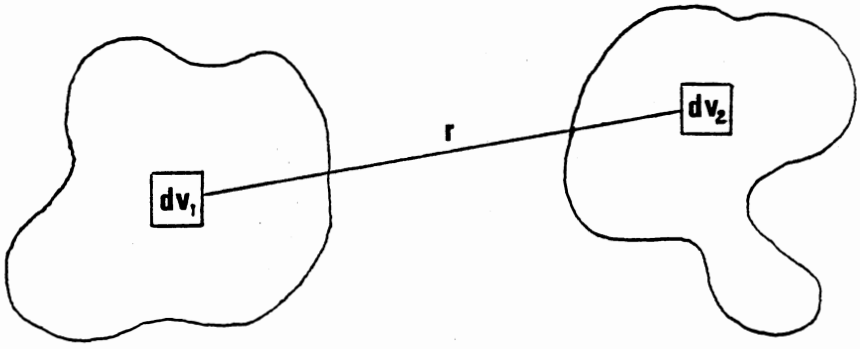

Figure 1. Geometry used to derive equation I.10.

Flat plates: The attraction energy per unit area for two parallel flat plates of the same material is given

$$V(r)_{mtt} = - A / 12 \pi H^2 \qquad \text{I.11}$$

where H is the separation of the two plates and the Hamaker constant, A, is given by

$$A = \pi^2 q^2 C \qquad \text{I.12}$$

Two spheres of unequal radius: Consider two spheres of radius a_1 and a_2 respectively, the interaction energy in the limit that a_1 and a_2 are much

greater than H is

$$V(r)_{att} \approx -(A / 6 H) \{ a_1 a_2 / (a_1 + a_2) \} \quad I.13$$

[Hiemenz, (1986); Israelachvili, (1985)]

Two spheres of equal radii: Considers two spheres of radius a separated by a distance R, the interaction energy, $V(r)_{att}$, is

$$V(r)_{att} = -(A/6) \{ [2a^2 / (R^2 - 4a^2)] + [2a^2 / R^2] + \ln [(R^2 - 4a^2) / R^2] \} \quad I.14$$

This interaction energy may be simplified, if the distance between the surfaces, H = R-2a, is much smaller than the radius a, then the attractive interaction may be approximated as

$$V(r)_{att} \approx -(A/12) \{ L/H + 2\ln(H/L) \} \quad I.15$$

$$\approx -(Aa/ 12 H)$$

where L = a + 3/4 H. [Overbeek, (1984); Overbeek, (1977)]

Two cylinders: Consider two cylinders of unequal radius R_1 and R_2 respectively and of length l, and a surface separation of H, where $H = R - R_1 - R_2$. The interaction energy may be approximated by

$$V(r)_{att} \approx -(A\, l/ 12 \sqrt{2} H^{3/2}) \{ R_1 R_2 / (R_1 + R_2) \}^{1/2}$$

Note: this interaction energy is for orientation of the cylinders such that the axes of symmetry are parallel to one another. The interaction energy for two cylinders of the same dimensions and oriented such that the axes

are perpendicular to one another, i.e. crossed cylinders, may be approximated by

$$V(r)_{att} \approx - (A / 6 H) \sqrt{R_1 R_2} \qquad I.16$$

[Israelachvili, (1985)]

Hamaker constants are calculated, theoretically, for the bulk material. These constants may be calculated via one of two methods. The first one starts from the microscopic properties of the individual molecules and assumes them to be additive. This was the original treatment used by Hamaker. The second method is a macroscopic or a continuum approach [Visser, (1972)]. This method was formulated by Lifshitz (1956) and later implemented for real systems by Parsegian (1969) and Russel, et. al. (1989), and uses a quantum electrodynamic approach based on bulk properties, e.g. the dielectric constant, of the material. Both methods account for the material of the particles as well as the medium in which they are embedded.

These constants may be determined experimentally, as well. Common experiments used to determine them are: flocculation experiments on the dispersions of colloidal particles; interactions of two crossed metal wires in electrolyte solutions; and film measurements. Visser (1972) gives an extensive survey of data obtained from these various methods. Table 2 is a condensed version of the data presented in Visser's survey.

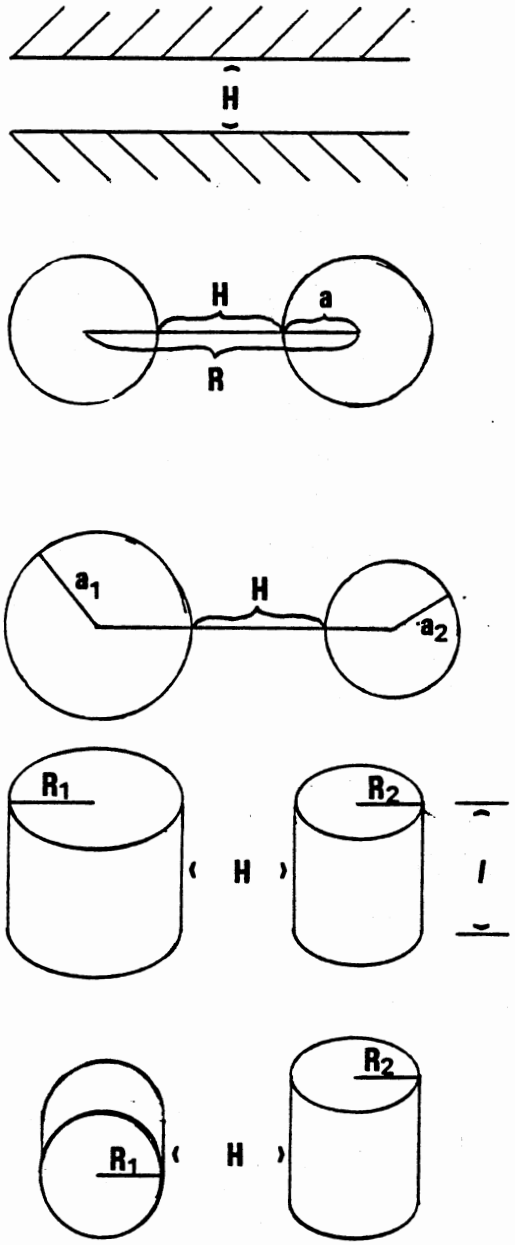

Figure 2. Different van der Waals interaction geometries.

TABLE 2

HAMAKER CONSTANTS IN AIR AND IN WATER,
ALL IN 10^{-20} J = 2.5 kT.

A	in Air	in Water
Water	4.4	0
Hydrocarbons	4-10	0.3-1
Oxides and Halides	6-15	0.5-5
Metals	15-50	5-30

[This is a reproduction of Table 1 in Overbeek (1984)]

Though the Hamaker expressions are conceptualy easy to understand, they do not adequately describe the observed behavior. Early corrections were made to account for retardation effects [Casmir, et. al. (1948)], however, these corrections were not sufficient. The descrepancy between the experimental and theoretical results lies in how the material contribution is calculated [Smith (1973)]. The Hamaker approach assumed the interactions between the molecules to be additive, however for many body interactions one would expect this assumption to fail. The Hamaker results, also, tend to diverge as one approaches the molecular dimensions. Therefore, the continuum approach based on the macroscopic properties would be expected to provide better results [Mahanty, et. al. (1976), Russel, et. al. (1989)].

Mahanty and Ninham (1976) proposed a correction to

the Hamaker expressions by using an effective Hamaker constant, based on the continuum approach, in equation I.12. This effective Hamaker constant, A_{eff}, would be the same as that used for flat plates, i.e. employing a form of the Derjaguin approximation:

$$A_{eff} = A_1(1 + (A_3 H)^{3/2})^{-2/3} \qquad I.17$$

Here H is the surface to surface separation, A_1 is given by

$$A_1 = \frac{3\hbar\omega}{16\sqrt{2}\,k_B T}\,\frac{(\bar{n}_0^2 - n_0^2)^2}{(\bar{n}_0^2 + n_0^2)^{3/2}}$$

and A_3 is given by

$$A_3 = \frac{n_0 \pi \omega (\bar{n}_0^2 + n_0^2)^{1/2}}{4\sqrt{2}\,c}$$

where $\hbar$ is Planck's constant, k_B is Boltzmann's onstant, c is the speed of light, w is the frequency for the dominant relaxation in the ultraviolet of the medium (for the experiments presented in this study w = 1.88 x 10^{16} 1/s), $\bar{n}_0$ the refractive index of the plates, and no the refractive index of the medium. Tests of this approximation have been made by Pailthorpe and Russel (1982) and the comparison of the multipole expansion calculations (Langbein, 1974) suggest that this simple form is sufficiently accurate for most purposes [Russel, 1989].

A second correction to the Hamaker expression is made to account for the electrolytes in the system. [Russel, 1989] Thus, the form for the interaction

between two spheres incorporating these corrections is

$$Va = -\frac{k_B T}{16 H} e^{-2\kappa H} - \frac{A_{eff}\, a}{12 H} \qquad I.18$$

where a is the particle radius, T the temperature in degrees Kelvin, and H is the surface separation [Russel, 1989].

Solvation Interactions

Colloidal suspensions are comprised of some type of macroscopic particle suspended in a fluid medium. The medium is composed of molecules of finite size, which interact with the each other as well as the suspended particle. These fluid interactions seem to affect how the colloidal particles can pack together, i.e. the fluid molecules seem to order about the colloidal particles, therefore the fluid has structure which cannot always be neglected. These particle-molecule interactions are referred to as solvation or structural interactions.

These forces have been measured in aqueous and non-aqueous media between surfaces [Langmuir, (1938); Horn, et. al. (1981, 1980)]. The surfaces commonly used are flat plates or curved cylinders of plain or coated mica. These experiments have led to the conclusion that these forces are "short ranged", i.e. they only interact over a few molecular diameters, and depend on the size, shape and packing of the molecules. This holds true for

macroscopic particles as well [Ninham, et. al. (1980); Israelachvili, (1985)]. The more detailed experiments [Horn, et. al. (1980, 1981)] show a discrete molecular structure of the solvent near the solid surfaces, thus, resulting in the oscillation of the force as a function of separation. These oscillations have a periodicity which correlates with the size of the molecules, and the magnitude of the force decays within a few molecular layers. See Figure 3. They also show that the molecules and walls can significantly effect the density profile and the oscillating density profile resulting in an oscillatory force of magnitude comparable to the conventional van der Waals interaction.

In most colloidal suspensions the medium of suspension is water. Since, water is unusual, there are some important solvation phenomena that can be related directly to it. These phenomena are hydrogen bonding - resulting in "cages" about the colloidal particles (see figure 4); the hydrophobic effect and hydrophilicity. The individual phenomena have been examined experimentally in great detail by Pashley [Pashley, (1981); Pashley, (1982)], Israelachvili [Israelachvili, (1978); Israelachvili, et. al., (1978); Israelachvili, et. al., (1979); Israelachvili, et. al., (1984); Israelachvili, et. al. (1984)], Horn [Horn, et. al., (1980); Horn, et. al., (1981)], Parsegian [Rau, et. al. (1984); Cowley, et. al. (1978); Parsegian, et. al.

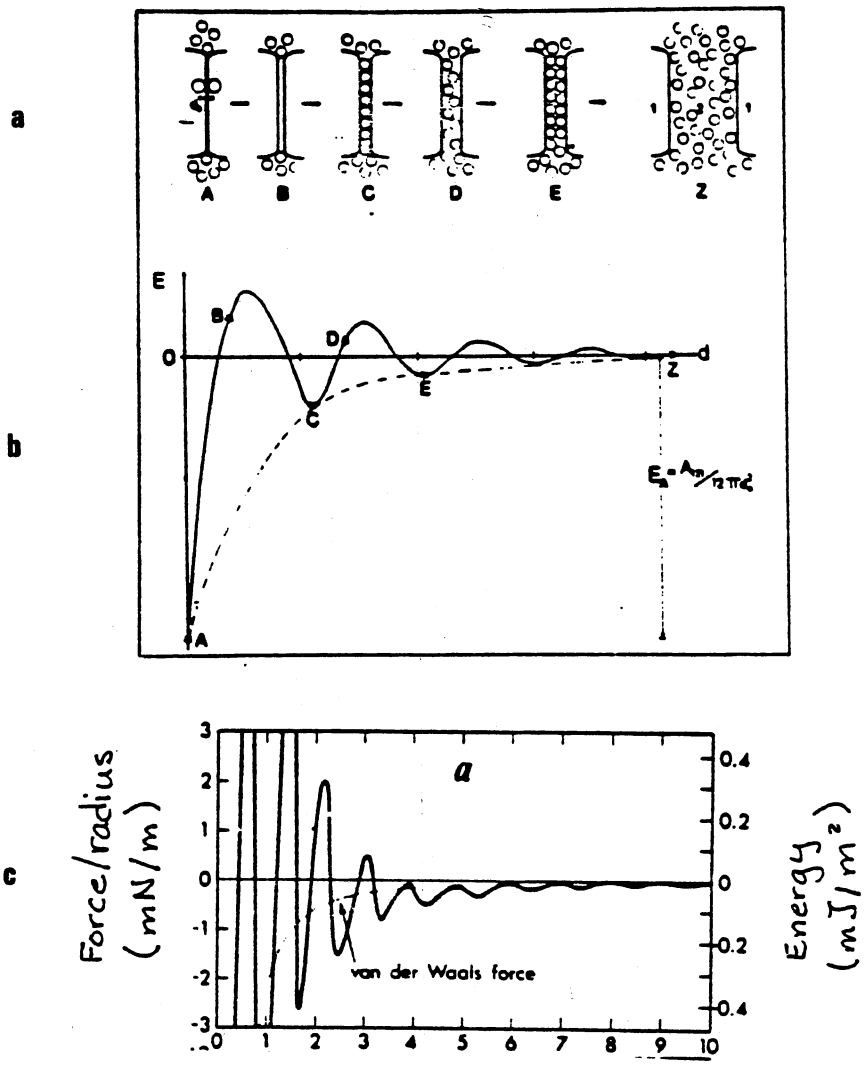

Figure 3. (a) Shows the molecular ordering as the separation changes. (b) The corresponding solvation pressure. (c) Measured force between two curved mica surfaces. For comparison, the theoretical continuum van der Waals force. [Israelachvili, (1985)]

(1987); Parsegian (1982)], and Claesson [Claesson, et. al., (1984)]. Theoretically these forces have been studies by Snook and Van Megen [Snook, et. al. (1980)], Gruen [Gruen, et. al., (1981)], and Marcelja. [Marcelja, et. al., (1976)]

However, in most colloidal suspensions the average separation between the particles remain greater than the range of solvation interactions. Hence the complication of the medium's structure can be neglected in most studies by assuming the medium is a continuum. Thus, only bulk properties, such as the dielectric constant, are used to describe the medium. Furthermore, the continuum acts to modify the existing forces between two macroscopic particles from that predicted between two particles in a vacuum as described previously.

Electrostatic Forces

In colloidal dispersions, if the only interaction present is a result of the dispersive forces which in most cases are attractive (and certainly attractive for like particles, as in the case of monodisperse suspension used in this study) the system would collapse through coagulation. Fortunately, this does not occur because of the presence of a repulsion arising from electrostatic considerations (Coulomb repulsion) [Israelachvili (1985)].

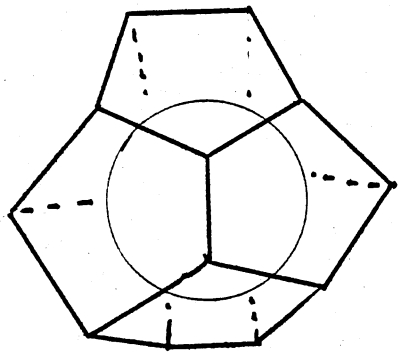

Figure 4. The solvation cages.

For charge stabilized systems, a suspension stabilized by Coulomb repulsion, the particles carry a charge. For latex particles the charge is generally negative; however, the overall suspension is electroneutral. The charges are carried via ions either solvated or attached to the particle surface, and an electric double layer is formed by the ions on the particle or surface and the solvated counterions located at the particle-solution interface. [Verwey, et. al. (1948); Hiemenz (1986)] The structure of the double layer surrounding the particle is similar to the ionic atmosphere described in the Debye-Huckel theory. [Overbeek, 1984] It is the overlap of these double-layers as the particles approach each other that causes the electrostatic repulsion.

The structure of the diffuse double layer (see Figure 5) was first given by Gouy, Chapman, Deby and Huckel [Verwey, et. al. (1948); Overbeek (1984); Chapmann (1913); Hogg, et. al. (1966)] and later modified by Stern to incorporate the finite size of the ions in solution [Verwey, et. al. (1948); Overbeek (1984)]. According to the model proposed by Gouy-Chapmann, the particle charge is considered as a smeared-out surface charge on the plane defining the surface. The countercharges carried by the medium are attracted or repelled by the surface according to the Boltzmann principle. The potential, which obeys the Poisson equation, at any point in the system, simplified for the case when the valence of the cations and anions are the same, is given by

$$\nabla^2\Psi = (8\pi cez / \varepsilon) \sinh (ze\Psi / k_BT) \qquad I.19$$

where Ψ is the potential, ∇^2 the Laplacian operator, is the dielectric constant of the medium, z is the valence of the ionic species in solution, c is the concentration of ions in solution, e is the electric charge, k_B is Boltzmann's constant and T is the temperature. This has been solved exactly by Gouy (1910) for the case of a single flat plate, however for cases of interacting plates or spheres, one generally employes approximate methods as the problem becomes difficult to solve analytically. Now restricting our discussion to a small Ψ approximation, equation I.19

reduces to

$$\nabla^2\psi = \kappa^2\psi \qquad \text{I.20}$$

where κ is the Debye-Huckel reciprocal length given by

$$\kappa^2 = 8\,ce^2z^2 / k_BT \qquad \text{I.21}$$

Thus, equation I.19 may be solved for the one dimensional symmetry of infinite plates by simplifying $\nabla^2\psi$ to $d^2\psi / dx^2$. This has solutions

$$\psi = A_1 \cosh \kappa x + A_2 \sinh \kappa x \qquad \text{I.22}$$

where A_1 and A_2 are constants that depend on the boundary conditions applied. For the case of two dissimilar plates with separation 2d, and boundary conditions (i) $\psi = \psi_{o1}$ at $x = 0$, and (ii) $\psi = \psi_{o2}$ at $x = 2d$ where ψ_{o1} and ψ_{o2} are the surface potentials of the plates 1 and 2 respectively. Equation I.22 becomes

$$\psi = \psi_{o1} \cosh \kappa x + \qquad \text{I.23}$$
$$\{ \psi_{o2} - \psi_{o1} \cosh 2\kappa d\}/\{\sinh 2\kappa d\} \sinh \kappa x$$

One can now obtain the interaction energy between two double layers. This interaction energy is equal to the change in the free energy of the double layer system when the plates are brought together from infinity i.e. [Hogg, et. al. (1966); Verwey, et. al. (1948)]

$$V_I = \Delta G = G_{2d} - G_\infty \qquad \text{I.24}$$

where G_{2d} is the free energy at the separation 2d and G_∞ is the free energy at infinity. Following Verwey, et. al. (1948) the free energy of a single double layer [Hogg, et. al. (1966)] is given by

$$G = - \sigma \psi_{\infty} / 2 \qquad \text{I.25}$$

where σ is the surface charge density and is given by

$$\sigma = \frac{\varepsilon}{4\pi} \left(\frac{d\psi}{dx}\right)_{x=0} \qquad \text{I.26}$$

Following Hogg, et. al. (1966) one obtains

$$G_{2d} = \frac{\varepsilon\kappa}{8\pi} \left[2 \psi_{01}\psi_{02} \operatorname{cosech} 2\kappa d - (\psi_{01}^2 + \psi_{02}^2) \coth 2\kappa d\right] \qquad \text{I.27}$$

and

$$G_{\infty} = \frac{\varepsilon\kappa}{8\pi} (\psi_{01}^2 + \psi_{02}^2) \qquad \text{I.28}$$

Therefore, V_R is

$$V_R = \frac{\varepsilon\kappa}{8\pi} \left[(\psi_{01}^2 + \psi_{02}^2)(1 - \coth 2\kappa d) + 2\psi_{01}\psi_{02} \operatorname{cosech} 2\kappa d\right] \qquad \text{I.29}$$

The interaction of infinite flat plates, can be used to obtain an expression for the interaction of two spherical particles using the Derjaguin approximation.

In the Derjaguin approximation, one considers the particle to be composed of infinitesimally small parallel rings each of which may be treated as a flat plate so long as the thickness of the double layer is small compared to the particle size [Verwey, et. al. (1948); Vold, et. al. (1983); Israelachvili (1985); Hogg, et. al. (1966)]. Thus, one can write the interaction between spherical particles as

$$V_R = \int_0^{\infty} 2 \, h' \pi \, V_R \, dh' \qquad \text{I.30}$$

where V_R is defined in equation I.29 and h' is the radius of the ring as shown in Figure 6. For the case where $a_1 \neq a_2$ and the geometry given in Figure 6, one can show that

$$V_R = \frac{\varepsilon a_1 a_2 (\psi_{o1}^2 + \psi_{o2}^2)}{4(a_1 + a_2)} \left\{ \frac{2\psi_{o1}\psi_{o2}}{(\psi_{o1}^2 + \psi_{o2}^2)} \ln \frac{1 + e^{-\kappa H}}{1 - e^{-\kappa H}} + \ln(1 - e^{-2\kappa H}) \right\} \quad \text{I.31}$$

provided h << a_1 and h << a_2 [Hogg, et. al. (1966)].

For the case of interest in this work a = a_1 = a_2 and ψ_{o1} = ψ_{o2} = ψ_o, equation I.31 reduces to

$$V_R = (a \psi_o^2 / 2) \ln (1 + \exp(-\kappa H_o)) \quad \text{I.32}$$

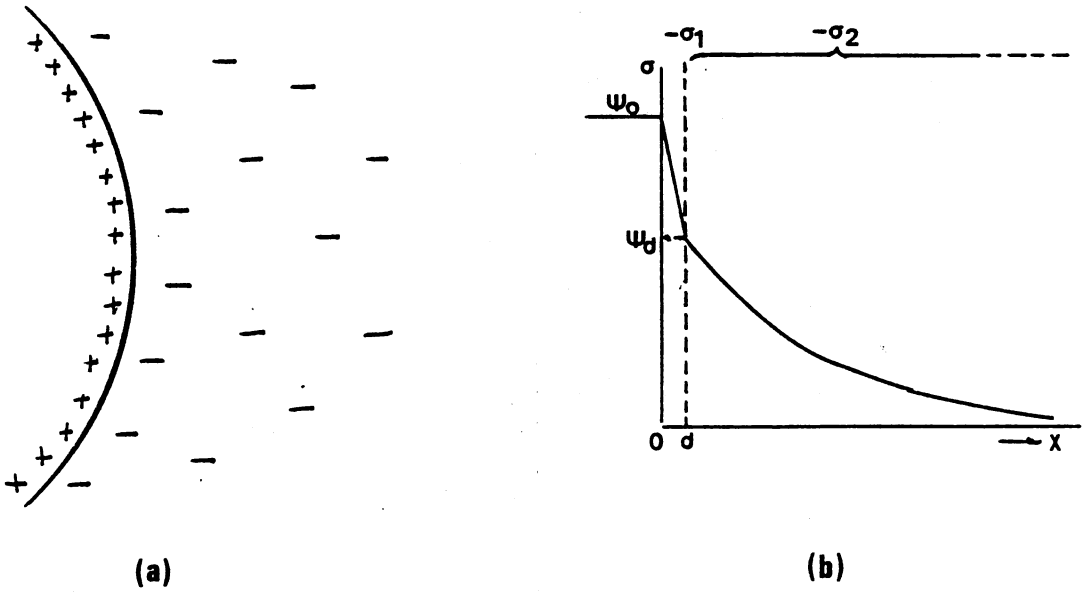

Figure 5. (a) Schematic of the diffuse Double-layer about a particle. (b) Representative Double-layer according to the theory of Stern [Verwey, et. al. (1948)].

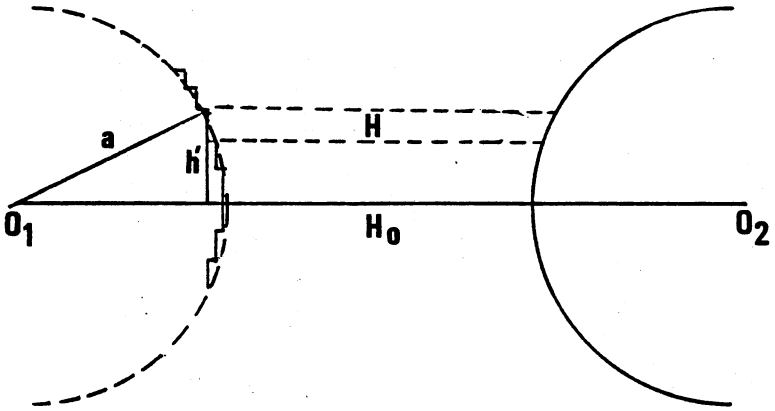

Figure 6. Illustrating the building up of repulsion between two spheres out of the repulsion between quasi-parallel layers. [Vold, et. al. (1983); Verwey, et. al. (1948)]

Steric Effects

In suspensions of colloidal particles, the particles are stabilized from aggregation predominantly via one of two mechanisms - charge stabilization or steric stabilization. The charge stabilization mechanism is based on the Coulomb type electrostatic repulsion previously discussed. However, steric stabilization is achieved by utilizing either osmotic effect or volume restriction effects.

In a sterically stabilized suspensions, the particles are composed of large segments or loops of a high molecular weight polymer, or are coated with chains or loops of a polymer. The solvent is chosen to

be appropriate for the attached polymer. Thus when two particles approach each other, they will be repelled by either a) the polymer chains attached to the particle surface lose entropy due to increased confinement causing the repulsion - this is the volume restriction effect; or b) the layers of the attached polymer chains interpenetrate, the higher polymers segment concentration between the particles causes a rise in the local osmotic pressure -the osmotic effect [Vrij (1976)]. (See figure 7)

The strength of this type of interaction may be evaluated by the following calculation. Consider a polymer chain of maximum length, l, attached to a colloidal particle (here approximated by a flat plate). This chain has a permanently attached end and the rest of the chain is free to move about in the hemisphere defined by, l, i.e. $V_i = 2\pi l^3 / 3$. (See figure 8) A second particle approaches to a surface to surface separation of H, thus reducing the volume in which the polymer is free to move to

$$V_f = \pi/3 \{2l^3 - (l - H)^2(2l + H)\} \qquad I.33$$

The attached polymers of both particles must occupy the same volume. Assuming the change in free energy is the same as that of an ideal solution undergoing the same concentration change, G is

$$G = - 2 k_B T \Gamma \ Ln \ (V_f / V_i) \qquad I.34$$

where k_B is the Boltzmann's constant, T is the

temperature and Γ is the amount of adsorption. For a chain of 4 nm at $\Gamma = 10^{13}$ cm^{-2} and H of 1 nm, the repulsion is 2 x 10^{5} kT per square micron [Vold, et. al. (1983)], this comparable to a double layer of $\varepsilon\Psi/kT = 5$ with $\kappa = 0.1$ nm^{-1}. However, the particles used in this study were charge stabilized, hence the steric forces discussed here are neglected form further consideration.

Particle Field Interactions

For the investigation considered here, it is important to consider how the particles in suspension are affected by the presence of an externally applied perturbation and the overall resulting implications to

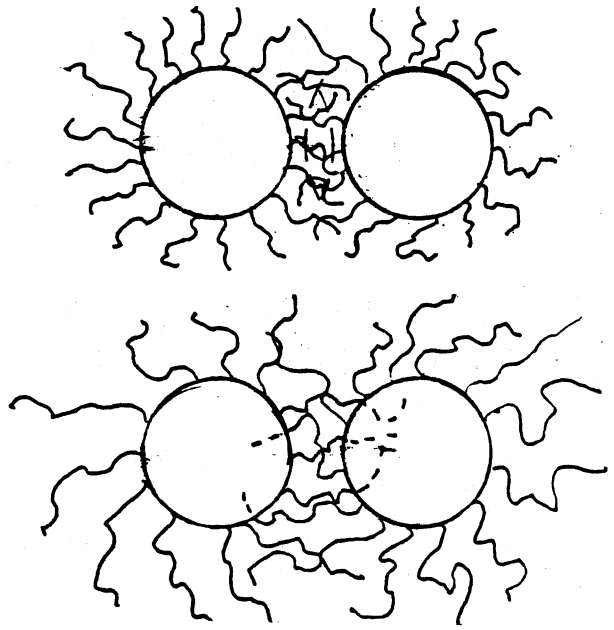

Figure 7. Illustrating the osmotic effect (top) and the volume restriction effect (bottom) in steric repulsion. [Overbeek (1984)]

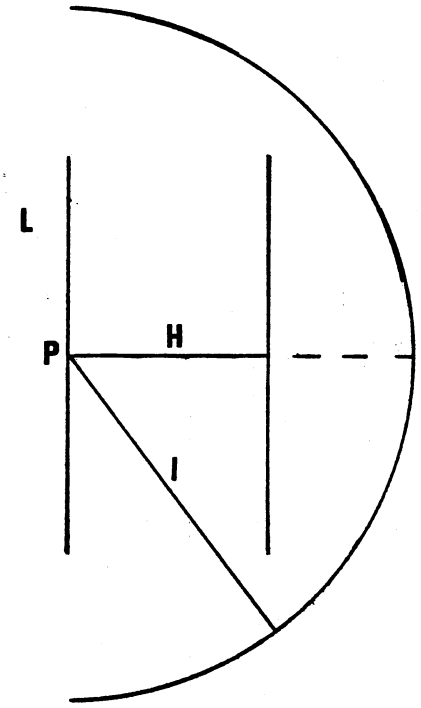

Figure 8. Geometry, coordinate system, and nomenclature for calculating the segment density of an absorbed polymer between approaching plate-like particles. [Vold, et. al. (1983)]

the system of particles. This study focuses on a single type of applied field, an oscillating electric field, there are several other commonly used externally applied fields such as a mechanical or an applied shear [Ackerson, et. al. (1984)]; gravitational [Russel, et. al. (1989); Prieve, et. al. (1987, 1989)]; or other types of applied electromagnetic fields [Chowdhury, et. al. (1985, 1988); Skjeltorp (1983, 1984, 1985)]. Here, one need only focus on those interactions induced by

applying an oscillating electric field and further focusing only on the organization occurring parallel the field lines; i.e. an applied parallel field. However, for the sake of completeness, a similar development for an applied magnetic field will be presented.

Parallel applied fields have been used previously in both the electric field and magnetic field cases. Fraden (1987) and Richetti, et. al. (1987) used the applied electric field to examine the association of colloidal particles in the presence of the field. While Skjeltorp (1983, 1984, 1985) and Popplewell, et. al. (1981, 1986, 1987) used the magnetic field, in these cases the studies in the parallel direction were done primarily as observations before examining the phenomena present perpendicular in closer detail. However, in all of these previous studies the concern has been to examine the behavior of the interparticle ordering in the presence of the field rather than a means of investigating the stabilization forces present in the suspension.

Electric Field Interactions

Consider a single dielectric sphere, when an uniform field is applied, the sphere becomes polarized and the sphere is said to have an induced dipole moment located at the center of the sphere. If one now considers the sphere to be located in a medium, one can

write the form of the induced moment taking into account the medium as

$$u = a^3 [(\varepsilon_p - \varepsilon_\omega)/(\varepsilon_p + 2\ \varepsilon_\omega)]\ E \qquad \text{I.35}$$

with ε_ω, ε_p being the complex dielectric constant of the medium (in the case presented here the medium is water) and the particle respectively, where $\varepsilon = \varepsilon' + i\ \varepsilon''$; a, the radius of the sphere; and E is the electric field (in c.g.s units) [Sauer (1985); Fraden (1987); Pohl (1978)]. Now consider that a second identical particle is placed in the medium along with the first, one would expect these particles to interact via a dipole-dipole interaction at large separation with energy

$$V = u^2\ (1 - 3\cos^2\theta)/\ \varepsilon_\omega\ r^3 \qquad \text{I.36}$$

where u is the dipole moment, r is the center to center distance and θ is the angle between the line connecting the centers and the external field. For this investigation $\theta = 0^\circ$ implies that the line of centers lies parallel to the field lines at infinite distance (the parallel field case) and at $\theta = 90^\circ$ the field lines are perpendicular to the line of centers (the perpendicular case). This is a pairwise interaction and one may assume in a dilute suspension of particles, the only interactions present are those pairwise interactions.

However, as the particles approach one another this approximation for the dipole moment is no longer valid.

Thus, one must consider how separation effects the dipole moment. This is difficult to do because in general this problem cannot be solved in a closed form. One approach proposed by Pohl (1978) is to calculate the energy required to bring two polarizable spheres to a center-to-center separation of r then extend the result to r = 2a. Thus, the energy (for the parallel case) at contact has the form

$$V = (r^3 E^2 / A) [(\varepsilon_p - \varepsilon_\omega) / (\varepsilon_p + 2 \varepsilon_\omega)]^2 \quad \text{I.36}$$

where A is the correction term and is given by

$$A = \{ 1 - (1/4) [(\varepsilon_p - \varepsilon_\omega) / (\varepsilon_p + 2 \varepsilon_\omega)] \} \quad \text{I.37}$$

and for the case under investigation here where $\varepsilon_\omega >> \varepsilon_p$ this correction is approximately 12.5 %.

A much more detailed and comprehensive approach was proposed by Sauer (1985). This approach was presented for conditions very similar to those used in this study, i.e. he was attempting to discuss the pearl chain formation (particles aligning in chains along the field lines). He used the asymptotic solutions, by expanding the potential in a power series and kept only the leading terms, to obtain

$$V = u^2 / \varepsilon_\omega d^3 \{ (1 - 3 \cos^2\theta)/ (1+\xi)^3 - s(1 + 3 \cos^2\theta)/8 (1 +\xi)^6 \} \quad \text{I.37}$$

where $r = d(1 + \xi)$ where $d = 2a$ and $s = Re\{(\varepsilon_p - \varepsilon_\omega) / (\varepsilon_p + 2 \varepsilon_\omega)\}$, and Re{} is the real part of the quantity enclosed. For $\varepsilon_p << \varepsilon_\omega$, this the correction due to second order terms is only approximately 12%, this

correction becomes less as ε_p approaches ε_ω. For the study presented here where $\varepsilon_p = 2.55$ and $\varepsilon_\omega = 78$, this correction is approximately 10%. Therefore, for experimental purposes the long range dipole-dipole interaction appears sufficient.

One may also consider the effects of adding particles to the chain. This has been considered by others [Jeffrey (1973), Jones (1986, 1987)] for conducting spheres. In these studies, the effective dipole moment of the entire chain was calculated by using the method of images for a chain composed of two or three spheres. The results presented show that for non-touching particles asymptotically approach the number of particles in the chain times the individual dipole moments as the surface to surface separation increases, which for the case of two or three spheres is quite rapid. However, the method presented becomes computationally difficult for more than three spheres and for non-conducting particles. Therefore, the dipole-dipole interaction seems to be sufficient for the purposes of this investigation.

Magnetic Field Interactions

In an applied magnetic field, the colloidal particle behaves as a magnetic hole [Skjeltorp (1983, 1984, 1985); Warner, et. al. (1985); Davies, et. al. (1985, 1986)]. To understand the implication of the

dipole hole, one must consider the system employed. In this case the colloidal suspension under investigation is a ferrofluid composite system. The composite system is comprised of colloidal particles (micron sized spheres) suspended in a ferrofluid. A ferrofluid is a colloidal suspension itself, in which nanometer sized ferrite particles are suspended in a carrier fluid, most generally a hydrocarbon such as kerosene or toulene. When a magnetic field is applied, alignment of the ferrite particle in the ferrofluid induces a dipole on the larger micron sized particle.

Here a parallel development to that given above is used. The dipole moment on the particle may be give as

$$u = 4 \pi ((\mu_m - \mu_f)/(\mu_m + 2 \mu_f)) a^3 H \qquad I.38$$

where μ_m, μ_f are the permeability of the sphere and the fluid respectively, a is the radius of the particle, and H is the uniform magnetic field applied. By noting that $\mu_m = \mu_o$, and $\mu_f = \mu_o(1 + \chi_f)$, one can simplify equation I.38 to [Warner, et. al. (1985)]

$$u = - v \chi_f H \qquad I.39$$

where v is the volume of the sphere, and χ_f is the effective susceptibility of the fluid (this is usually supplied by the manufacturer of the fluid).

Therefore, the interaction energy between two micron sized particles suspended in the ferrofluid may be written approximately as

$$V = u^2 (1 - 3 \cos^2\theta)/r^3 \qquad I.40$$

which is identical in form to equation I.36. The particle experiences an attractive interaction when the field is applied in a parallel direction, and a repulsive interaction when the field is applied in a perpendicular direction [Skjeltorp (1983, 1984, 1985)].

These induced dipole interactions in both the electric field and the magnetic field cases induce structure in the colloidal samples. Skjeltorp (1983, 1984, 1985) observes that when the field is applied parallel to the layer of particles the particles form chains (Figure 9a) and when the field is applied perpendicularly, a two-dimensional lattice structure is formed (Figure 9b). Both configurations have been examined in terms of Monte Carlo simulations; including the stability of the lattice structure [Davies, et. al. (1985, 1986)]. An applied electric field produces the same behavior as in the ferrofluid composite systems. When the field is applied in a parallel direction, chaining is observed (Figure 9a); and when the field is in a perpendicular direction, a triangular two dimensional lattice structure is observed (Figure 9b) [Fraden (1987); Richetti, et. al. (1987)].

The Total Colloidal Particle Interactions

To this point the interactions experienced by the particles suspended in a colloidal solution have been examined in terms of individual interactions, i.e. van

der Waals, dipole-dipole, double-layer repulsion, etc. However, it is improbable that only one interaction is

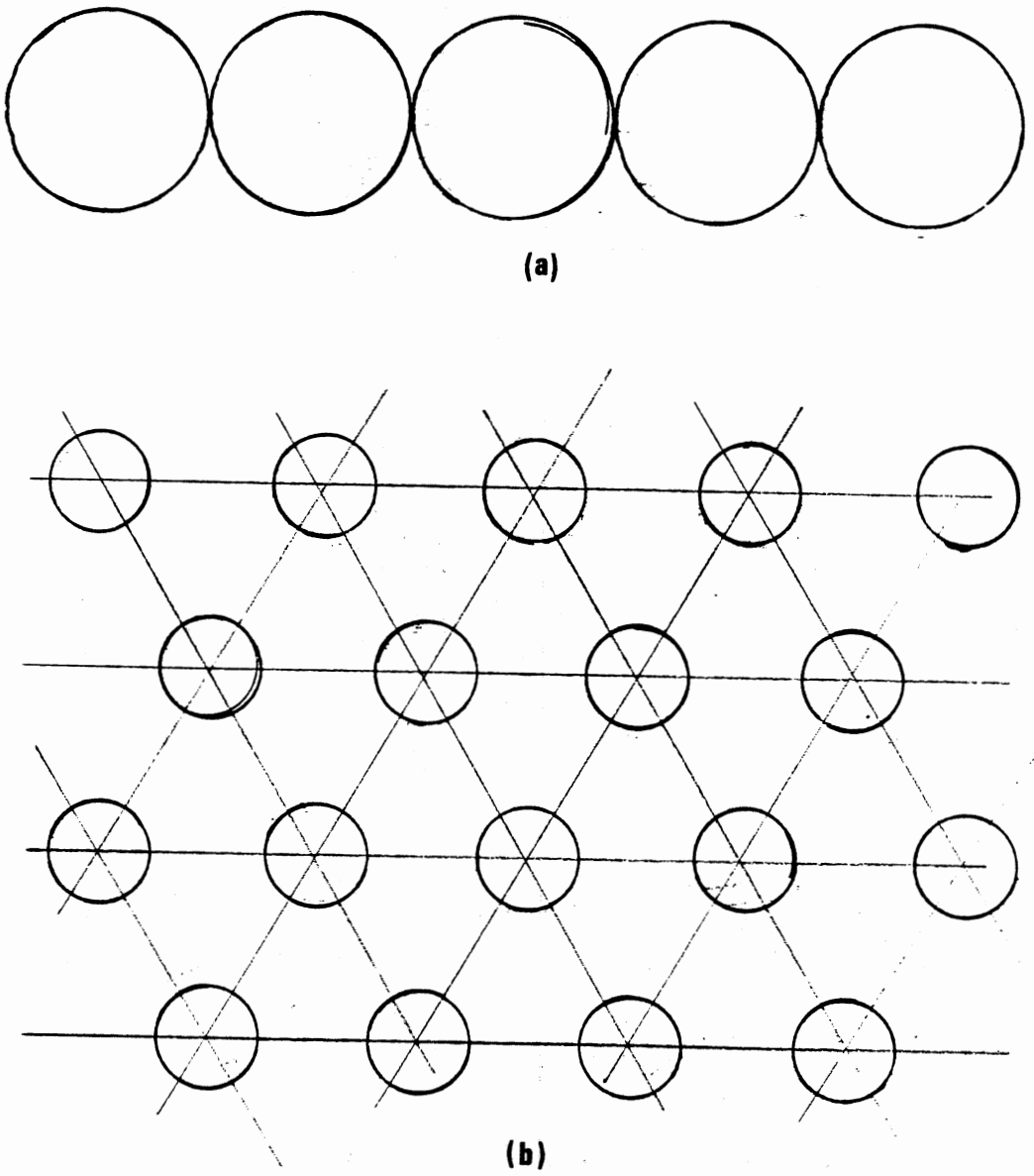

Figure 9. Illustrating the configurations of the suspended particles when the field a) is applied in the parallel direction and b) is applied in the perpendicular direction.

present in the colloidal suspension. If for example, only van der Waals forces were present the suspension would collapse, i.e. the particles would be drawn into contact with one another causing aggregation. Thus, one must consider combinations of interactions to understand the phenomena present in sample systems.

The most generally accepted theory for the stability of charged particle colloidal systems was proposed by Derjaguin, Landau, Verwey, and Overbeek (DLVO) [Verwey, et. al. (1948); Overbeek (1984); Israelachvili (1985); Hiemenz (1967); Vold, et. al. (1983)]. This theory combines the elements of van der Waals interactions with those of the electrostatic interactions by a direct addition of the two interactions. This is given by the combination of the free energies of the attraction and repulsion to give the total free energy of interaction

$$V_t = V_{att} + V_{rep} \qquad \text{I.41}$$

where V_{att} is the attractive interaction due to the van der Waals interactions and V_{rep} is the repulsive force due to the electrostatic repulsion.

Figure 10 shows schematically the various types of interactions potentials that can occur between two surfaces under the combined action of these two interactions. From the schematic it is seen that van der Waals forces exceed the double layer repulsion at

small distances since it obeys a power law. Depending on the electrolyte concentration and the surface charge density one of the following may occur: [Israelachvili, (1985)]

a) For highly charged surfaces in a dilute electrolyte, there is a strong long range repulsion that peaks between 1 and 4 nm.

b) In more concentrated electrolyte solutions there is a significant secondary minimum (usually beyond 4 nm). The potential energy minimum at contact is the primary minimum.

c) For surfaces of low charge density, the energy barrier will always be lower than that of higher electrolytic solutions and above some electrolyte concentration-the colloidal particles will begin to coagulate. It is this phenomenon that forms the basis of the DLVO theory of stability, i.e the particles will coagulate when the secondary minimum has a depth less than kT.

d) As the surface charge approaches zero the interaction curve approaches a pure van der Waals interaction.

DLVO theory is generally accepted as correct under the conditions for which it was derived, i.e. [Lyklema, (1981)]

> -- The sol must be dilute such that the potential of the mean force may be replaced by the average potential.

-- No other interaction forces are operative besides van der Waals attraction and double

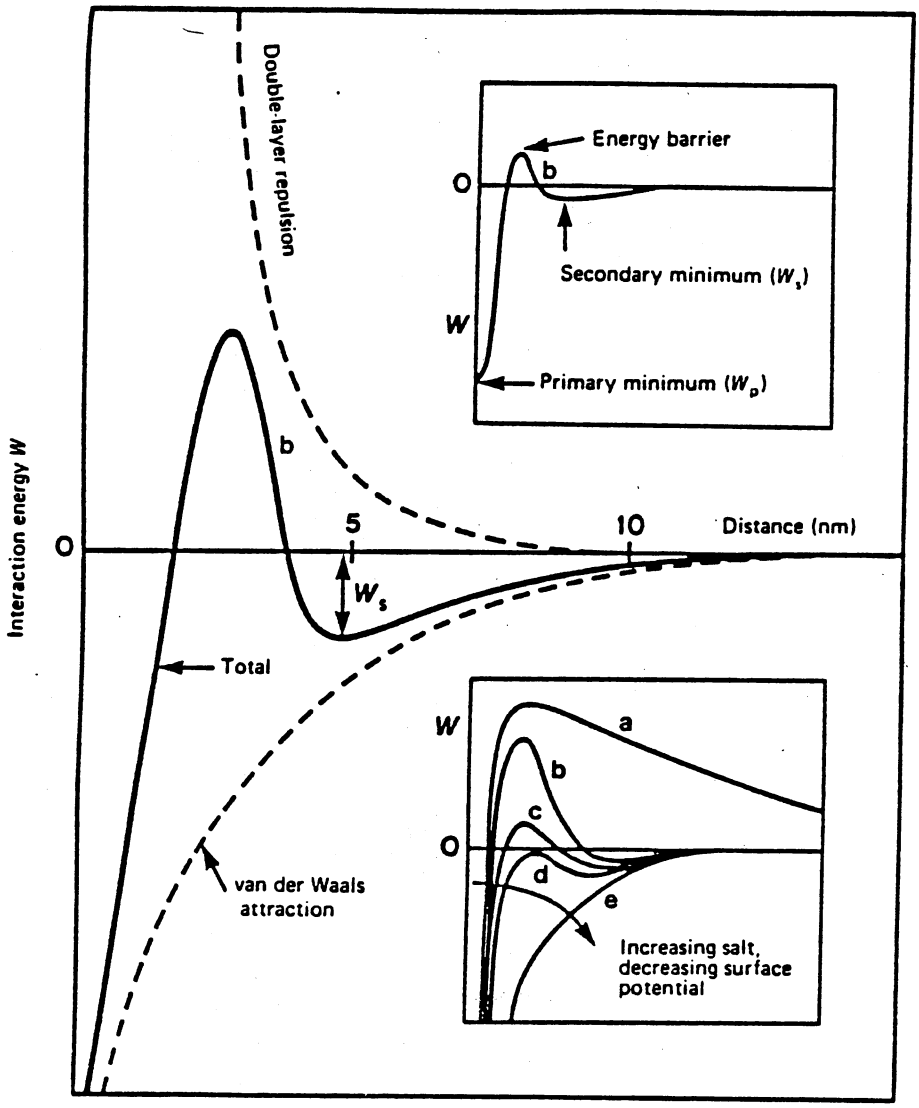

Figure 10. Schematic energy vs. distance profiles of DLVO interactions. (a) Surfaces repel strongly. (b) Surfaces come to a stable equilibrium at secondary minimum. (c) Surfaces come into secondary minimum. (d) Surfaces may remain in secondary minimum or adhere. (e) Surfaces and colloids coalesce rapidly. [Israelachvili (1985)]

layer repulsion.

-- The geometry of the particles must be relatively simple, i.e. spheres, flat plates.

-- The double layers must be purely diffuse.

-- Upon overlap, the double layers relax sufficiently fast to remain in thermodynamic equilibrium.

This chapter has presented those interactions that are present in colloidal suspensions, forces which will be tested directly by the experiments described in this thesis.

CHAPTER II

EXPERIMENTAL TESTS OF MICROSCOPIC FORCES

In the previous chapter, the interactions that one may encounter in a colloidal suspension were discussed. However, the means by which these interactions are examined were either only briefly mentioned or not discussed at all. Over the years several techniques have been applied to this problem. For example, van der Waals forces have been examined using soap films and biological membranes by Overbeek (1960), Joosen (1984), and Parsegian (1987). Stabilization forces have been measured using flocculation studies like those of Melik (1985). These techniques are generally arduous and the information obtained from the experiments is difficult to interpret. More direct techniques have been used like those of Israelachvili and Prieve briefly discussed earlier. This chapter will focus primarily on those techniques used by Israelachvili and Prieve as well as examine the experiments by Richetti, et. al. and Fraden who used a similar experimental design to that used in this study.

The Macroscopic-Macroscopic Technique

A macroscopic-macroscopic technique (M-M) was developed by Isrealachvili, et. al. [J. N. Isrealachvili, et. al. (1988, 1976, 1977 and 1983); J. N. Isrealachvili (1977); R. M. Pashley (1980); P. Claesson, et.al. (1983); and R. G. Horn, et. al. (1981)] In this method, two macroscopic surfaces either flat plates or crossed curved cylinders are brought together using a spring. The separation of the surfaces is monitored using an optical interference technique. Thus, the force is measured directly. Therefore, one can obtain fairly readily a force versus separation relationship.

The surfaces used in these experiments are mica sheets placed either on curved glass cylinders - which is shown in Figure 11 - or glass flat plates. Mica was chosen for these studies because the surfaces are molecularly smooth. Typically experiments conducted using this apparatus use ruby muscovite mica. The separation between the two surfaces is controlled by the three stage mechanism depicted in Figure 11. The separation is measured by monitoring the beam interference fringes and the fringes are continually monitored in a spectrometer. The forces are measured by suddenly reversing the voltage in the piezoelectric crystal which expands or contracts by a known amount.

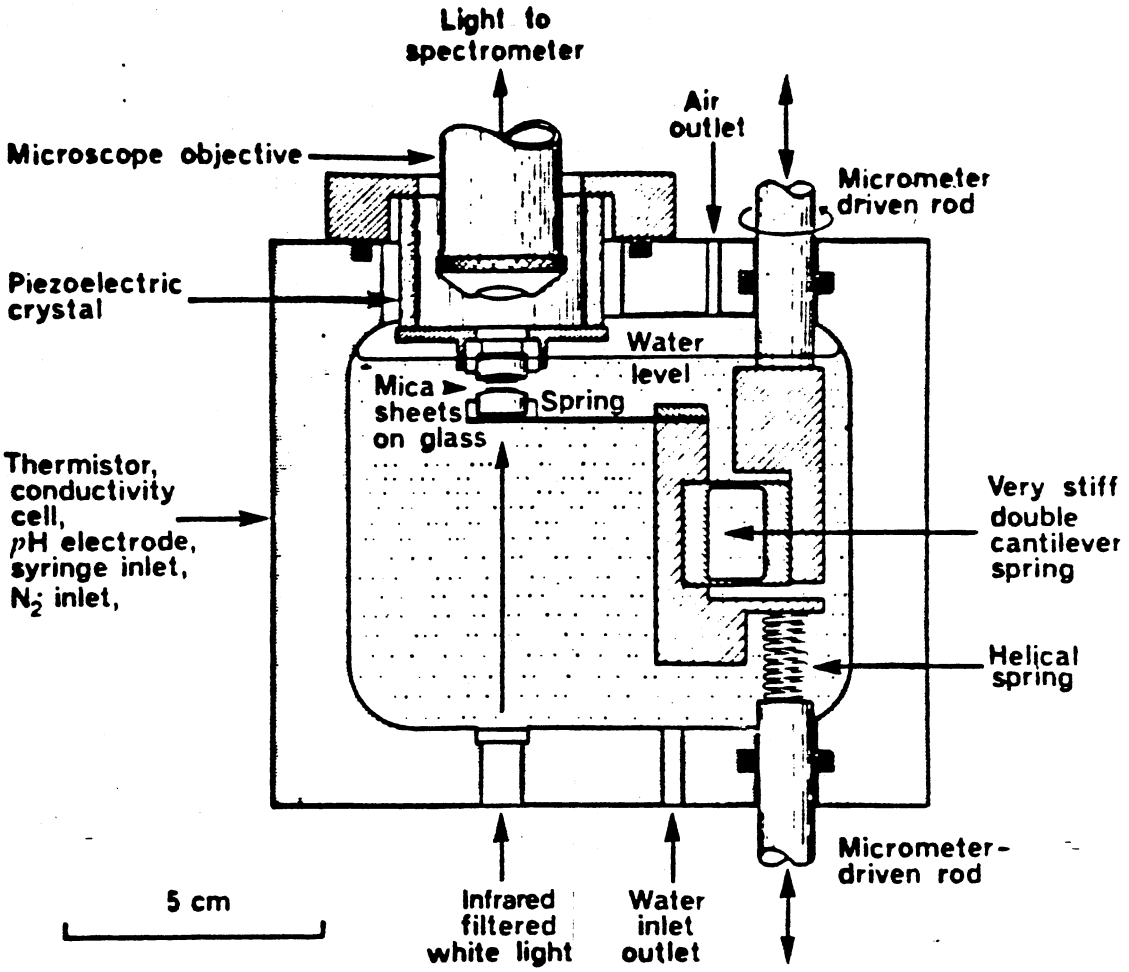

Figure 11. Schematic drawing of the apparatus to measure the forces in the M-M. [Israelachvili (1976)]

The resulting change in separation between the plates is measured optically and the difference in the two values is then multiplied by the stiffness of the spring, thus determining the force.

This method provides a straight forward means of

obtaining force versus separation measurements. Various solvents may be used in this system, allowing for the modelling of various colloidal systems as well as the investigation of the hydration forces - those forces due to liquid structure. The major drawback to this experimental technique of importance in regard to colloidal systems is that this technique only models the system. The surfaces are larger than the actual colloidal particle, and affects due to thermal motion are totally neglected.

The result of modelling the colloidal system is that it leaves open questions related to the differences between the two systems. For example: here two macroscopic surfaces are used, will the forces observed carry directly over to the microscopic colloidal system? Does the plate's electronic double adequately mimic the particle's? The system used in M-M has no thermal motion - the plates are stationary - how does the thermal motion of the colloidal particles change the observed forces? In the continuum approach for van der Waals interactions, the wavelength of the light as it approaches the particle size becomes an important parameter - therefore, how does this effect the forces observed?

The Macroscopic-Microscopic Technique

The macroscopic-microscopic technique (M-m) carries the investigation one step closer to an actual colloidal system than that of the M-M technique. Here the forces are measured between a flat plate and a colloidal sized particle. This technique developed by Prieve, et.al. [D.C. Prieve, et. al. (1987, 1989)] provides a novel use of total-internal-reflection microscopy (TIRM) to measure the separation of the plate and the particle.

When light strikes a planar interface from a more optically dense medium at an angle of incidence greater than the critical angle, total internal reflection results. Although all the light energy is ultimately reflected back into the more dense medium, there is an optical disturbance in the less dense medium which takes the form of an evanescent wave. However, a particle may intercept this wave and scatter in proportion to is distance from the surface. Thus, the intensity of the light scattered by the sphere in this evanescent wave is measured and can be translated into a separation distance - this is the basic principle of TIRM. TIRM is generally used to inspect optical surfaces for damage.

This M-m technique uses gravity to bring the particle into near contact with that of the plate. The particles used were polystyrene latex microspheres 10.04 um in diameter - large enough so settling can occur. The plate used in the experiment was an ordinary

microscope slide that was carefully washed. The force is determined through a force balance between the double-layer repulsion and gravity. The van der Waals attraction between the sphere and the plate was neglected in these experiments based on the assumption that for a large sphere the force due to gravity will dominate the attraction. So, once again a simple force versus separation experiment has been obtained. However, one must account for the thermal motion of the particle, as a distribution of heights is measured in a given experiment.

Prieve, et.al. estimates the interaction of the plate and sphere via the sum of the double-layer potential and the gravitational potential. This total interaction incorporates the thermal motion of the particle, thus, more closely approximating a true colloidal system. Here, the double-layer potential (as discussed earlier) between a spherical particle and a flat plate in a 1:1 electrolyte may be approximated by

$$V_{DL}(H) = B \exp(-\kappa H) \qquad \text{II.1}$$

where H is the separation, $1/\kappa$ is the Debye length and B is given by

$$B = 16\ \varepsilon a (k_B T / e)^2 \tanh(e \Psi_1 / 4 k_B T) \times \tanh(e \Psi_2 / 4 k_B T) \qquad \text{II.2}$$

where Ψ_1 and Ψ_2 are the Stern potentials of the particle and plate, ε the dielectric constant of the

medium, e is the electronic charge, k_B is Boltzmann's constant, T is the temperature and a is the particle radius. This approximation is valid when $\kappa a \gg \kappa H \gg 1$. The contribution due to gravity

$$V_{GR}(H) = (4/3)\,\pi a^3\,(\Delta\rho)\,g\,H = GH \qquad \text{II.3}$$

where $\Delta\rho$ is the difference in density between the particle and the medium and g is the acceleration due to gravity.

Adding equations II.1 and II.3, the total potential is given by

$$V_{TOT}(H) = B \exp(-\kappa H) + GH \qquad \text{II.4}$$

This function has a single minimum at a separation, H_1, given by

$$H_1 = \ln(\kappa B / G) \qquad \text{II.5}$$

By using equation II.5, the value B may be eliminated from equation II.4. Rearranging, equation II.4 becomes

$$[V_{TOT}(H) - V_{TOT}(H_1)] / k_B T = (G / k_B T)(\exp(-x) - 1 + x) \qquad \text{II.6}$$

where $x = \kappa(h - h_1)$ is the displacement from the most probable distance normalized with respect to Debye length. Experiments have shown agreement with theoretical predictions (Figure 12) at larger separations by adjusting the specific gravity of the polystyrene sphere by 2%, while smaller separations there was poor agreement. The origin of this poor agreement was felt to be due to either the contributions

of the colloidal forces being incorrect or a failure to include the van der Waals forces. However, the theoretical prediction now seems in perfect agreement with the data due to an earlier error in the calculation of ionic strength. [Prieve, et. al. (1989)]

Thus, although this technique furthers the previous studies, it still leaves important unanswered questions. We still are only modeling a colloidal system. Will the forces still behave in the same manner? What will happen when the van der Waals interactions are taken into consideration?

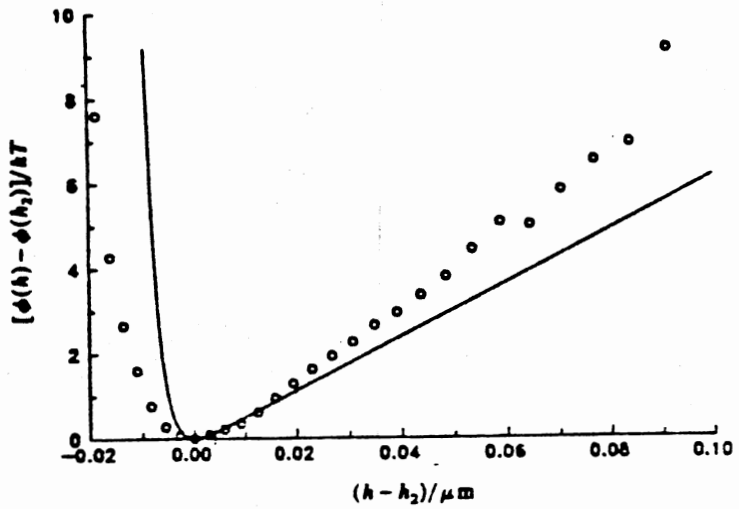

Figure 12. Potential-energy profile deduced from the scattering intensity. The solid line is their theoretical prediction. [D. C. Prieve, et. al. (1987)]

The Microscopic-Microscopic Technique

The microscopic-microscopic technique (m-m) is the technique developed for this study. Here the microscopic forces are measured between colloidal microscopic spheres, extending both studies previously discussed. This technique employs an externally applied field to induce a dipole in the particle, as discussed in the previous chapter. Once the induced dipoles are formed in the particles, they will align in chains parallel to the lines of force of the applied field. The interaction of the particles is controlled by the amplitude of the applied field and the stabilization forces present. These stabilization forces are the forces of interest in this study. The interaction between the particles controls their separation as in the other studies.

This technique of applying an electric field to a colloidal sample and focusing on the formations along the field lines has been used previously. Richetti, et.al. (1987) used this method to examine the behavior of interparticle ordering in suspensions subjected to an external homogeneous electric field. This particular study presented qualitative and preliminary quantitative results. Fraden (1987) used the technique to examine

the linear aggregation of the colloidal particles. This study focused primarily on the kinetics of the colloidal aggregate formation. However, Fraden did examine some of this linear aggregation data in a similar manner to that of Richetti, et.al. as a comparison.

The Richetti, et.al. experimental conditions are very similar to those used in this study. The sample cell is comprised of glass plates separated by two parallel wires 100 um in diameter, and the wires are separated by a gap of 4 mm. These parallel wires are the capacitor plates across which an AC voltage is applied in order to produce an electric field. The frequency used is 1 MHz. Presumably this frequency is high enough that the counterion cloud surrounding the particle cannot follow the applied field. The reason an AC field is applied rather than a DC field is to avoid hydrolysis.

Qualitatively, this study showed that the particles would align in chains along the field lines. Figure 13 are the photomicrographs obtained by Richetti, et.al. for various field strengths. These formations can be easily studied using static light scattering techniques. Figure 14 shows the corresponding diffraction patterns obtained from similar structures as those in figure 13. Under the course of this investigation it was noted that the first order diffraction peak shifted as a function

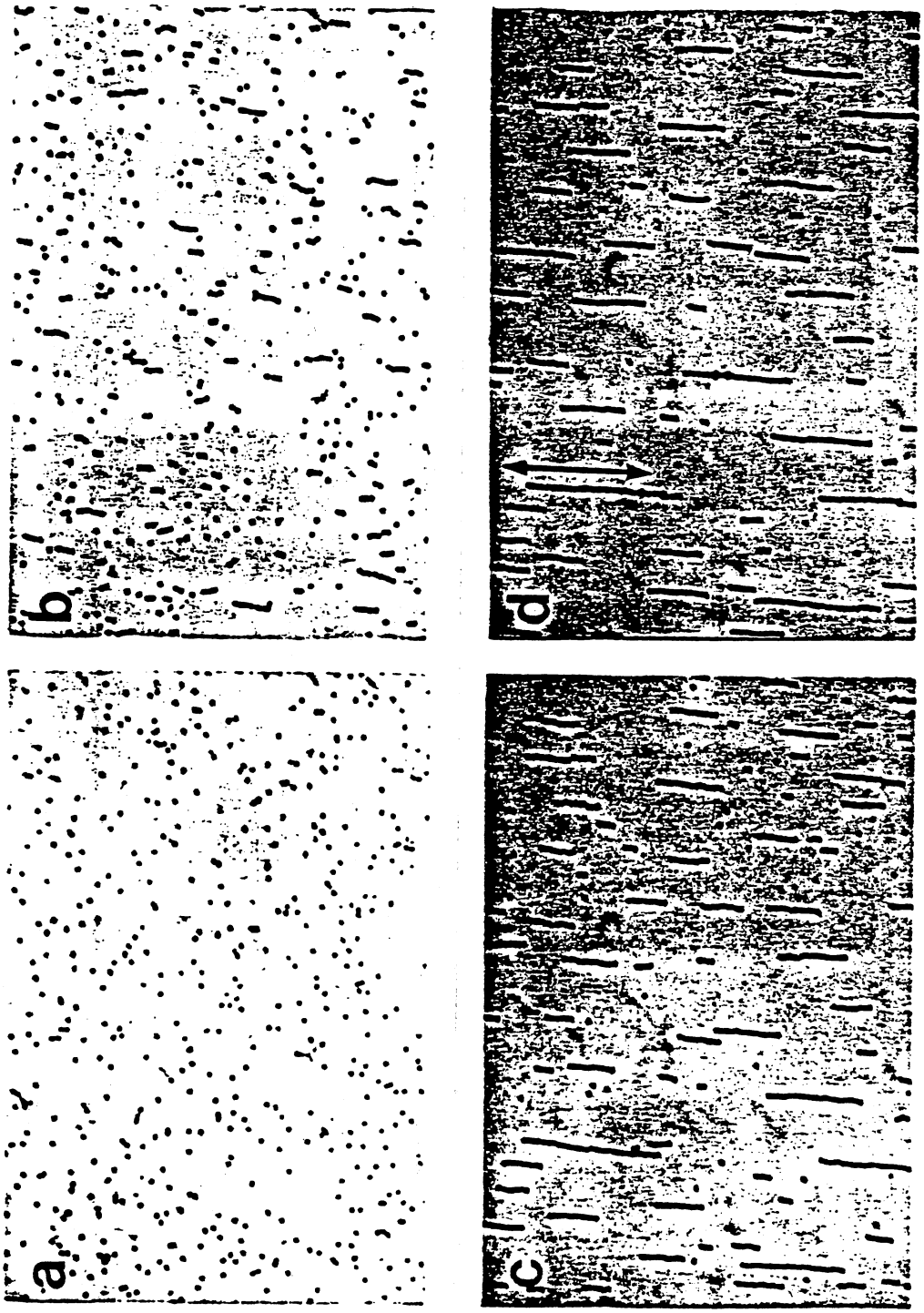

Figure 13. The photomicrographs obtained by Richetti, et. al. (1987) for 2.1 um sphere with an AC electric field applied in the direction of the arrow. a) E = 0 V/cm, b) E = 22 V/cm, c) E = 30.5 V/cm and d) E = 52 V/cm.

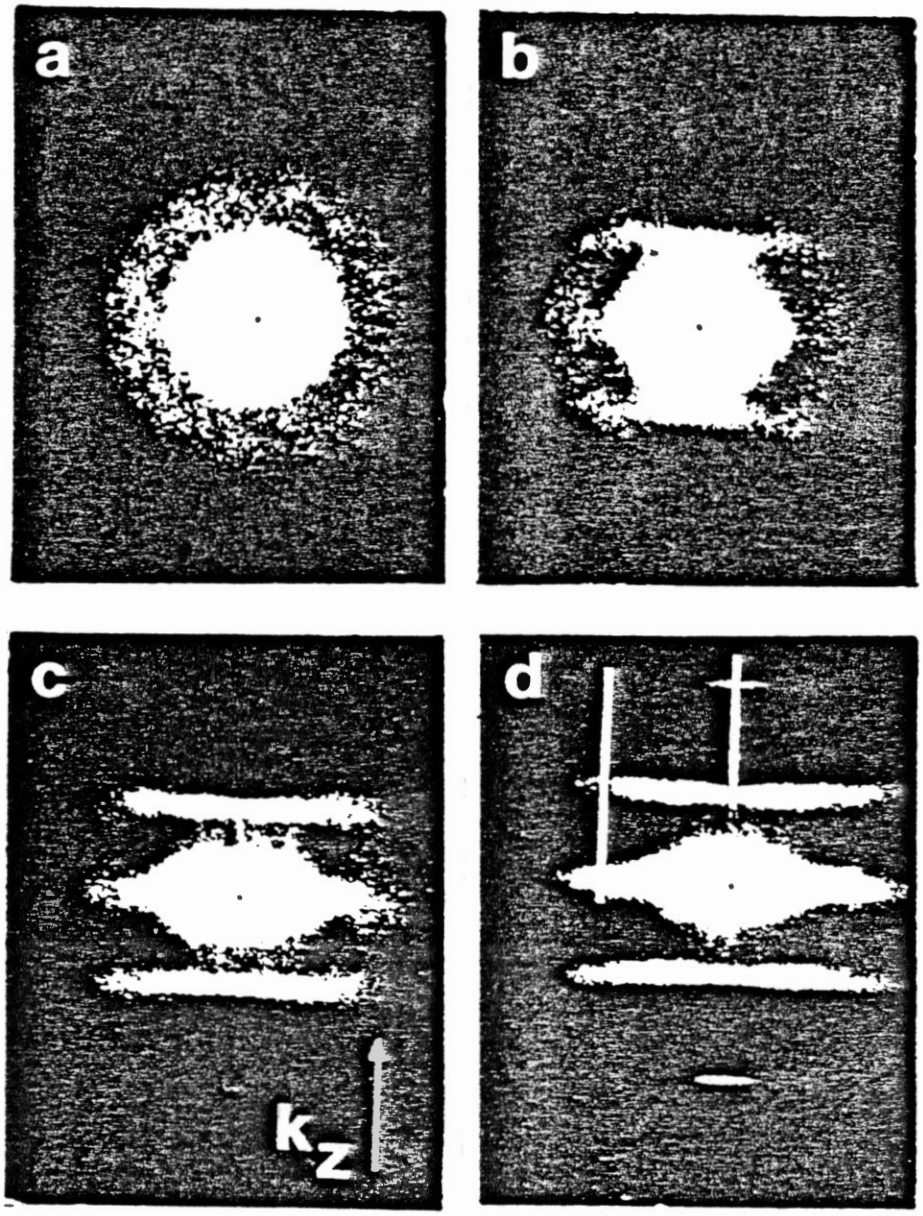

Figure 14. (a) Scattered light intensity distributions obtained with a HeNe laser by Richetti, et. al. (1987). a) E = 0 V/cm, b) E = 17.5 V/cm, c) 26 V/cm and d) 52 V/cm. .

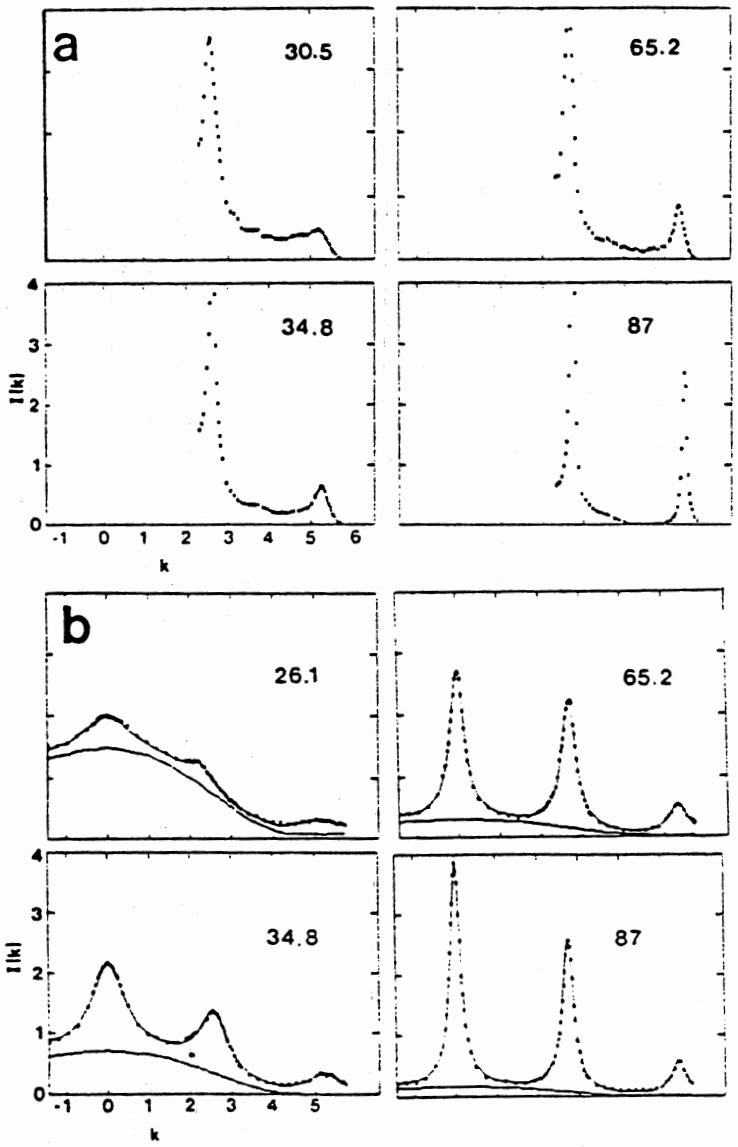

Figure 14. (b) Scattered intensity scans obtained by Richetti, et. al. (1987) for various values of E. a) $k_x = 0$ and b) $k_x = 4.2 \times 10^4$ cm^{-1}.

of applied field. All of the these experimental features have been observed in the study presented here.

Richetti, et.al. attempted to explain this observed behavior using a thermal fluctuation theory based on dipole attraction between two particles. This theoretical analysis begins by expressing the average particle separation, a, as

$$a = \frac{\int R \exp(-V(R) / k_B T) \, dR}{\int \exp(-V(R) / k_B T) \, dR} \qquad \text{II.7}$$

where R is the particle separation, k_B is Boltzmann's constants, T is temperature, and V(R) is the pairwise potential which in this case was assumed to be

$$V(R) = \frac{\langle u(t)^2 \rangle - 3 \langle (u(t) R)^2 \rangle}{|R|^3} \qquad \text{II.8}$$

where $u(t) = (-r^3 E(t) /2)$ is the time dependent dipole moment, E(t) is the time dependent electric field, r is the particle radius. Equation II.8 reduces to the form of equation I.36, after the time averages have been taken. The interaction energy for the case under investigation, the parallel applied field, reduces to

$$V(R) = (- r^6 E^2) / (16 |R|^3). \qquad \text{II.9}$$

For any V(R), such that V(R) approaches zero, the average particle separation approaches infinity. If a change of variables is made, i.e. $x = (R - 2r)/2r$, where 2r is the particle diameter, and one expands V(R) though a Taylor series about R = 2r, keeping only the

constant and first derivative terms, one may obtain upon rearrangement

$$1 - \Phi / \Phi = k_B T / V'(R)|_{2r} \qquad \text{II.10}$$

where Φ is equal to 2r/a (Richetti, et. al. uses an effective particle diameter, 2r, in their approach while Fraden and this study do not modify the particle diameter) and is taken to be a measure of particle volume fraction in a chain of particles. $V'(R)|_{2r}$ is the first derivative of the interaction evaluated at 2r. Employing the dipole energy, equation II.10 becomes

$$1 - \Phi / \Phi = (128\ k_B T) / (3\ r^3 E^2). \qquad \text{II.11}$$

Figure 15 is a plot of the experimental data in view of this theoretical explanation. The experimentally determined slope is given as 3.3×10^{-4} erg/cm^3 which must be compared with the theoretically determined slope making an experimental correction for the particle radius, i.e. the effective radius, of 2.6 erg/cm^3. Therefore, it is apparent that even though the results are qualitatively correct, there is some theoretical or experimental error involved in this study.

In an attempt to understand this discrepancy, Fraden examined his linear aggregation data in a similar manner to that describe previously. He made an initial modification to the dipole moment used by Richetti, et. al. Fraden used the dipole moment presented in equation I.35, and the interaction potential given in equation

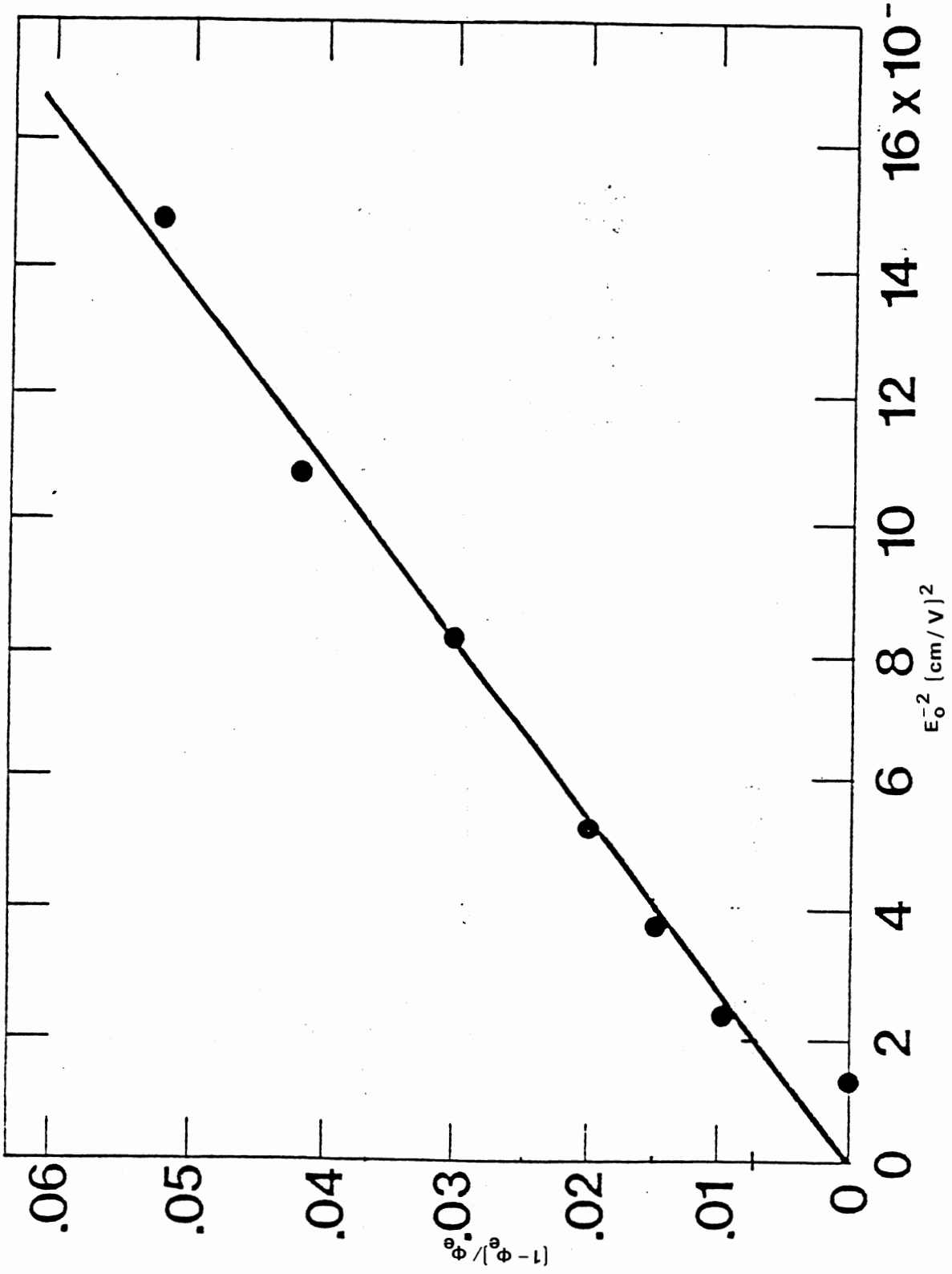

Figure 15. Experimental packing fraction ϕ_e versus applied field from Richetti, et. al. study.

I.36. Conducting the same analysis as Richetti, et. al., he obtained for equation II.11

$$1 - \Phi / \Phi = (128\ k_B\ T) / (3\ \varepsilon_\omega\ r^3\ E^2). \qquad \text{II.12}$$

This produces a reduction in the theoretical slope to of 3.3×10^{-2} erg/cm^3 which is still 2 orders of magnitude smaller than the theoretical prediction of Richetti, et. al. Upon comparison with theory, the data Fraden collected are a factor of ten larger than that predicted by theory, however, his data was collected using an image processing technique rather than a light scattering technique and there is some question as to the accuracy of the particle-particle separation measurements.

There are some significant problems in both of these methods. First in the Richetti, et. al. experiments, the particles are allowed to settle on one of the glass plates, therefore, it is unclear as to whether or not the field seen by the particles is uniform. Second in the Richetti, et. al. technique, one is obliged to question the origin of equation II.10, as well as the corrections made to the particle size. Equation II.10 is obtained by assuming as approximate form for the real potential (see figure 16). It can be shown that using this approximation one obtains the scattering function for hard spheres [Ackerson, et. al. (1989)]. Therefore, equation II.10 results from an

erroneous mathematical manipulation. Neither study takes into account the stabilization forces present in the colloidal suspensions, therefore not accounting for possibly significant effects due to these interactions.

This Microscopic - Microscopic Technique and Statistical Correction

The experimental technique used for this investigation is very similar to that used by Richetti, et. al. The sample cell was designed to allow for light scattering measurements, while the applied field is generated by a simple capacitor comprised of two parallel pieces of copper tape across which an

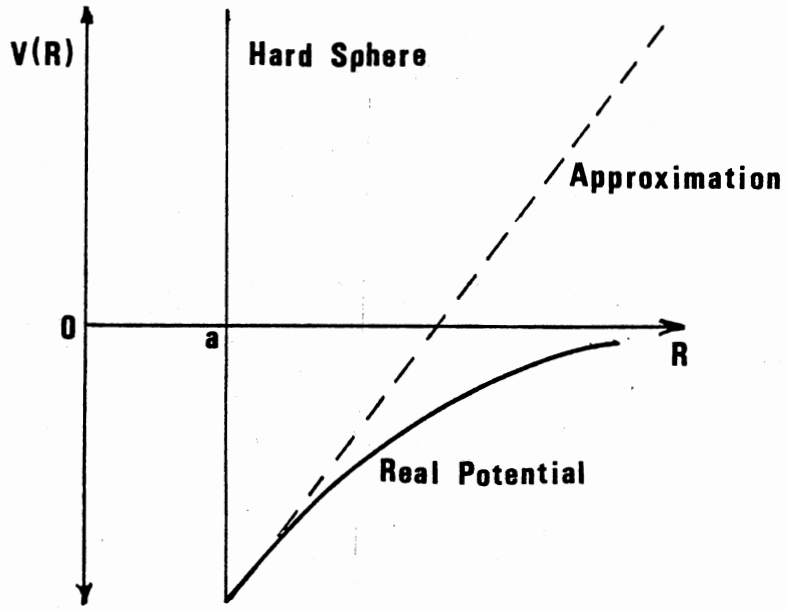

Figure 16. The potential used by Richetti, et. al.

oscillating voltage is applied. The chain formations are monitored via a light scattering technique, but here we are concerned primarily with the measured average particle separation from the diffraction pattern.

The separation of the particles is measured via a simple light scattering technique as in Richetti, et.

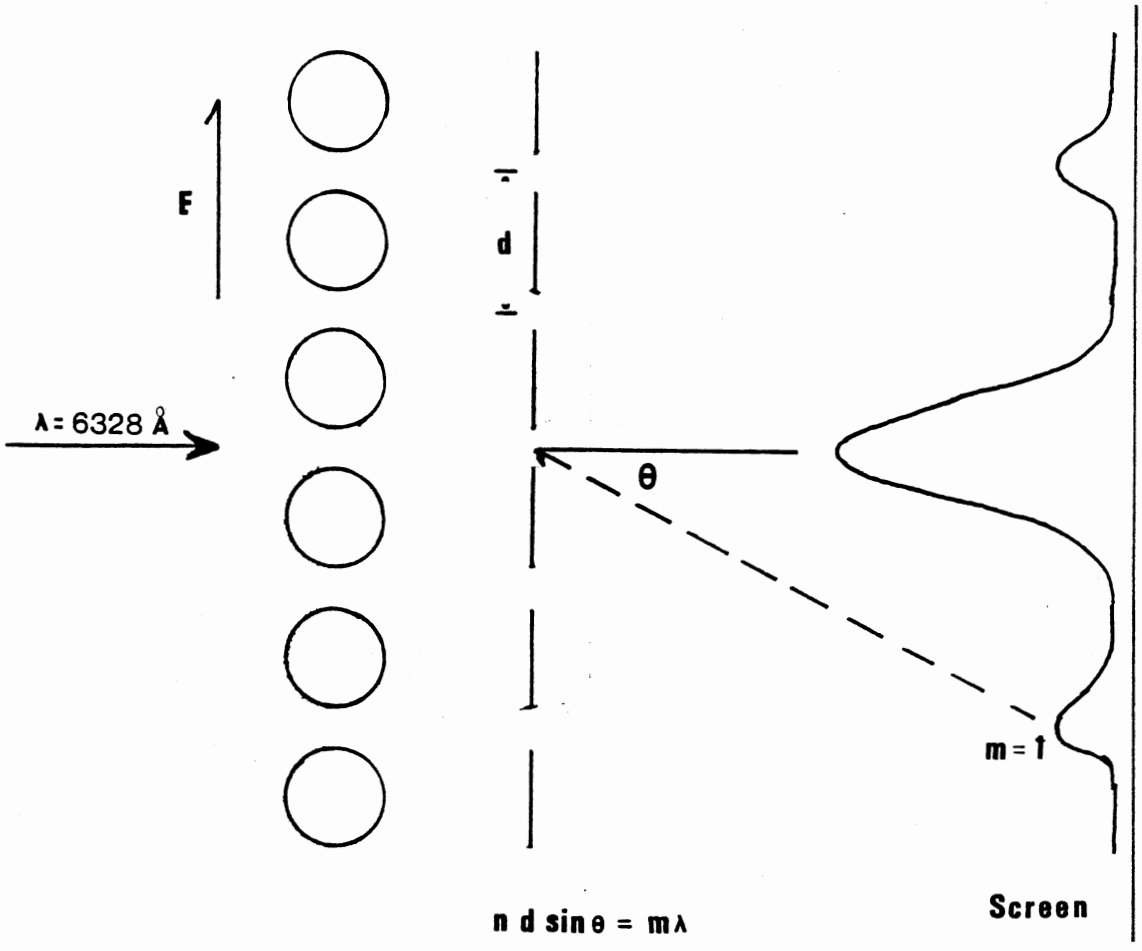

Figure 13. Schematic of the diffraction grating.

al. When the particles align in the chains, they comprise a diffraction grating (Figure 17). Using simple diffraction grating theory, one can obtain the average center to center separation of the particles from the scattering pattern, i.e.

$$d \sin\theta = m\lambda \qquad \text{II.13}$$

where d is the average center to center separation, θ is defined in Figure 17, λ the wavelength of light, and m is the order of the diffracted maxima. At this point, another aspect of diffraction grating theory should be presented. The number of lines in the grating determines the intensity and the sharpness of the diffraction pattern, e.g. if this were only a double slit experiment the intensity of the pattern is given by

$$I = Im\,(\cos\gamma)^2\,(\sin\alpha/\alpha)^2 \qquad \text{II.14}$$

with γ and α defined by

$$\gamma = (\pi d/\lambda)\sin\theta \qquad \text{II.15}$$

$$\alpha = (\pi H/\lambda)\sin\theta \qquad \text{II.16}$$

where d is the distance between centers of slits (the center to center distance of the spheres), λ is the wavelength of light and H is the slit width (the surface to surface separation of the spheres. Equation II.14 can be extended to incorporate an increase in the number of slits

$$I = Im\,(\sin N\gamma/\sin\gamma)^2\,(\sin\alpha/\alpha)^2 \qquad \text{II.17}$$

where γ and α are defined by equations II.15 and II.16 and N is the number of slits [F. A. Jenkins and H. E. White, Fundamentals of Optics, (McGraw-Hill, N.Y. 1976)]. For N = 2, equation II.17 reduces to equation II.14. Figure 18 is a plot of equation II.17 for three different values of N. Thus, intensity is dependent on

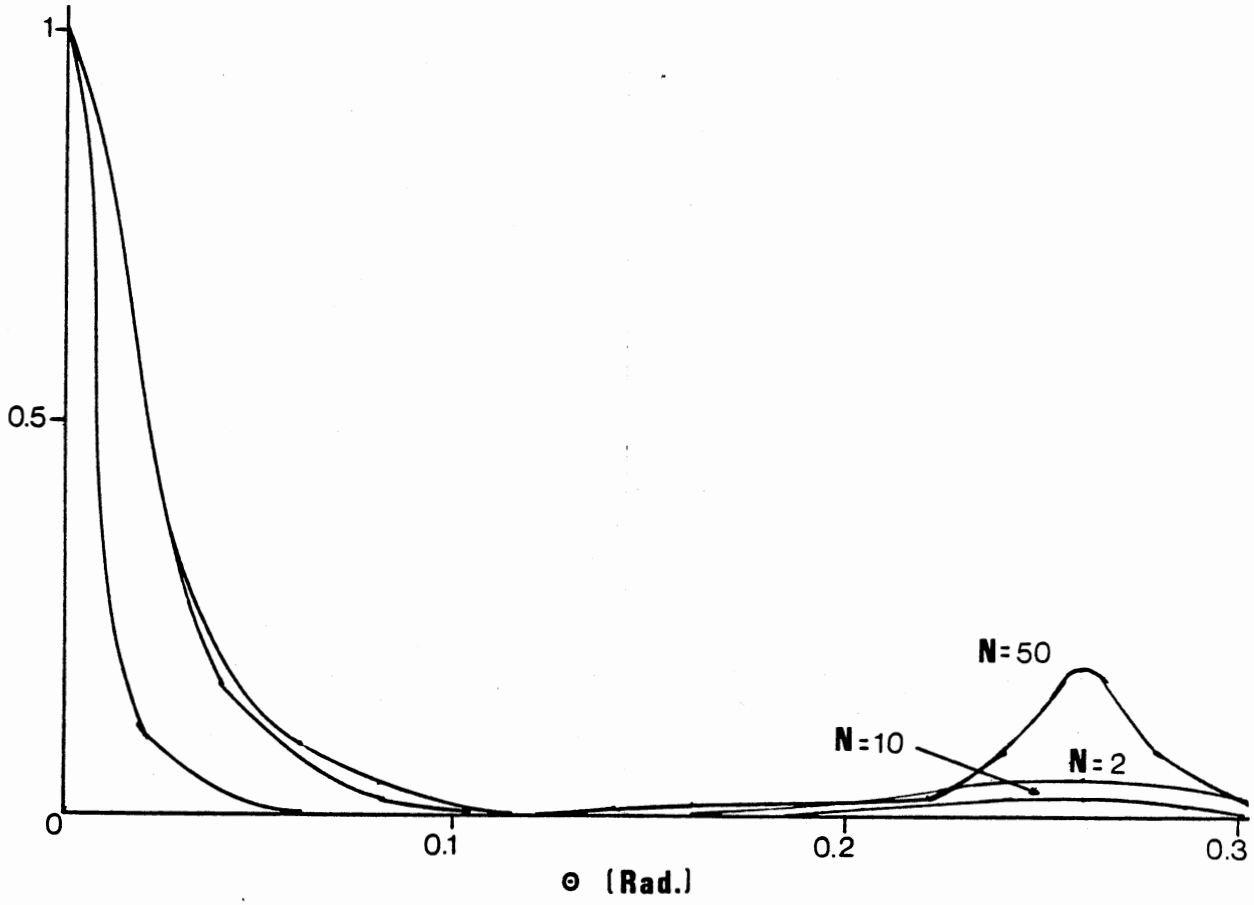

Figure 18. A plot of the intensity produced from a diffraction grating versus angle for three values of N.

the number of lines in the diffraction grating and the position of the diffracted maxima is not.

The average particle separation is dependent upon a balance between the interaction colloidal stabilization forces and the induced dipole caused by the applied field which is known. This is similar to the force balance in the M-m technique between the stabilization forces and the force due to gravity. Therefore, the m-m technique proposed here balances the forces using an applied field while monitoring the average separation of the particles, as the amplitude of the field is increased.

The Statistical Formulation

If there were no effects due to the presence of thermal motion (this would be the case at absolute zero) the m-m method would be a simple applied force versus separation measurement with the separation determined using diffraction theory. However, effects due to thermal motion are present, therefore a statistical theory must be developed similar to that used by Prieve, et. al. in the M-m study and Richetti, et. al. and Fraden in their m-m studies.

For the investigation presented here, a statistical theory based on the one-dimensional Tonks' gas is

developed. A similar Tonks' gas development has been presented previously by Munster (1969). However, the Munster form for the scattering function becomes

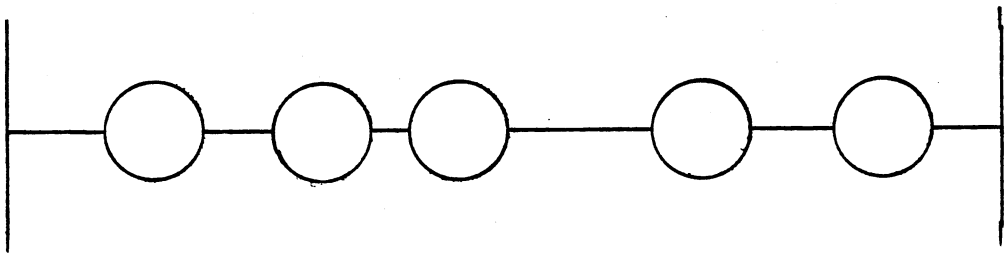

Figure 19. The configuration of particles used to develop the statistical correction.

difficult to use for the testing of various potential forms; therefore, a new development was necessary [Ackerson, et. al. 1989]. A Tonks' gas, first proposed by L. Tonks in 1936 [L. Tonks, 1936], is a gas restricted to only one-dimension. If one assumes the gas to be in equilibrium, the molecules cannot exchange places, (i.e. molecule 3 is confined to move only between molecules 2 and 4) and the molecules only experience nearest neighbor interactions; one can exactly solve the equation of state for this gas and express the result in terms of a single integral for

arbitrary potentials. Thus, the Tonks' gas is an excellent base for development of a statistical theory to explain the one dimensional phenomena.

For the Tonks' gas configuration (Figure 19) the partition function is expressed in general as [Munster, B. J. Ackerson, et. al. 1989],

$$Z = \iiint dX^3 \ldots \exp(-\beta V) \qquad \text{II.18}$$

and specifically for this configuration

$$Z = \int_0^L \exp(-\beta V(L-X_N)) \int_0^{X_N} \exp(-\beta V(X_N-X_{N-1}) \quad \ldots \int_0^{X_2} \exp(-\beta V(X_2-X_1)) \exp(-\beta V(X_1)) \; dX_1 dX_2 \ldots dX_3 \qquad \text{II.19}$$

where is $1/k_B T$, and V(X) is the pairwise interaction, and X_1 is referenced to zero and X_N to L. By applying the convolution theorem, one finds

$$\mathcal{L}Z = \int_0^{\infty} \exp(-sL)\, Z \, dL \qquad \text{II.20}$$
$$= [\, \Phi(s)]^{N+1}$$

where

$$\Phi(s) = \int_0^{\infty} \exp(-sr) \exp(-\beta V(r))\, dr. \qquad \text{II.21}$$

Now consider the scattering function for this configuration in the single scattered Born approximation

$$I(k) = (1/N) \left\langle \sum_{i,j} \exp(ik\,(r_i - r_j)) \right\rangle \qquad \text{II.22}$$

Equation II.22 can be rewritten in the form

$$I(k) = (1/N) \left[\langle N \rangle + \left\langle \sum_{i \neq j} \exp(ik\,(r_i - r_j)) \right\rangle \right.$$
$$\left. \left\langle \sum_{i \neq j} \exp(ik\,(r_i - r_j)) \right\rangle \right]$$
$$= 1 + (S/N) + (S^{*}/N) \qquad \text{II.23}$$

where

$$S = \langle \sum_{i\neq j} \exp(ik\,(r_i - r_j)) \rangle .$$

Recall, the Tonks' gas particles have fixed order, thus for $i>j$

$$r_i - r_j = (r_i - r_{i-1}) + (r_{i-1} - r_{i-2}) + \ldots + (r_{j+1} - r_j).$$

So, S becomes

$$S = (1/Z) \sum_{i\neq j}^{N} \sum_{i=1}^{N} \int_0^L \exp(-\beta V(L-X_N)) \int_0^{X_N} \exp(-\beta V(X_N - X_{N-1})) \ldots \int_0^{X_{i+1}} \exp(-\beta V(X_{i+1} - X_i)) \int_0^{X_i} \exp(ik(X_i - X_{i-1})) \exp(-\beta V(X_i - X_{i-1})) \ldots \int_0^{X_{j+1}} \exp(ik(X_{j+1} - X_j)) \exp(-\beta V(X_{j+1} - X_j)) \ldots \int_0^{X_2} \exp(-\beta V(X_2 - X_1)) \exp(-\beta V(X_1))\, dX_1 dX_2 \ldots dX_N \qquad \text{II.24}$$

As with the partition function, apply the convolution theorem to the numerator to find

$$\begin{aligned} LN &= L(ZS) \\ &= \sum_{i\neq j}^{N} \sum_{i=1}^{N} [\Phi(s)]^{N-i+1} [\Psi(s)]^{i-j} [\Phi(s)]^{j} \\ &= \sum\sum [\Phi(s)]^{N+1} [\Psi(s) / \Phi(s)]^{i-j} \\ &= [\Phi(s)]^{N+1} \sum\sum [\Psi(s) / \Phi(s)]^{i-j} \end{aligned} \qquad \text{II.25}$$

where

$$\Psi(s) = \int_0^{\infty} \exp(-(s-ik)r) \exp(-\beta V(r))\, dr.$$

Now take the Laplace inverse to regain N

$$N = \sum_{i=2}^{N} \sum_{i=1}^{i-1} (1/2\pi i) \int_{c-i\infty}^{c+i\infty} \exp(Ls) [\Phi(s)]^{N+1} [\Psi(s) / \Phi(s)]^{i-j}\, ds$$

By using the method of steepest descents and carefully choosing the contour of integration, c, such that the phase remains stationary on the real axis, the integral becomes

$$I \cong (\exp((N+1)f(c))/2) \int_{-\infty}^{\infty} \exp(-(N+1)f''(c)y^2/2)\, X(c)\, dy$$

where

$$f(c) = (Lc/(N+1)) + \ln \Phi(c)$$

and

$$X(c) = [\Psi(c) / \Phi(c)]^{i-j}$$

and c is chosen such that $f'(c) = 0$.

If one assumes, X(c) varies slowly compared to the exponential, a simple a gaussian integral results, and integrating I becomes

$$I = (\exp((N+1)f(c))\ X(c))*(2\ (N+1)f''(c))^{-1/2} \qquad \text{II.26}$$

Similarly, the partition function becomes

$$Z = (\exp((N+1)f(c))*(2\ (N+1)f''(c))^{-1/2}$$

Thus, the numerator becomes

$$N_{i,j} = Z\ [\Psi(c) / \Phi(c)]^{i-j} \qquad \text{II.27}$$

where

$$X(c) = [\Psi(c) / \Phi(c)]^{i-j}.$$

and the normalized scattering function is

$$S = N/Z = \sum_{i=2}^{N} \sum_{i=1}^{i-1} (\Psi / \Phi)^{i-j} \qquad \text{II.28}$$

The summation is a geometric series; thus, the scattering intensity is given by

$$I(k) = 1 + S/N + S^*/N \qquad \text{II.29}$$

$$= 1 + [\Psi/\Phi - \Psi] + [\Psi / \Phi - \Psi]^*$$

where

$$\Psi(c) = \int_0^{\infty} \exp(-cr)\ \exp(ikr)\ \exp(-\beta V(r))\ dr \qquad \text{II.30}$$

and

$$\Phi(c) = \lim_{c \to 0} \Psi(c) \qquad \text{II.31}$$

where c depends on the concentration, k is the scattered wave vector, and V(r) is the pair potential of

interaction between the particles. By evaluating equation II.30 numerically (Appendix A is a sample computer program used to evaluate this integral.), one can obtain the scattered intensity as a function of the scattered wave vector, equation I.29. Thus, one can develop a theoretical diffraction pattern given a form for the pair interaction potential. From this theoretical development, one can obtain, for example, the positions of the diffraction peaks which can be compared directly with the experimental data.

Therefore, the m-m technique provides a direct means of examining forces in a colloid system - not a model system - and provides a method by which one can compare several pair potentials relatively easily by using the statistical method described here. With this development, one can use either system - the electric field in water or the ferrofluid composite - thereby investigating the stabilization forces in different systems. Given this method one can now examine in much greater detail the experiment applied in this study.

CHAPTER III

EXPERIMENTAL CONFIGURATION AND EXPERIMENTAL TECHNIQUE

Introduction

The focus of this study is to investigate the stabilization forces present in a colloidal suspension. As discussed previously, the experimental technique uses an applied electric field to induce a dipole-dipole interaction between the particles while monitoring their separation via a simple light scattering technique. Thus, the method allows one to measure the particle separation as a function of the applied field. It is the purpose of this chapter to discuss the development and tests of the apparatus and procedure used in this study.

For the investigation, one must have:

1) A sample cell with a means of measuring the applied voltage, thus, allowing for the determination of the applied electric field.

2) An accurate representation of the diffraction pattern produced by applying such a field. It was necessary to have an precise measure of peak location and intensity, in addition a measure of the separation of the sample from the data collection device in

order to accurately determine the scattering angle.

3) A sample adequately characterized to allow for the accurate determination of the constants necessary to estimate the theoretical stabilization forces present in the colloidal suspension under investigation.

The basic experimental configuration used for this study is remarkably simple. While, the primary investigation discussed here is based on an applied electric field, the configuration used for this study may be modified to look at other systems. The configuration may be easily modified to study the affects of an applied magnetic field.

Basic Configuration

The configuration is comprised of the following equipment:

a) a Spectra Physics Stabilite Model 120 HeNe laser (15 mV)
b) an optical bench
c) a lens (optional)
d) a sample platform (and corresponding apparatus for field application)
e) a converted computer printer - i.e. the optical scanner
f) A/D converter
g) an Apple II plus computer

Figure 20 shows how the above equipment was utilized. The sample platform is a sample cell holder designed for the particular sample cell in use. The

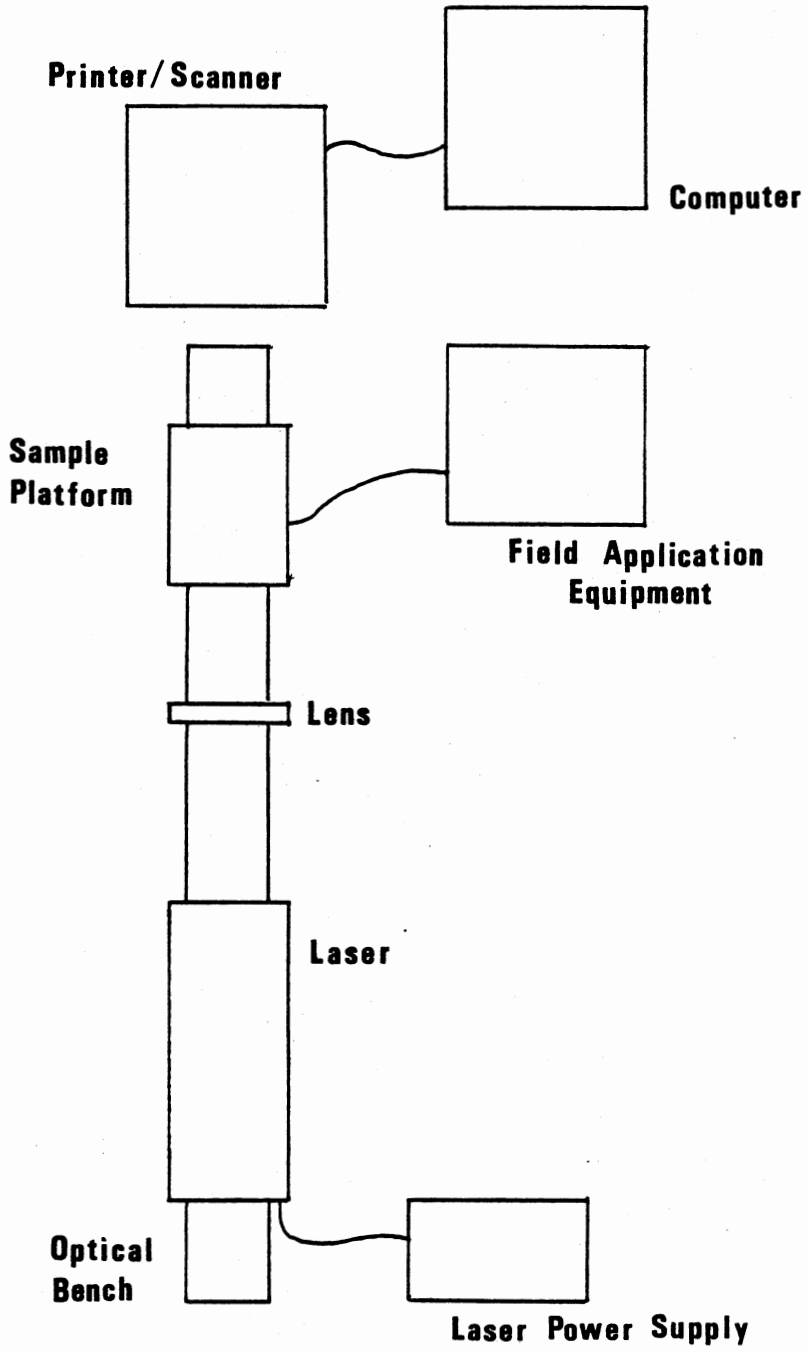

Figure 20. Schematic of the experimental configuration.

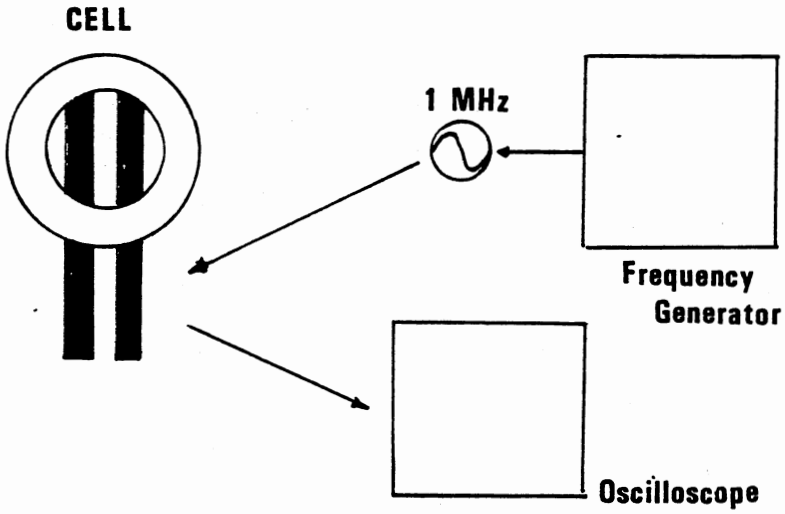

Figure 21. The electric field sample apparatus.

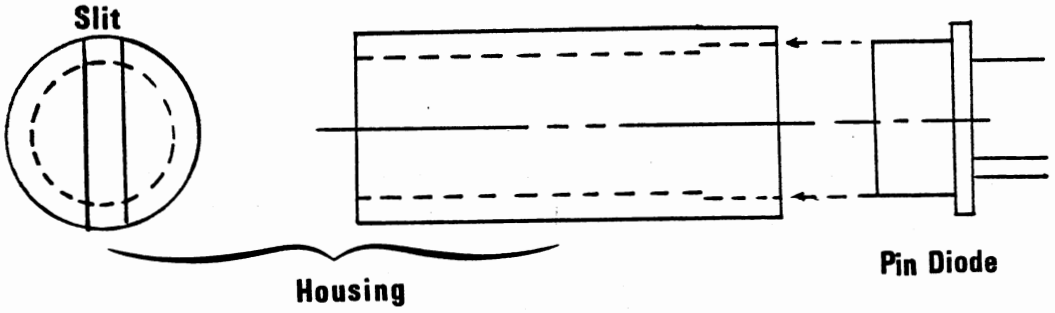

Figure 22. Schematic of pin-diode and housing.

platform is a means of carefully positioning the sample into the experimental configuration. A additional apparatus required to conduct the electric field experiments (Figure 21) are the cell designed for the electric field experiments, a Tektronix FG 501A 2 MHz Function Generator, and a Hitachi V-152 F 15 MHz oscilloscope.

The Modified Printer

A regular computer printer was modified to be used as an optical scanner. The print head was removed and replaced with an attachment that contained the 7180 photo pin diode and housing (See Figure 22). The print head position is quite accurately positioned in printing to produce good quality print and was felt to be accurate for our studies. At each print position a signal is sent from the printer to trigger an A/D converter, a reading is taken from the pin diode through the A/D converter, and stored in computer memory. There are 512 points taken across the scan.

Using this scanning system, one can accurately measure the intensity distribution of the diffraction pattern. The system was tested for both resolution and distortion, by using a simple block test. The test was conducted by placing a block (8.40 cm wide) just in front of the plane defined by the sweep of the pin

diode. The block had sharp edges and was illuminated from behind, therefore, a silhouette of know size and shape was produced. A scan was taken, recorded and a hard copy produced (Figure 23). As one can see there is a sharp decrease in the intensity as the diode reached the first edge of the block and sharp increase in the intensity as it passes the second edge. The intensity changes over a few data points as one would expect due to the bending of light around the edges of the block. The width of the block determined from the scan was 8.38 cm. It appears that the scanning system devised is an accurate and a reliable collection device.

Electric Field Cell

Several experimental cells were tried for this experiment. Two basic designs were used for this cell, however, after modifications only one cell type was used to conduct the experiments. Figure 24 shows the first cell design used to determine if such experiments were feasible. Figure 25 shows the ultimate experimental cell design.

Key elements of the cell are the capacitor plates and the transparent walls. The transparent walls allow the light scattering to be conducted in the cell. The

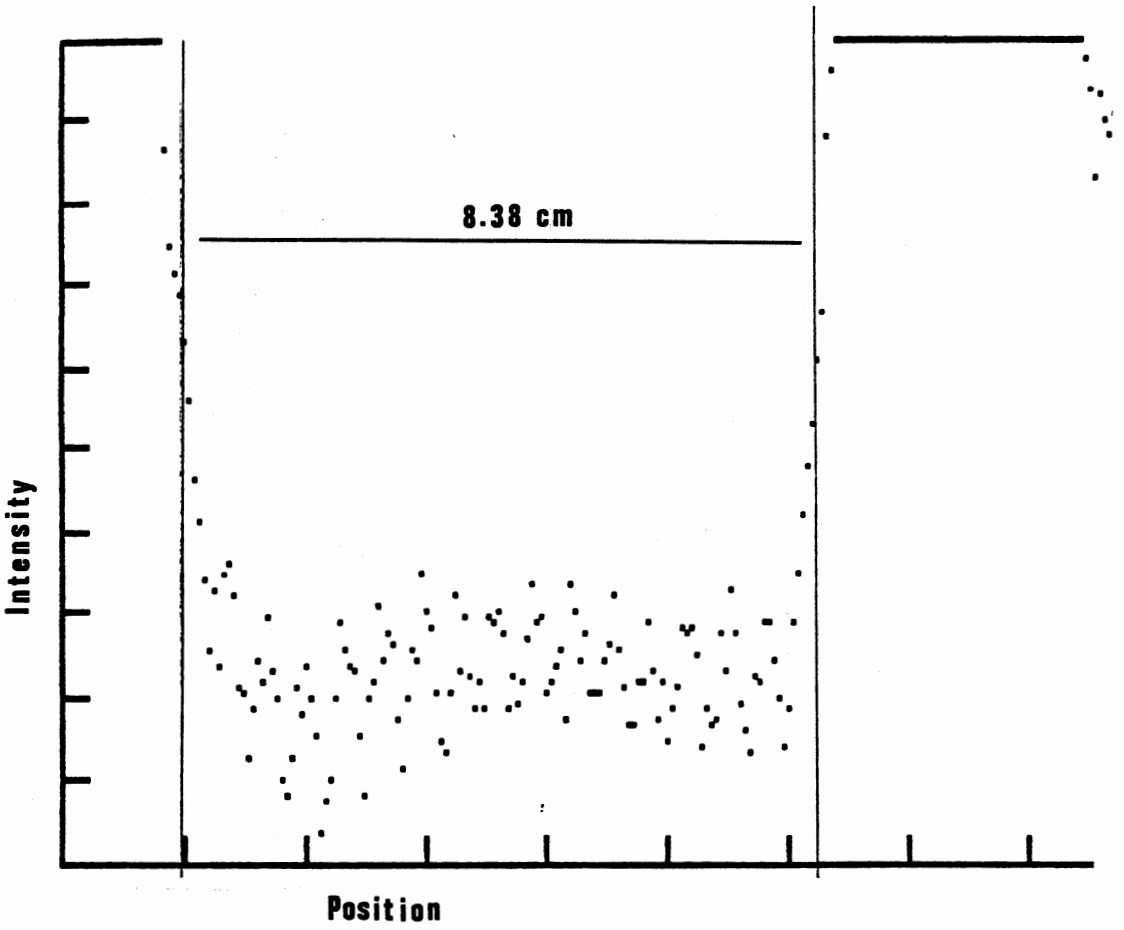

Figure 23. The scan produced from the block test.

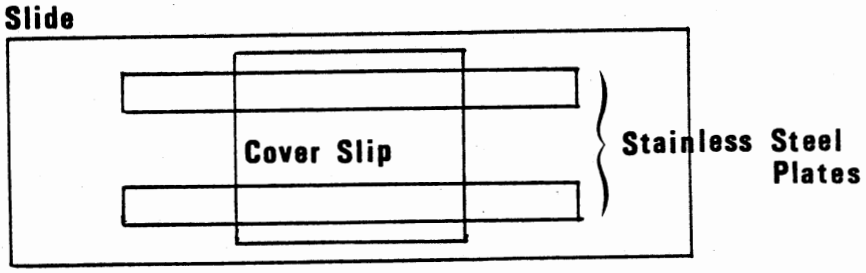

Figure 24. Schematic original electric field sample cell.

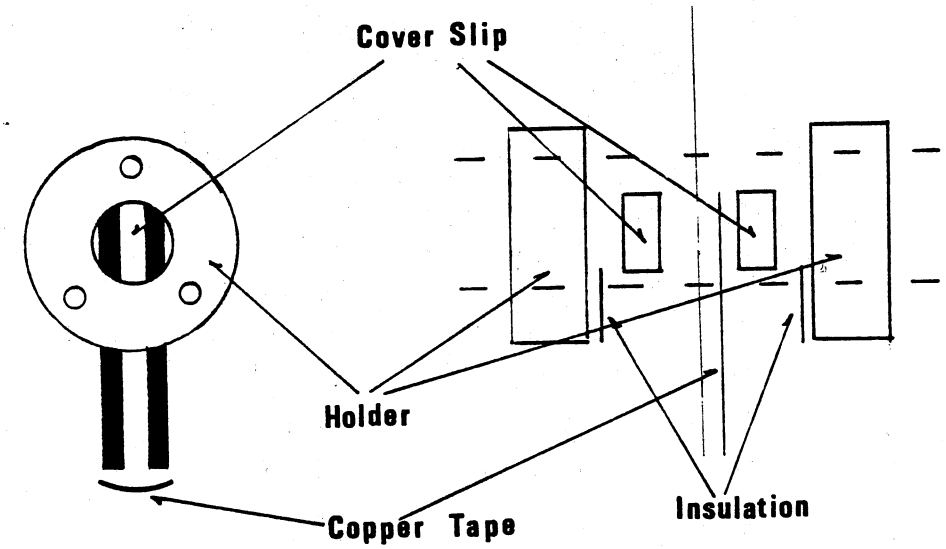

Figure 25. Schematic of the sample cell used for this study.

capacitor plates are the most important feature of the cell. Several different types of plate materials may be employed, e.g. stainless steel strips, copper strips, and copper tape. Important features of the capacitor to consider are the thickness and the separation of the plates.

The original cell used the stainless steel plates of thickness 0.05 cm and a separation of 0.02 cm. In this cell the plates were epoxied to a microscopic slide. The gap was filled with the sample and covered with a microscopic cover slip. With this cell, the original experimental tests were carried out. The major

problem encountered using this experimental design is that the sample has a tendency to evaporate or flow out of the cell, thus, making it difficult to conduct long experiments. However, the data taken using this cell clearly demonstrated that the experiment could be undertaken and qualitatively was the same as that taken with the improved cell design.

The improved cell design was needed to correct the problem faced with the original design. In this cell copper tape was used for the capacitor plates. This tape is 0.0102 cm in thickness and had a separation of 0.08 cm in most cases. (With the copper tape, several separations were tried.) The copper tape was insulated from the walls of the cell holder with either paper or for the most part tape so as not to short out the capacitor. The walls of the cell were circular microscopic cover slips 0.2 mm in thickness and 18 mm in diameter. This cell design allowed for much longer experimental runtime and was much easier to employ. Evaporation and cell leakage was reduced to minor problem and only after much longer periods of time. With the original cell design experiments usually only lasted for about one hour, and with the improved design experiment could generally last for three to four hours.

For the experiments conducted in this study, the maximum applied voltage was 30 volts peak to peak (VPP),

which corresponds to a maximum applied electric field of 26,500 V/m (265 V/cm). The minimum applied field for each run was dependent on the intensity of the observed pattern. For all of the samples studied, an intense pattern was observed at the maximum applied field. As the applied field was reduced, the intensity reduced until at some point the intensity of the first order diffracted maxima could not be detected accurately which determined the lowest applied field for that sample. For the case of the highest ionic strength used (0.01 M KNO_3), this would generally occur at an applied voltage of 21 VPP or a field of 18,600 V/m (186 V/cm).

A concern for this study is the field uniformity, since one assumes that the spheres in suspension experience a uniform applied field. In the case of this sample cell, the length of the capacitor plates is 1 cm, i.e. the plates run completely across the wall of the cell, and measurements were conducted by scattering light only from the central region of the cell. Thus, one would expect no fringe effects from the ends of the plates. In addition, the capacity of the region between the plates is higher than the region beyond the edges of the plates, implying that the fringe effects may be neglected.

Samples

The samples were comprised of polyvinyltoluene (PVT) particles suspended in water. The physical characteristics of the particles used in this investigation are given in Table 3. The PVT particle was originally chosen such that one could conduct magnetic field experiments with the same particle used for the electric field experiments, these particles do not to dissolve in some of the ferrofluids used for the ferrofluid composite system while our polystyrene particles do dissolve. The original qualitative measurements were done by using the PVT particles direct from the manufacturer, and qualitative measurements were also made on 2.0 um polystyrene particles in order to insure that the PVT particles did not differ significantly from the results obtained by Richetti, et. al. and Fraden. Later studies were conducted by using a variable ionic strength and well characterizable particles. Potassium nitrate (KNO_3), a 1:1 electrolyte, was chosen for this study because it is the same used by Isrealachivili, et. al. in his m-m.

The 1:1 electrolyte notation is a means of representing the valency of the ions in solution. For example, in the case of KNO_3 or NaCl, the z_+ value for the positive cation in solution is equal to one as well

TABLE 3

THE PHYSICAL INFORMATION ABOUT THE PARTICLES USED IN THIS STUDY

	Lot. No. 6402	Lot. No. 10-55-7
Mean Diameter	2.02	2.12
Std. Dev.	.0135	.0466
Per Cent solids as provided by the Manufacturer	0.7%	8.2%
Density (g/ml) (@ 20 degrees C)	1.027	1.027
Refractive Index (@ 590 nm)	1.5808	1.5973
Area per charge group (A^2/charge group)	544	420

TABLE 4

SUMMARY OF THE ZETA POTENTIAL MEASUREMENTS PROVIDED BY THE MANUFACTURER. THESE MEASUREMENTS WERE TAKEN USING A PEN KEM SYSTEM 3000 INSTRUMENT.

Solution	Measured Zeta Potential (mV)
0.1 M NaCl	-16.4
0.01 M NaCl	-38.9
0.005 M KNO_3	-65.6
	-54.5
0.001 M KNO_3	-68.8
0.0005 M KNO_3	-45.7
0.00005 M KNO_3	-11.5 *
	-18.8 *

* Measurements at this ionic strength seem to be difficult. Two other measurements at this ionic strength were provided one at -7.91 mV and a second at-69.9 mV.

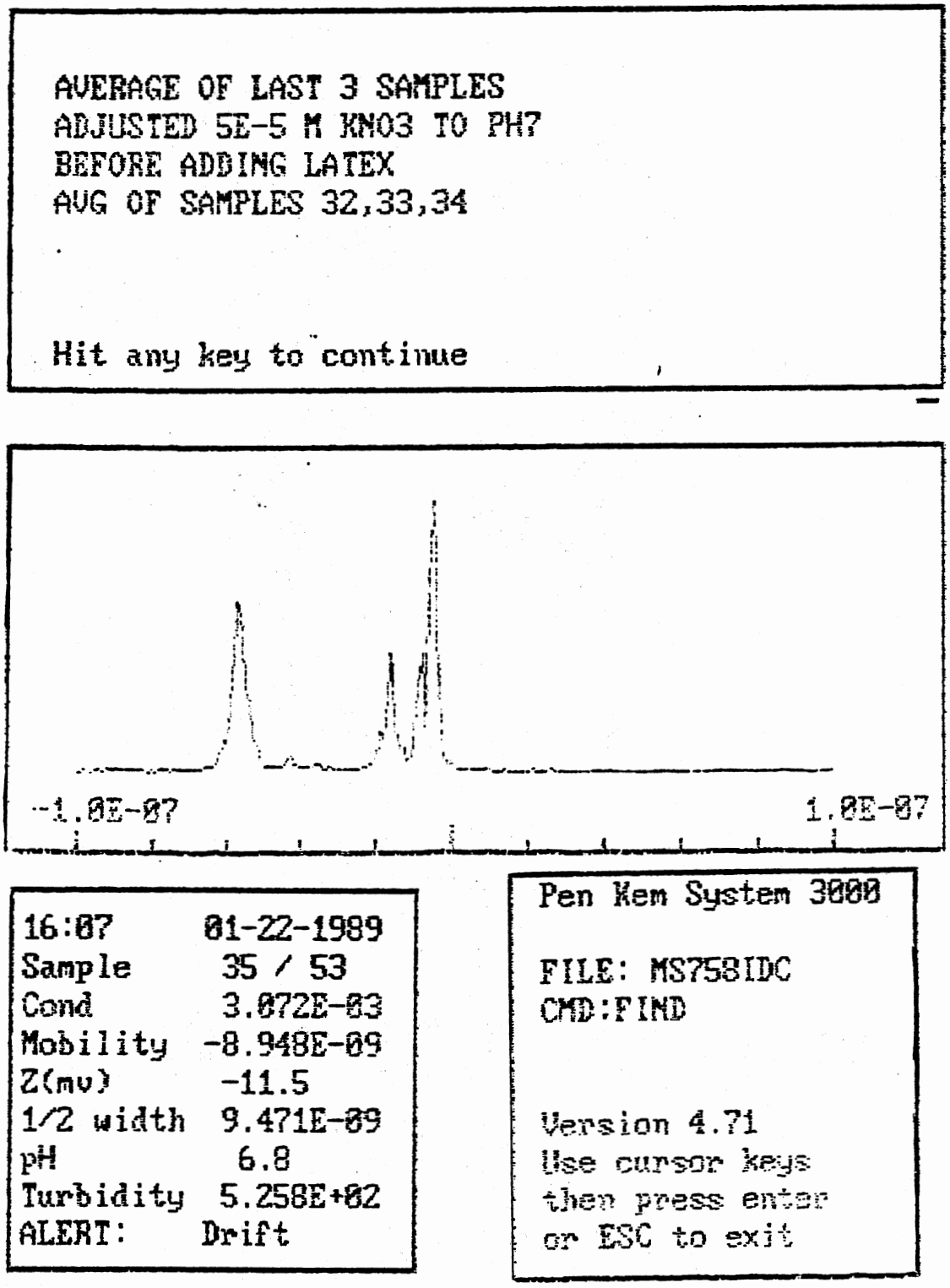

Figure 26. Dielectrophoretic measurement of the zeta potential of the PVT particles in 0.00005 M KNO_3.

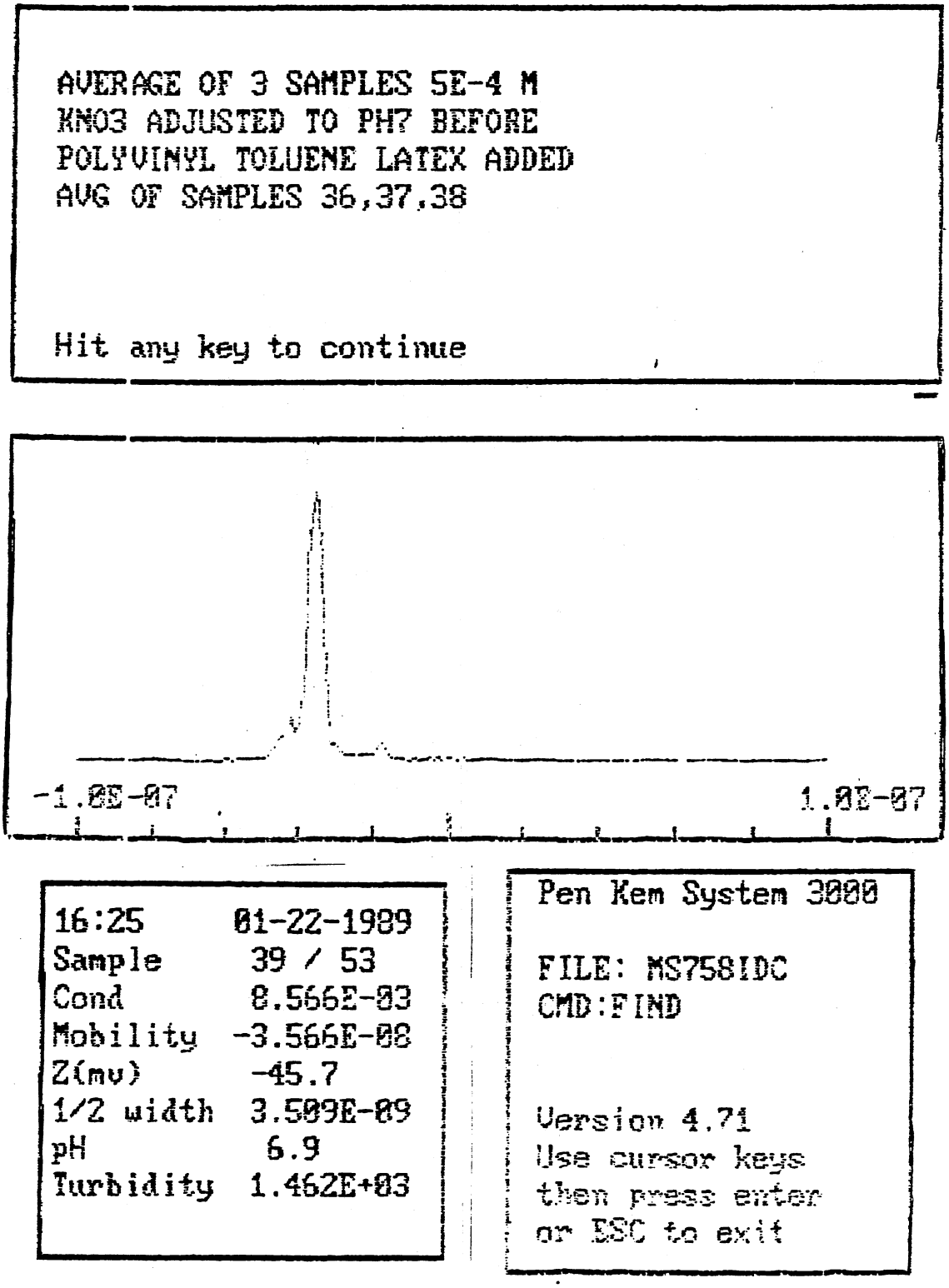

Figure 27. Dielectrophoretic measurement of the zeta potential of the PVT particles in 0.0005 M KNO_3.

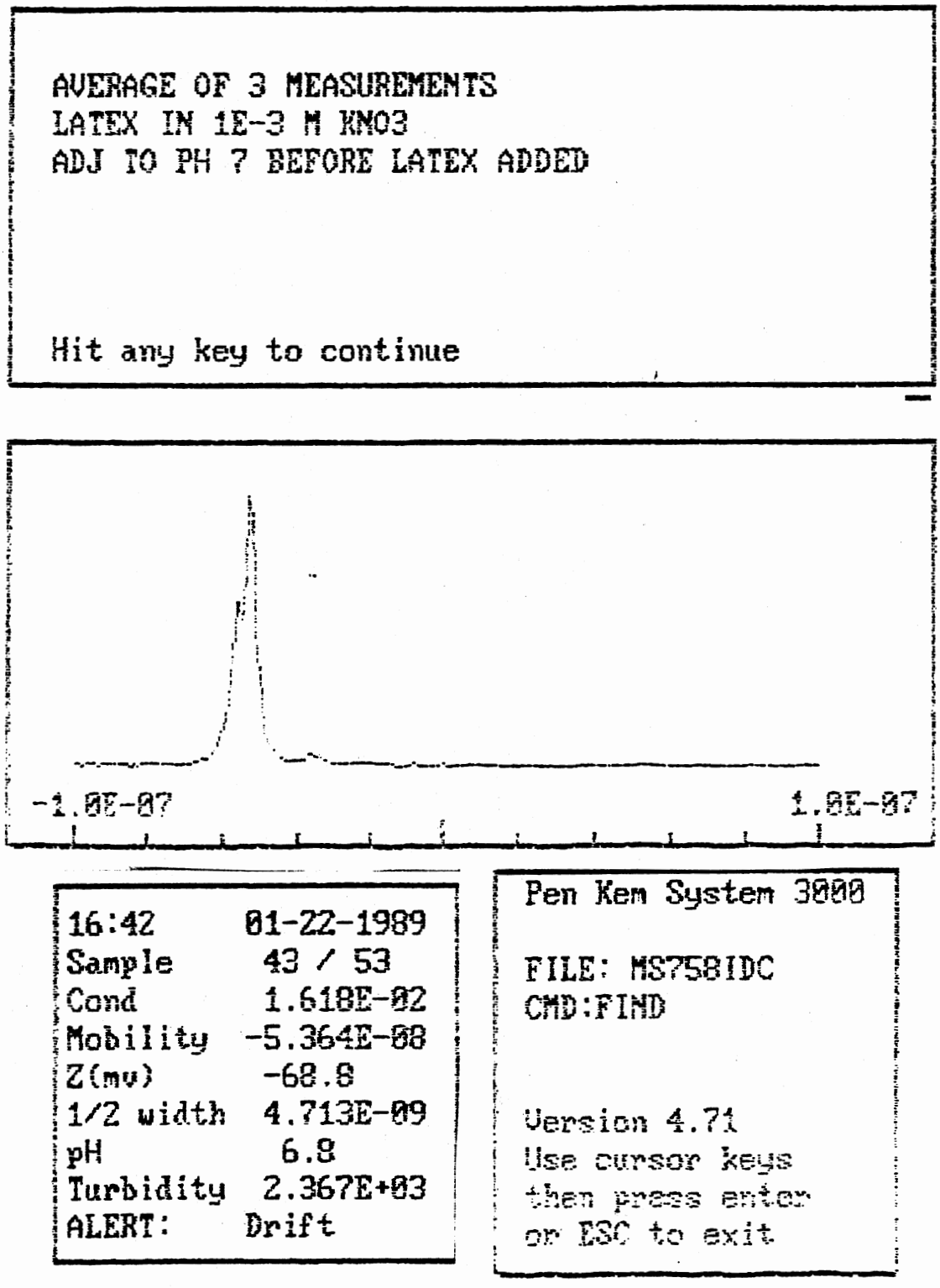

Figure 28. Dielectrophoretic measurement of the zeta potential of the PVT particles in 0.001 M KNO_3.

AVERAGE OF 3 SAMPLES, 5E-3M
PH 7 ADJUSTED BEFORE LATEX
ADDED

Hit any key to continue

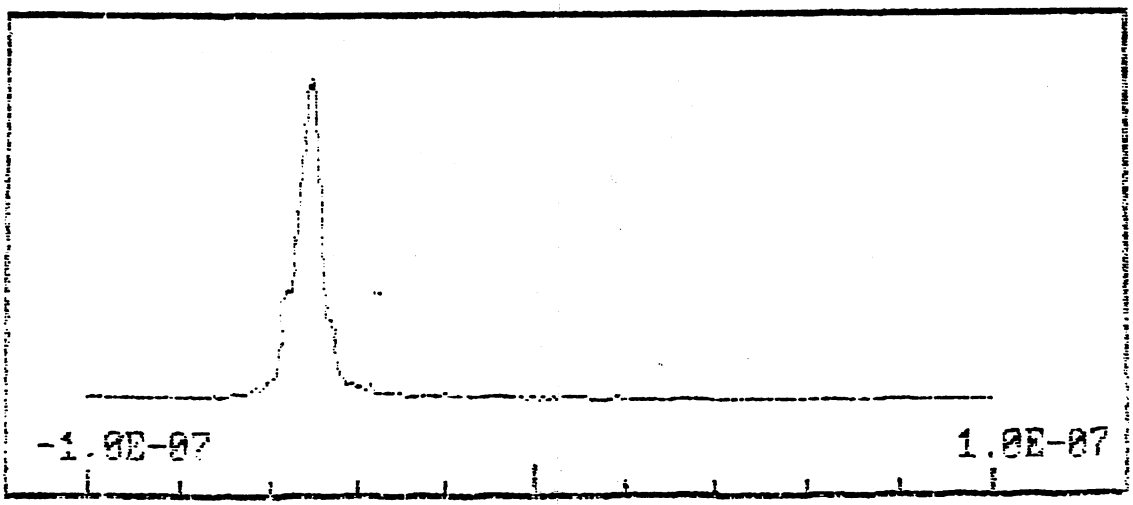

17:03	01-22-1989
Sample	47 / 52
Cond	6.958E-02
Mobility	-5.113E-08
Z(mv)	-65.6
1/2 width	5.018E-09
pH	6.7
Turbidity	4.328E+03

Pen Kem System 3000

FILE: MS758IDC
CMD:FIND

Version 4.71
Use cursor keys
then press enter
or ESC to exit

Figure 29. Dielectrophoretic measurement of the zeta potential of the PVT particles in 0.005 M KNO_3.

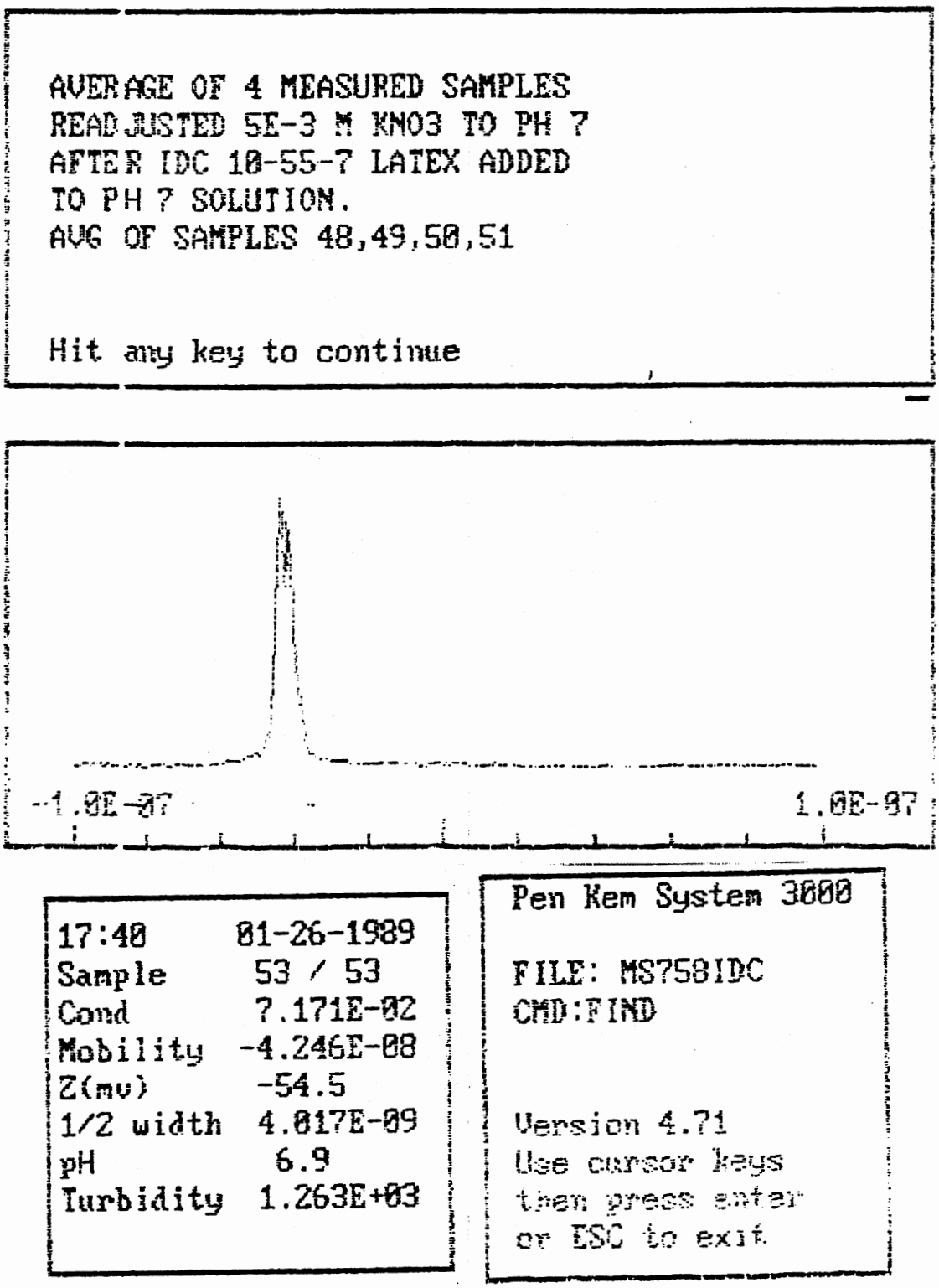

Figure 30. Dielectrophoretic measurement of the zeta potential of the PVT particles in 0.005 M KNO_3.

AVERAGE OF FIVE RUNS
IDC LATEX 10-55-7
LATEX IN 0.01M NACL
ONE DROP LATEX IN 100ML

Hit any key to continue

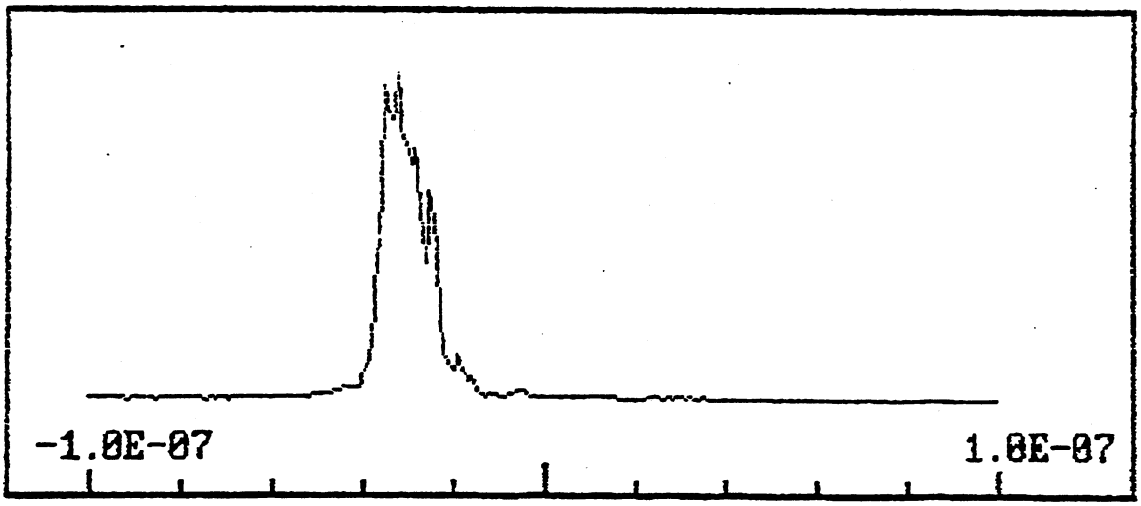

Date	10-30-1988
Sample	6 / 12
Cond	1.182E-01
Mobility	-3.034E-08
Z(mv)	-38.9
1/2 width	7.832E-09
pH	
Turbidity	1.767E+03

Pen Kem System 3000

FILE: LJIDC1008
CMD:FIND

Use cursor keys
then press enter
or ESC to exit

Figure 31. Dielectrophoretic measurement of the zeta potential of the PVT particles in 0.01 M NaCl.

AVERAGE OF FIVE RUNS
IDC LATEX 10-55-7
LATEX IN 0.1M NACL
ONE DROP LATEX IN 100ML

Hit any key to continue

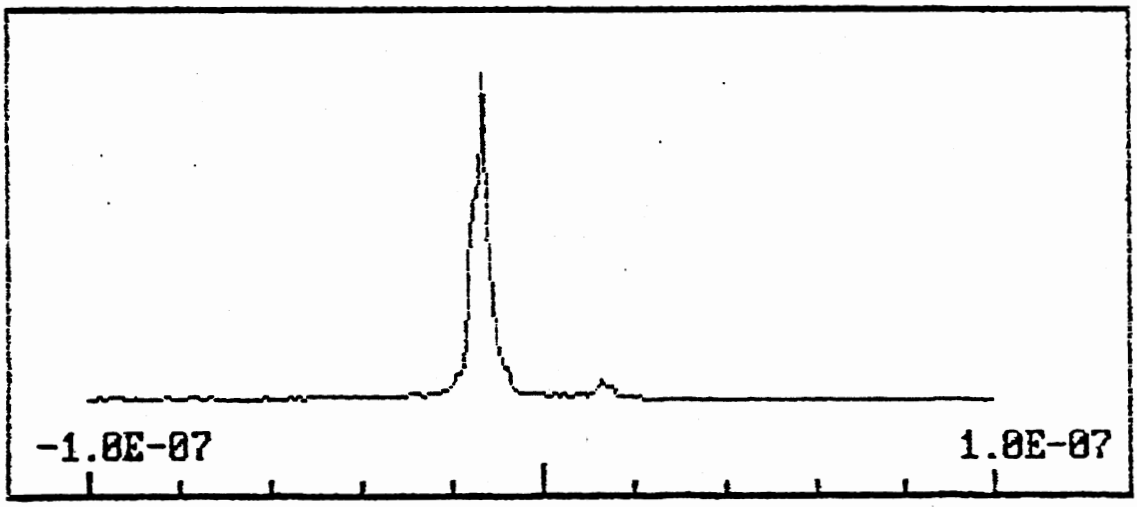

Date	10-30-1988
Sample	12 / 12
Cond	1.071E+00
Mobility	-1.277E-08
Z(mv)	-16.4
1/2 width	3.667E-09
pH	
Turbidity	1.193E+04

Pen Kem System 3000

FILE: LJIDC1088
CMD:FIND

Use cursor keys
then press enter
or ESC to exit

Figure 32. Dielectrophoretic measurement of the zeta potential of the PVT particles in 0.1 M NaCl.

as the z_- value for the negative anion. Thus, one can represent Na_2NO_2 as a 2:1 electrolyte.

Additional characterizing information was obtained from the manufacturer regarding the 2.12 um PVT particles. The manufacturer (Interfacial Dynamics Corporation) provided several different electrophetic mobility measurements in various ionic solutions for this particular particle. Figures 26 - 32 are reproductions of the actual electrophoretic measurements made on the lot of particles used for this study. The measurements made in the KNO_3 solutions were made at similar ionic strengths to those used in this study. Table 4 provides a summary of the measured zeta potentials of the particles from Figures 26 - 32 and additional measurements provided by the manufacturer.

The values reported by the manufacturer are zeta potentials. There has been some discussion about whether or not a zeta potential is a true surface potential or even whether the zeta potential has been properly defined in the various experimental determinations of the potential [Private Communication]. The general consensus is that the zeta potential is the equivalent to the Stern potential, i.e. the potential at the distance of closet approach of an ion to the surface of the particle [D.H. Everett,

1988].

With properly characterizable particles, one can select particular variables to modify and control during the course of study. One can choose to vary experimental parameters such as the charge on the particle, the screening length (by controlling the ionic strength), the pH of the solution, the particle size, the shape, and the surface chemistry. The study presented here is a function of the ionic strength. By changing the ionic strength of the solution one can modify the Debye-length, how the particle are screened from one another in solution. Thus, this investigation is concentrated on the effects resulting from changes in the double-layer repulsion properties of the sample.

In order to accurately determine the ionic strength, the samples supplied from the manufacturer were deionized. The samples were deionized using a BIO-RAD ion exchange resin (An analytical grade mixed bed resin AG501-x8(D); 20-50 mesh; fully regenerated; Control number 27180) with the ratio of resin to sample in solution was approximately one to two. Samples were deionized by standing for a week in the resin with periodic tumbling. After this step, the samples were prepared by mixing 10 ul of the particles into 10 ul of a selected ionic solution. The solution and the particles were mixed and the sample cell was sealed.

Prior to loading the sample for the first time, the cell was cleaned by rinsing the cell with a cleaning solution, followed by rinsing the with deionized water, then rinsing the cell three to five times with the Barnsted water (Barnsted water is purified by passing the water through a series of ion exchange filters producing highly deionized water.) and allowing the cell to dry. After the first run was completed, the sample was changed. Prior to loading the second sample, the cell was rinsed four to six times with the Barnsted water and allowed to dry. The experiments were conducted by increasing the ionic strength to reduce the effects of contamination from the previous samples.

An ionic solution was prepared by dissolving 1.395 grams of potassium nitrate [KNO_3] into 100 ml of Barnsted water. Four other solutions were prepared by dilution.

A comparative solution was made to mimic the experimental samples. It would have been very costly to use an exact solution due the volumes required in order to a make conductivity measurement. For a given sample, the conductivity was measured on a solution composed of 5 ml Barnsted water (the same water used to make the ionic solutions, conductivity of approximately 1 umho) and 5 ml of the KNO_3 solution. (Recall that the sample solutions used in the actual experiments were a mixture

10 ul of the deionized particles and 10 ul KNO_3 solution.) The conductivity cell was rinsed between each measurement with deionized water until the lowest conductivity was recorded. The sample was put into the cell several times, until the conductivity measurements read the same value between measurements. This process was repeated for each sample. The value measured was an experimental conductivity, G, where G is defined as

$$G = K\zeta \qquad \text{III.1}$$

where K is the conductivity cell constant (for the cell used K = 0.68), and ζ is the "specific conductance". Table 5 gives the measured values for G at 23 degrees C. These values were corrected to 25 degrees C. The G values were also corrected for the water background such that the G value obtained is due strictly to the KNO_3 ions. From the G value the specific conductance was obtained.

From the specific conductance, the ionic concentration was determined. (See Table 5) This concentration value was used to determine the Debye screening length for a 1:1 electrolyte. KNO_3 is a 1:1 electrolyte. This experimental Debye lengths using the method outlined in by Isrealachvili [Isrealachvili (1984)]. The Debye length is given by

TABLE 5

THE RAW AND REDUCED DATA OBTAINED
FROM CONDUCTIVITY MEASUREMENTS

	Concentration of the KNO_3 solution (M)				
	0.0000138 umho	0.000138 umho	0.00138 umho	0.0138 mmho	0.138 mmho
1.	3.1	8.5	65	.60	5.0
2.	3.15	9.0	67.5	.60	5.25
3.	3.2	9.1	67.5	.60	5.25
4.	3.2	9.25	67.5	.60	5.25
5.	3.2	9.25	67.5		5.25
6.	3.2	9.25			
G(23 C)	3.2	9.25	67.5	.60	5.25
G(25 C)	3.3	9.62	70.2	.624	5.46
ζ	umho/cm	umho/cm	umho/cm	mmho/cm	mmho/cm
	3.4	12.6	103.2	.918	8.03
Conc.	M (x105)	M (x105)	M (x104)	M (x103)	M (x102)
	2.4	8.7	7.2	6.6	6.3
$K(m^{-1})$	(x10-7)	(x10-7)	(x10-7)	(x10-8)	(x10-8)
	1.6	3.1	8.8	2.7	8.2

$$1/K = \left[(\varepsilon k_B T) / (4\pi \Sigma_i n_i e_i^2) \right]^{1/2} \qquad \text{III.2}$$

$$= 0.3045/\sqrt{c} \quad \text{nm}$$

This result was verified by Hiemenz [Hiemenz, 1986]. These values were used when evaluating the experimental data.

The Basic Experimental Procedure for Data Collection

The experimental procedure is as follows:

1. A sample is chosen and the sample cell is filled.

2. The sample cell is placed into the experimental apparatus given on page 67.

3. The maximum field is applied to allow for a strong diffraction pattern to form, in most cases a strong pattern form in less than 15 minutes, however, the sample was generally left for 30 minutes prior to taking data.

4. A given run of data is signal averaged over ten individual scans, to reduce noise and stored on disk.

5. The field is reduced and a another run is taken and saved. This process is repeated until the diffraction cannot be measured.

6. Once a complete series is taken the data are removed from the disk and printed. While taking the data from the disk, the particle form factor is divided out of the run. The particle form factor was measured prior to applying the maximum field. The computer programs used in this study are given in Appendix A.

7. The separation of the first diffracted peak is measured in centimeters from the zeroth order peak. This measurement

determines the scattering angle which is related to the average separation of the particles.

The raw data obtained in these studies are the scattering angle and the value of the applied field. While the technique is simple in concept, we must carefully examine this method for the following potential problems:

(1) Is the decreasing electric field method of the data collection correct? Are there hysteresis effects?

(2) It is apparent that there are time dependent effects; is the system at an equilibrium? How significant are these effects?

(3) Are there particle concentration effects present?

(4) How are the data corrected for the cell walls? These questions were examined in careful detail.

Corrections to the Raw Data

The raw data collected are the applied voltage and a representation of the intensity distribution of the diffraction pattern as it would appear on a screen. However, the diffraction pattern is a result of the scattering of the individual particles in solution, the ordered structure of the particles, and the cell walls. Thus, certain corrections must be made to the raw data

in order to accurately determine the "average" center to center separation of the particles.

Consider a single finite sized scatter (the geometry is given in Figure 33), in this case the scatter is a sphere. It can be assumed that this scatter is a collection of induced point dipoles which scatter light to a detector, such that there is no significant internal multiple scattering. This is general assumption of the Rayleigh-Gans-Debye scattering

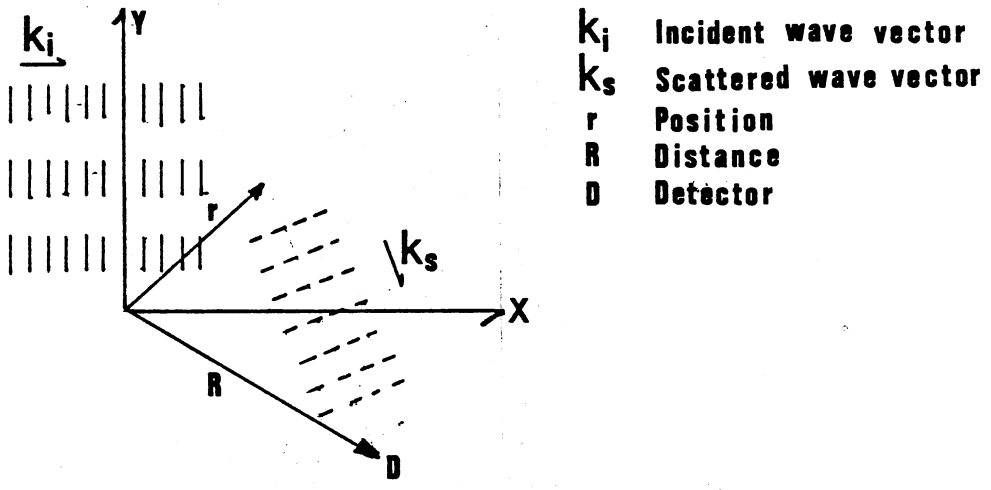

Figure 33. Scattering by a point object.

theory. The validity of this theory depends on the probability of internal scattering is small, i.e.

$$2ka(m-1) \ll 1 \qquad \text{III.3}$$

where 2k(m-1) is the inverse of a length estimating the distance between scattering events of a single photon and a is the particle size.

The total scattered field is given by summing the individual fields produced by collection of dipoles in the particles [Kerker (1969)]

$$E_T = \int_V E_s \, dV$$
$$= \int_V A \exp(i(\vec{k}\cdot\vec{r} - wt)) \, d^3r \qquad \text{III.4}$$

where A is the amplitude of the field.

Solving equation III.4 for the case of a sphere, on obtains

$$E_T = A \exp(-iwt) \int_0^s r^2 \, dr \int_0^{2\pi} d\Phi \int_{-1}^{1} \exp(ikr\cos\alpha) \, d\cos\alpha$$
$$= A \exp(-iwt) \, (3/u^3) \, (\sin u - u \cos u) \, a^3 \qquad \text{III.5}$$

where u = ka. Therefore, the scattered intensity for a single sphere may be written as

$$I \propto |E_T|^2$$
$$= A^2 a^6 [(3/u^3) (\sin u - u \cos u)]^2$$
$$= A^2 a^6 P(ka) \qquad \text{III.6}$$

where P(ka) is known as the particle form factor. This factor is dependent on the shape of the particle, thus, for a different shape one would expect a different functional dependence on u. For large particles - Mie theory is necessary but provides the same qualitative structure of P(k).

Now consider a random dispersion of identical spheres of size a. In equation III.5, the particle in

question is sitting at the origin, thus one must modify this by adding a phase factor to account for positions other than the origin, rewriting equation III.5

$$E = A\, a^{\Theta}\, (P(ka))^{1/2} \exp(i(\vec{k}\cdot\vec{r} - wt)). \qquad \text{III.7}$$

The total scattering from a random dispersion of N particles is simply a sum over a positions, i.e.

$$E_T = A\, a_{\Theta}\, (P(ka))^{1/2} \exp(-iwt) \sum_{i=1}^{N} \exp(i\vec{k}\cdot\vec{r}) \qquad \text{III.8}$$

By taking a positional average, one may calculate the scattered intensity of the dispersion,

$$I(k) \propto |A|^2\, a^6\, P(ka) \left\langle \sum_{i,j}^{N} \exp(i\vec{k}\cdot\vec{r}_i)\, \exp(-i\vec{k}\cdot\vec{r}_j) \right\rangle \qquad \text{III.9}$$

There are N identical terms in which i = j and $\langle 1 \rangle = 1$, thus

$$I(k) \propto N\, |A|^2\, a^6\, P(ka) * \left(1 + (1/N)\left\langle \sum_{i\neq j}^{N} \exp(i\vec{k}\cdot(\vec{r}_i - \vec{r}_j)) \right\rangle\right) \qquad \text{III.10}$$

Recall, the dispersion is comprised of identical particles, therefore the remaining average may be written as

$$\left\langle \sum \exp(ik\cdot(\vec{r}_i - \vec{r}_j)) \right\rangle = N\,(N-1)\, \langle \exp(i\vec{k}\cdot(\vec{r}_i - \vec{r}_j)) \rangle$$

For independent particles, the averages over particles i and j may be preformed independently or

$$\langle \exp(i\vec{k}\cdot(\vec{r}_i - \vec{r}_j)) \rangle = \langle \exp(ikr_i) \rangle \langle \exp(ikr_j) \rangle$$

$$= 0 \text{ for } k \neq 0$$

The averages are zero because $\exp(ikr_i)$ takes on all values on the unit circle uniformly as r varies over its full range. Therefore, equation III.10 becomes

$$I(k) \propto N\, |A|^2\, a^6\, P(ka) \qquad \text{III.11}$$

Thus in a random dispersion, the measured intensity is just the sum of the individual contributions of all the spheres without the interparticle interference. Experimentally, it means that one can measure P(ka) from a dispersion containing many of spheres. In this study, P(ka) was measured by recording the diffraction pattern of the colloidal dispersion prior to applying the electric field and stored for later use.

Now consider a dispersion of particles that interact with one another, such is the case for the dispersion used in this study when the field was applied to the sample. One can obtain information about the structure induced by the particle interaction from the scattering pattern produced. This structural information in the dispersion can be described by the pair correlation function $g(r_1,r_2)$. This function is defined as

$$g(r_1,r_2) = P(r_1,r_2) / n^2 \qquad \text{III.12}$$

where n is the particle number density, and the function $P(r_1,r_2)\ d^3r_1\ d^3r_2$ is the probability that particle 1 is at position r_1, while a second particle is at r_2. Explicitly the function P(r1,r2) is defined as

$$P(r_1,r_2)\ d^3r_1\ d^3r_2 = \frac{N(N-1)\ d^3r_1\ d^3r_2 \int\cdots\int \exp(-\mathbf{V}/k_BT)\ d^3r_3 \ldots d^3r_N}{\int\cdots\int \exp(-\mathbf{V}/k_BT)\ d^3r_1 \ldots\ d^3r_N}$$

where $\mathbf{V}$ is the interaction potential of the total system which is dependent on the coordinates r_1. The

average scattered intensity

$$\langle I(k)\rangle \propto \langle |E_T|^2 \rangle$$

$$= c\,P(k) \left\langle (1/N)\sum_{i}^{N}\sum_{j}^{N} \exp(ik(r_i - r_j)) \right\rangle \qquad \text{III.13}$$

where c is a constant dependent on experimental parameters, and P(k) is the particle form factor. Since the particles are identical, one can argue that the average can be written as

$$\langle \exp(i\mathbf{k}\cdot(\vec{r}_1 - \vec{r}_j)) \rangle$$

$$= \iint \frac{\exp(i\vec{k}\cdot(\vec{r}_1 - \vec{r}_2)) \int \cdots \int \exp(-V/k_B T)\, d^3r_1 \ldots d^3r_N}{\int \cdots \int \exp(-V/k_B T)\, d^3r_1 \ldots d^3r_N}$$

Rewriting in terms of $P(r_1, r_2)$

$$\langle \Sigma\Sigma \exp(i\vec{k}\cdot(\vec{r}_1 - \vec{r}_j)) \rangle =$$

$$N + \iint \exp(i\vec{k}\cdot(\vec{r}_1 - \vec{r}_2) P(r_1, r_2)\, d^3r_1\, d^3r_2 \qquad \text{III.14}$$

In a system with translational symmetry (e.g. $P(r_1, r_2) = P(r_1 - r_2)$) and using relative coordinates, one can now write the average in terms of the pair correlation function g(r),

$$\langle \Sigma\Sigma \exp(i\vec{k}\cdot(\vec{r}_1 - \vec{r}_j)) \rangle = N + Nn \int g(r) \exp(i\vec{k}\cdot\vec{r})\, d^3r \qquad \text{III.15}$$

The integral

$$\int \exp(i\vec{k}\cdot\vec{r})\, d^3r = \delta(k)$$

only contributes at $k = 0$, therefore one can define a new function S(k), known as the static structure factor, as

$$S(k) = (1/N) \Sigma \langle \exp(i\vec{k}\cdot(\vec{r}i - \vec{r}j)) \rangle \qquad \text{III.16}$$

Finally, one can write for the scattered intensity

$$I(k) = c\,P(k)\,S(k) \qquad \text{III.17}$$

This result is important for the study presented

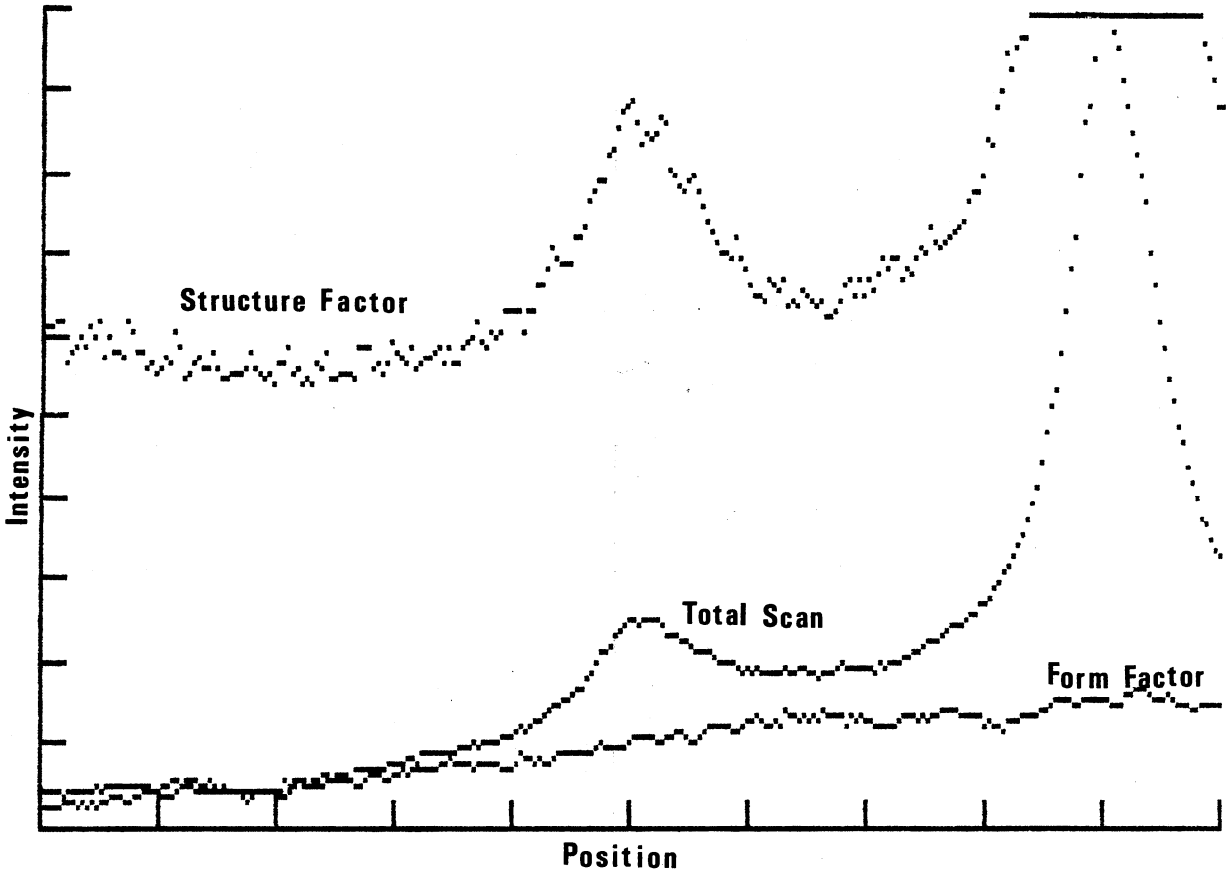

Figure 34. A superposition of the total scan, the form factor, and the structure factor (the structure factor is printed on a different scale than the total scan).

here primarily because this states that one may lift out the structure factor simply by dividing out the form factor (experimentally, this division was carried out by a computer program. See Appendix A). Figure 34 is a

superposition of the total scan, the form factor, and the structure factor resulting from the division of the total scan by the form factor. The center to center separation is based on the structure factor result.

Once the structure factor scan was determined a hard copy of the scan was printed. From the hard copy scan the separation of the zeroth and first order intensity maxima was measured. This measurement was made by locating the centers of the first and zeroth order peak and measuring the separation in centimeters with a vernier calipers. Figure 35 is a representative peak to peak measurement.

Given the peak to peak measurement, the scattering angle was determined by using

$$\Theta = \sin^{-1} ((1/1.333 \sin (\tan^{-1} (x/s)) \quad \text{III.18}$$

where 1.333 is the refractive index of water, x and s are defined by the geometries presented in Figure 36. Given the scattering angle the average particle separation can be obtained from the grating theory presented in Chapter II.

A test of consistency of equation III.18 the diffraction grating theory and particle size was made by irreversibly coagulating the particles under a maximum applied field. One can form permanent chains using a

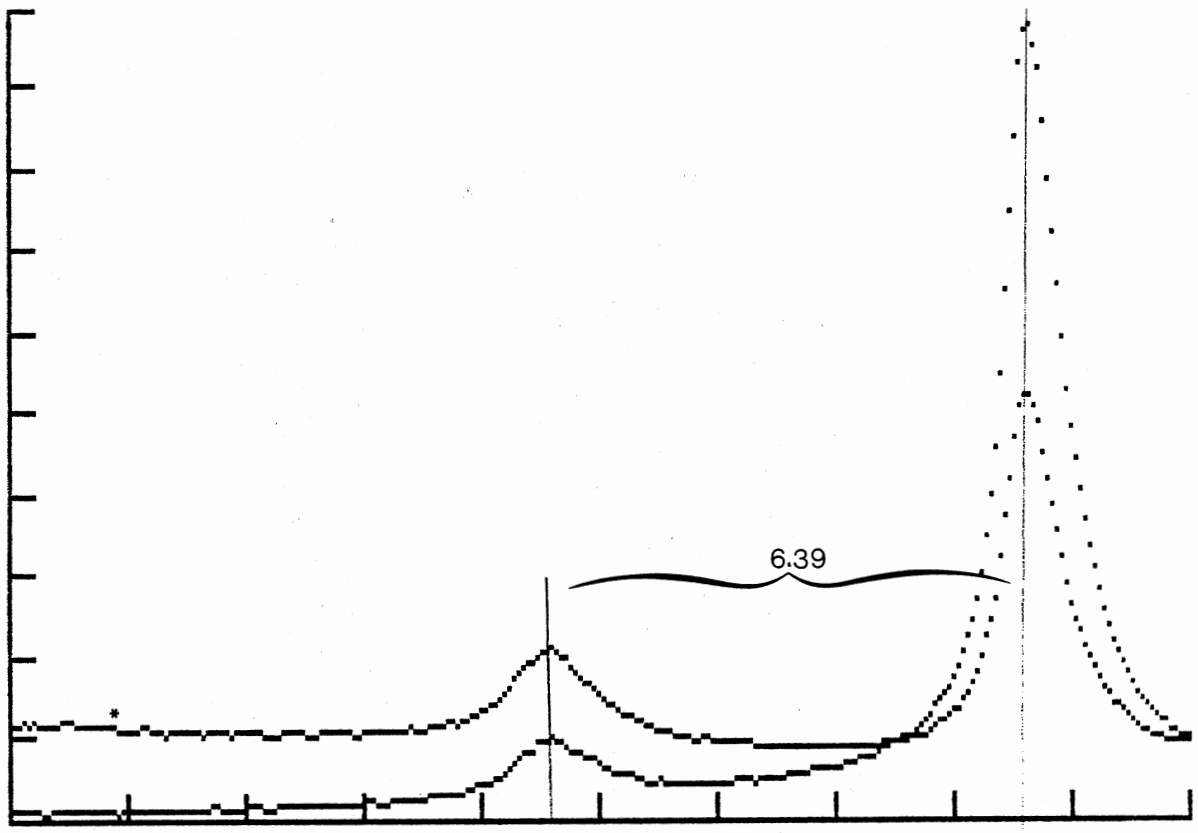

Figure 35. Representative peak to peak measurement.

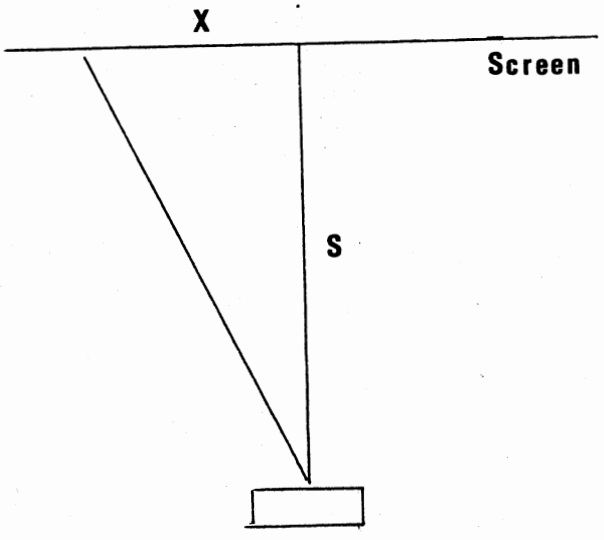

Figure 36. Scattering Geometry

high ionic strength solution and applying a maximum field. Here 2.02 um particles in 0.138 M KNO3 formed permanent chains by applying a 30 VPP field. Under these conditions, one would expect that the center to center separation determined from the diffraction pattern to be equal to the particle size. The particle size was determined to be 2.02 $\pm$ 0.01 um. See Appendix B for the error analysis of this system. These coagulated systems were microscopically observed to insure that (i) the samples were indeed coagulated, and (ii) the chains were straight. In samples at lower applied electric fields there is some kinking or bending of the chains which will be discussed in a later chapter.

Time Dependent Effects

The samples were tested for time dependent effects. Scans of the diffraction pattern were taken at various times under constant field conditions. Figure 37 shows the development of the diffraction pattern as a function of time.

It is obvious that the intensity is time dependent. However, this study is only concerned with the position of the first order intensity maximum (i.e. average particle separation) versus the applied field, and it was found that the position rapidly stabilizes in time.

An intuitive explanation for the observed behavior is that of the diffraction grating. As discussed in Chapter II, the intensity of the diffraction pattern is dependent on the number of particles in the chain, however, the position of the diffracted peak is not. Thus, it may be assumed that a local position equilibrium occurs, therefore, allowing for the use of the Tonks' gas formulation to interpret the observed phenomena. From microscopic observations, the number of particles in the chain increases with time. Thus, the large structure of the system is not equilibrated until a single long chain is formed in the cell.

Test for Hystersis

The experiment was conducted primarily by applying the maximum field, taking a data scan, reducing the applied field, taking a data scan, and so on until the first order diffraction peak was unable to be accurately detected. The concern here is: can the rate of equilibrium of the "local" average particle separation be affected by the experimental technique? Therefore, a hystersis test was conducted. For this test a series of scans was taken by starting at a field where, after a period of time, the diffraction pattern could be detected; then raising the applied feld until the maximum applied field was reached. This series was

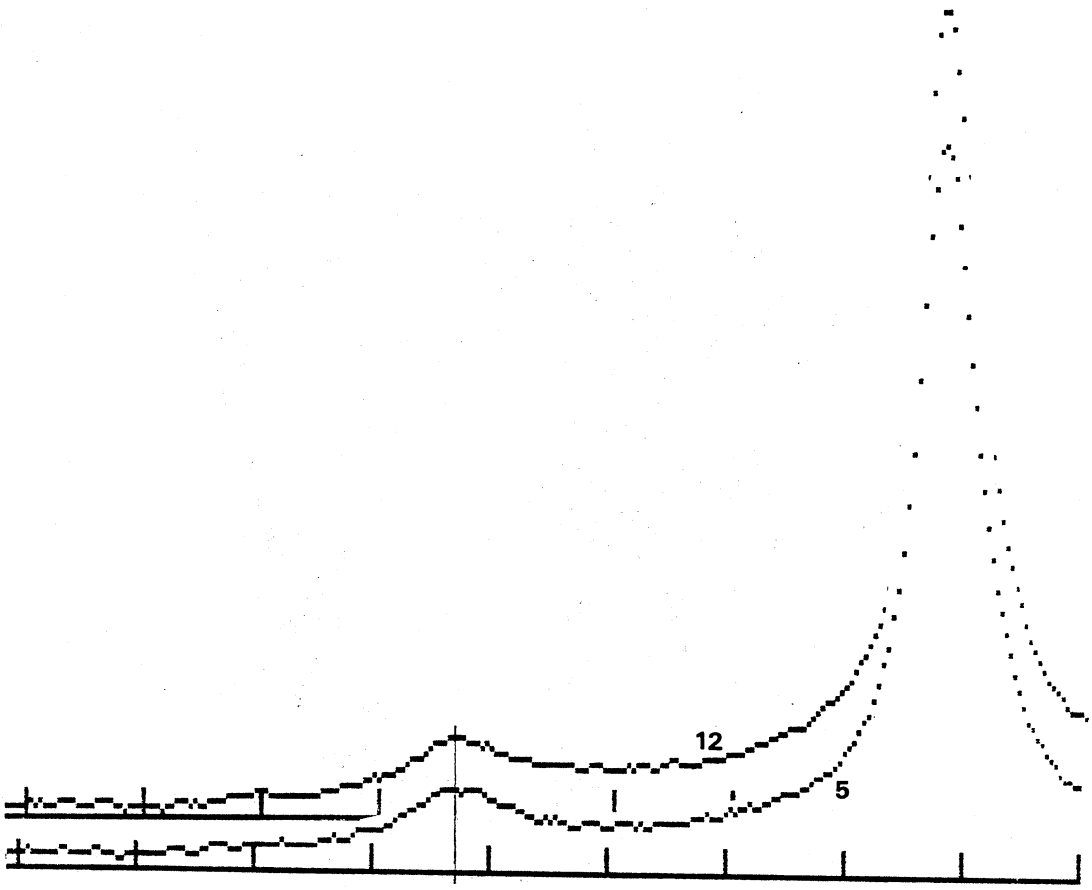

Figure 37. Development of the diffraction pattern as a function of time (@ 5 minutes and 12 minutes).

analyzed and compared with a corresponding falling run. This test determined that there was no measurable difference between the position of the diffracted peak of the rising scans and falling scans. However, there is a great variation in the intensity measurements.

This discrepancy between the intensity measurements can be easily explained in terms of the time dependent phenomena. At the low end of the applied field the

induced dipole interaction is weak and it takes a long time for the chains to form. As the field is increased the dipole interaction is strong and the less time it takes to form the chains. Recall that the position or the separation between the particles is not time dependent, but the intensity of the diffracted peak is dependent on the time. Thus, the advantages of starting at the high field and the resulting technique of lowering the field are it takes less time for the chains to form and the intensities are much greater.

Position of Scan

The experimental scans of the diffraction pattern were not made through k = 0. The primary reason for this is that if the scans were made through k = 0, the pin diode would have passed through the laser beam. Since, the computer programs used determine relative intensities, the intensity at this point would have washed out the important information. Thus, the position of the scan line was tested to ensure that the diffraction pattern did not vary in k_y.

The applied field was held constant and the detection device was raised and lowered while taking a series of data scans. The position of the diffracted peak was unaffected by the position of the scan line, however, the ability of the pin diode to pick up the

diffracted peak was limited at certain positions because of destructive interference due to the form factor of the particle. The optimum scan line was chosen to be 2 to 4 cm above or below the plane defined by the laser beam (The sample was generally 10 to 20 cm away.).

Concentration Effects

As seen previously, the intensity of the diffraction pattern increases as the number of particles in the chain increases. Therefore, if one increases or decreases the concentration of the particles in the suspension one would expect at the very least an effect on the intensity of the pattern on similar time scales. However, we must be ascertain if there effects on the position of the diffracted peak as a function of concentration.

A concern was that the Tonks' gas theory predicts an increase in the one dimensional pressure as the number density of particles increases. This increase of pressure produces a reduction in the center-to-center distance. However, the Tonks' gas theory predicts that in a range of applied electric fields, corresponding to the region investigated experimentally, the theory is independent of concentration affects. Thus, it was necessary to test various concentrations of samples to verify an independence on concentration in agreement

with the theoretical predictions.

Several different concentrations were tested. (The series of concentrations used was dependent on the particles used for the particular sample.) It was found using various particles and concentrations, the position of the diffracted peak was not dependent on the concentration used, while the intensity of the peak was affected. This again can be understood intuitively using the diffraction grating argument as used previously, i.e. the more particles in the chain the stronger the intensity of the diffracted peak.

One other concentration related phenomenon is that of double chaining, see Figure 55. This phenomenon was observed in a magnetic ferrofluid composite system at high concentrations of particles at high applied magnetic fields. Thus, it was necessary to verify that this either occurred or did not occur in the electric field cases. The observation conducted microscopically showed no signs of the double chaining phenomena at the concentrations employed in this study or the applied fields. (The maximum concentration used in this study was 8% sd.)

Frequency Effects

The electric field used was produced by an applying an oscillating voltage at 1 MHz across a set of

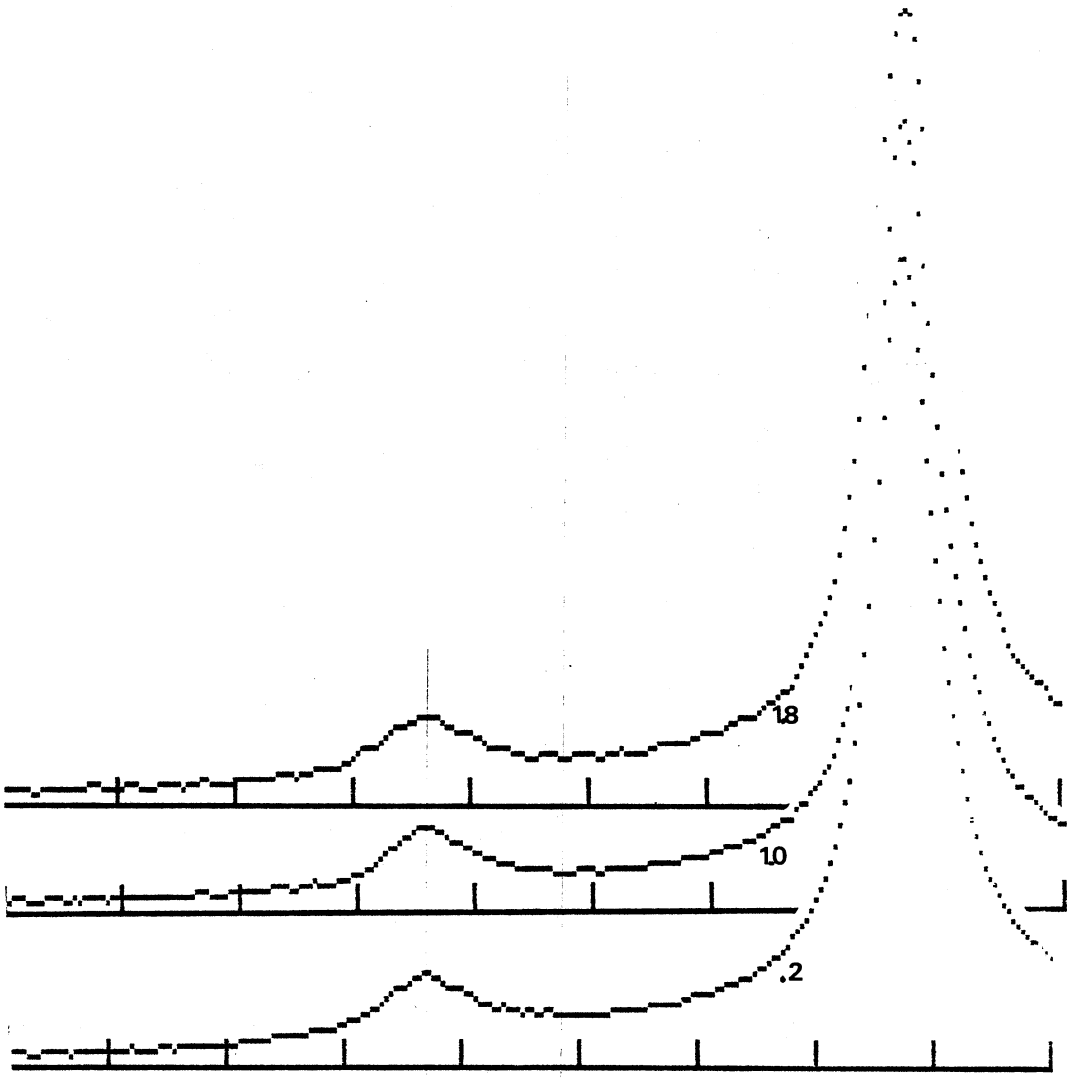

Figure 38. Frequency Study - The superposition of scans at .2 MHz, 1 MHz, and 1.8 MHz.

capacitor plates. This oscillating field was employed to counteract the problem of hydrolysis one encounters when a static voltage is applied. However, the oscillating field does have its disadvantages, because

the dielectric constant is frequency dependent, and the ions in the solution may follow the field. These frequency dependent effects may be unknown.

The ion mobility was of great concern in these the experiments. If the frequency is too small, the ions in solution will have time to diffuse during a cycle. This leads to the distortion of the ion clouds about the particles, as well as the hopping of ions from surface to surface. These parameters were not considered in the theoretical development, and the ion cloud distort would make data interpretation difficult. Therefore, a frequency must be chosen high enough that this diffusion process can be neglected which is 1 MHz in this case. [Richetti, et. al. (1987), Fraden (1987)] However, to ensure that we were not in a roll off region due to small particle separation, a test was conducted using 10 ul of 2.12 um PVT particles in 10 ul of 0.0138 M KNO_3 solution by varying the frequency from $2x10^5$ Hz to $20x10^5$ Hz. (Figure 39) This test showed that there was no measurable affects due to frequency over this range.

Another frequency effect that must be considered is the change of the dielectric constant over the range of ionic strengths and the frequency employed in this investigation. The dielectric constant is a frequency dependent quantity, Table 6, shows the dependence of the

quantity on frequency for four different ionic strengths. (These data were provided for this study by Dr. Lange, Oklahoma State University.) As one can readily see, only the imaginary portion of the dielectric constant seems to be drastically affected by the frequency and ionic strength. For the three lowest ionic strengths, the effect is negligible, however, at the highest ionic strength tested there is a larger effect. This result provides some explanation as to why one encounters a conduction effect; that the highest applied voltage in the 0.138 M KNO_3 is only measured to be 27 VPP. For this study, it was concluded that the effects due to frequency were negligible under the range of ionic strengths used.

Conclusions

The method and the instrumentation were vigorously tested to insure that the measurements were accurate and reliable. The results of the investigations conducted not only proved that the method was viable, but also provided a great deal of insight into the nature of the experimental systems. This insight was needed in order to fully understand the nature of the results obtained.

TABLE 6

THE REAL AND IMAGINARY PARTS OF THE DIELECTRIC CONSTANT AS A FUNCTION OF FREQUENCY

Conductivity(mohs/m)= 1.14E-6			
Freq(mhz)	Real D.C.	ImagK/Ko	ATTEN(dB/m)
1	78	0	0
2	78	0	0
5	78	0	0
7	78	0	0
10	78	0	0
20	78	0	0
40	78	0	0
50	78	0	0
70	78	0	0
80	78	0	0
90	78	0	0
100	78	0	0
120	78	0	0
150	78	0	0
175	78	0	0
200	78	0	0

Conductivity(mohs/m)= .000114			
Freq(mhz)	Real D.C.	ImagK/Ko	ATTEN(dB/m)
1	78.01	.01349	.02111
2	78	.003374	.02112
5	78	0	0
7	78	0	0
10	78	0	0
20	78	0	0
40	78	0	0
50	78	0	0
70	78	0	0
80	78	0	0
90	78	0	0
100	78	0	0
120	78	0	0
150	78	0	0
175	78	0	0
200	78	0	0

Conductivity(mohs/m)= .00114			
Freq(mhz)	Real D.C.	ImagK/Ko	ATTEN(dB/m
1	79.33	1.327	.2094
2	78.34	.3359	.2107
5	78.05	.05395	.2111
7	78.03	.02753	.2111
10	78.01	.01349	.2111
20	78	.003374	.2112
40	78	0	0
50	78	0	0
70	78	0	0
80	78	0	0
90	78	0	0
100	78	0	0
120	78	0	0
150	78	0	0
175	78	0	0
200	78	0	0

Conductivity(mohs/m)= .0114			
Freq(mhz)	Real D.C.	ImagK/Ko	ATTEN(dB/m)
1	148.8	70.76	1.529
2	103.4	25.44	1.834
5	83.07	5.069	2.046
7	80.66	2.663	2.077
10	79.33	1.327	2.094
20	78.34	.3359	2.107
40	78.08	.08426	2.111
50	78.05	.05395	2.111
70	78.03	.02753	2.111
80	78.02	.02108	2.112
90	78.02	.01666	2.112
100	78.01	.01349	2.111
120	78.01	.009371	2.112
150	78.01	.005998	2.112
175	78	.004407	2.112
200	78	.003374	2.112

CHAPTER IV

RESULTS AND CONCLUSIONS

Introduction

Recall that the initial experiment was designed to understand the ordering phenomena found when applying a parallel electric field to a sample comprised of latex particles. Similar experiments to the one proposed for this study were previously conducted by Richetti, et. al. and Fraden. As discussed in Chapter II, there were certain problems in the theory used to explain the behavior observed, because it did not quantitatively explain their results nor account for any of the stabilization forces present. Therefore, a new theory based on the Tonks' gas was developed for this study, allowing one to investigate not only the observed phenomena but the stabilization forces present in colloidal systems. This investigation, not only addresses the problems of the studies presented by Richetti, et. al. (1987) and Fraden (1987) but extends other work done in the investigations of interparticle forces as discussed previously.

Several experimental parameters could have been

adjusted, such as pH, ionic strength, surface chemistry, shape, etc., in order to test the nature of the stabilization forces present. By changing the ionic strength, one can directly modify the double-layer repulsion between the particles, therefore, one may expect observable changes in the manner in which the particles interact. This variable interaction should provide a meaningful insight into the total interaction between the particles and test the validity of the present theory.

In this work ionic strength studies were conducted on two sets of particles. One set of particles was used for the initial qualitative studies to insure that the experimental and theoretical methods were feasible. The particles used for this study were not as well characterized as the particles used for the more detailed quantitative study, where the zeta potentials had been measured. Both sets of particles underwent the same method of preparation and the same experimental tests as described in the previous chapter.

Qualitative Results of the Ionic Strength Study

The qualitative behavior observed in this study was the same as observed in the previous investigations presented by Fraden and Richetti, et. al. In all the

samples observed the average particle separation decreased as a function of the applied field. In neither of these other investigations were the effects of a change in ionic strength addressed.

The first noticeable affect, in the present work, is that the particle separation is not only dependent on the field strength but also on the ionic strength. The field required to induce chaining behavior is much greater in the lower ionic strength samples than the higher ones. The average particle separation is greater in the lower ionic strength samples for corresponding applied fields than at higher concentrations of KNO_3. The intensity of the observed diffraction pattern is much less for the lower ionic strength samples than those at higher ionic strengths, evidently this is due to having fewer particles in the chains at the lower ionic strengths. Microscopic observations showed that the Brownian motion in the chains was greater at corresponding electric fields at the lower ionic strengths than the higher ones, which will also diminish the intensity maxima. All of the evidence points to the fact that the more deionized the sample is, the greater the double-layer repulsion between particles.

Not only was the Brownian motion greater in samples at lower ionic strengths at corresponding electric fields, but generally in samples at lower field

strengths. As the Brownian motion increases, the chains develop kinks or bends and deviates from the assumed straight chain diffraction grating. Therefore, one may be concerned that this observed kinking shows up in the observed diffraction pattern and is responsible for the shift observed in the first order diffraction peak. However, recall that the average particle separation is smallest at the highest applied electric field. The separation of the first order diffracted maxima from the zeroth order maxima is greater at the higher applied fields than the lower applied fields. Thus, over the course of an experimental run, as the measurements were taken from high field to low field, the first order diffracted peak shifts inward toward the zeroth order peak.

This kinking effect may be estimated. Figure 39 shows two chains. The first chain has bends or kinks in it as one would experimentally observe in lower ionic strength solutions or at lower applied fields. The second chain shows a chain without the kinks or bends which can be experimentally observed at certain ionic strengths and at higher applied field conditions. Each chain contains the same number of particles. From this picture it is seen that the kinks reduce the overall length of the chain at a fixed center to center separation of particles.

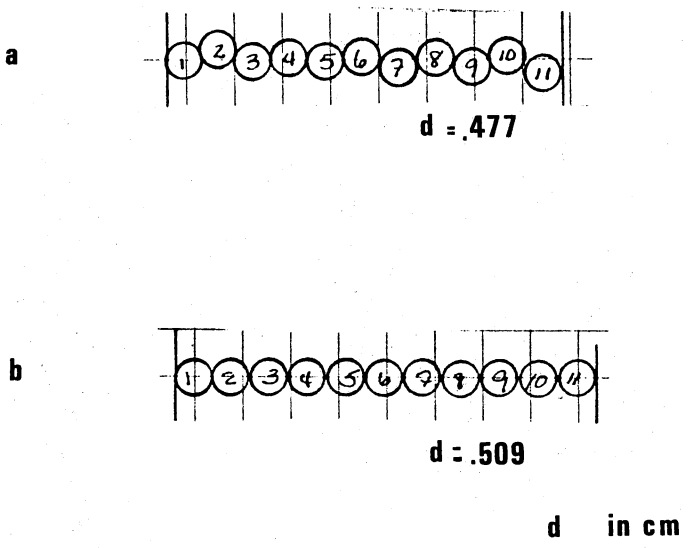

Figure 39. a) A chain exhibiting bending or kinking.
b) A straight chain.

The bends cause a decrease in the average projection of the particle center to center separation as measured parallel to the average direction of the straight chain formation. This result may also be seen in k-space. Using the simple diffraction grating theory, the first order diffraction maxima, m = 1, would occur at

$$\theta = \sin^{-1} (m\lambda/d)$$

$$= \sin^{-1} (6328\times10^{-10}/.477\times10^{-2})$$

$$= 0.0076 \text{ degrees}$$

for chain one of Figure 39 and at

$\theta = \sin^{-1} (6328 \times 10^{-10} / .509 \times 10^{-2})$

$= 0.0071$ degrees

for the second chain in Figure 39. This implies that if the bending or kinking of the chain as the field is decreased is responsible for the observed shift in the first order diffraction, the peak would shift away from the zeroth order peak, which is contradictory to the experimentally observed phenomena.

Additionally, this kinking behavior was examined microscopically. At the lowest ionic strength used (the worst case of kinking or bending) a micrograph was taken. From this micrograph two chains were chosen and the deviation from a line parallel to the field line was estimated. This deviation was approximately 3 degrees, and no fluctuation was greater than 13 degrees. The deviation would have to be greater than 10 degrees to produce an error in the particle of significance.

Quantitative Results of Ionic Strength

Given the qualitative behavior of the systems under investigation and the idea that a force balance between the particles was present in the systems, a theoretical development was obtained in order to provide a quantitative understanding of the observed phenomena.

This theoretical development is based on a Tonks' gas. A Tonks' gas is a one dimensional gas in which the particles experience only nearest neighbor interactions, the particles cannot exchange places along the chain, and the particles are in equilibrium. This theoretical development was presented in Chapter II.

From this theoretical development, one can obtain an intensity scan similar to that obtained experimentally. From this theoretical intensity scan one can make predictions of the scattered intensity maxima positions in k-space versus the strengths of the applied electric field. Thus, one has a means to test the various forms of the interparticle interactions present in the system via this Tonks' gas theory.

First we make a few comments concerning the validity of the Tonks' gas approach. The Tonks' gas requires that there are only nearest neighbor interactions. To the first approximations this is valid as the particles are larger than the typical range of interaction. Furthermore, the particles cannot exchange places along the chain. From microscopic observations this fact seems to be verified. Finally it is assumed that the particles are in equilibrium. At best they are only in a local equilibrium as deduced from time dependent studies.

From a previous chapter, it was pointed out that

there are time dependent effects in the intensity of the diffraction peaks implying that the system is not in a global equilibrium state. However, there were no observed time dependent effects in the position versus field measurements implying that the system is in local equilibrium. Therefore, we take the chains to be in local equilibrium and our analysis is only valid in the discussion of intensity maxima position versus field effects. This approach should not be used to analyze any of the observed intensity effects.

Thus one has the potential of checking the consistency of the various interparticle interactions. The interactions chosen to be examined were based on the DLVO theory outline in Chapter I. This theory has been generally accepted as correct for the interpretations of the stabilization forces present in colloidal systems. This theory states that the total potential experienced by the particles is a sum, assuming additivity, of the attractive van der Waals potential and the coulomb repulsive potential, i.e.

$$V_t = V_a + V_r$$

Thus, the pair potential for the systems under investigation here can be written as

$$V(r) = V_{dipole} + V_t$$

where for convenience of the analysis Vdipole is the dimensionless form of equation I.36 when θ = 0 degrees

$V_{dipole} = A / X^3$

where X is a dimensionless separation variable, and A is a constant dependent on the strength of the applied field, particle size and dielectric constant

$A = [\varepsilon_w a^3 E^2] / [4 k_B T]$.

Here ε_w is the dielectric constant of water, a is the particle radius, E is applied electric field, k_B the Boltzmann constant, and T is the temperature in degrees kelvin.

One could have chosen another form such as the forms presented in earlier chapters for the dipole interaction. However, these other forms for the dipole interaction involve sample corrections as discussed previously in Chapter I. Thus, for this study this seems to be a valid approximation.

The forms chosen for the repulsion and the attraction follow those presented by Verwey and Overbeek [1948]. The repulsion term is based on the Derjaguin approximation for spheres, and is given by the dimensionless form of equation I.32,

$V_r = [a \varepsilon_w \Psi^2 / 2 k_B T] \ln (1 + \exp(-K\, 2a(x-1)))$

where x is the dimensionless separation variable, a is the particle radius, k_B the Boltzmann constant, T is the temperature, K is the inverse Debye length, and Ψ is the surface potential of the particle. Generally the value of Ψ was used as a fitting parameter in this study, as

this was least well known or unknown experimentally. The van der Waals attraction used is an approximation for spheres given by Verwey and Overbeek [1948] in equation I.15. The dimensionless form of the approximation is by

$$Va = - A / [k_B T 24(x-1)]$$

where x is the dimensionless separation variable, and A is the Hamaker constant.

The initial fit to the 2.02 um data, used a theoretically determined value for the Hamaker constant

$$A = 1.4 \times 10^{-13} \text{ ergs.}$$

This value given in Isrealachvili [1985] and Visser [1972] was obtained for polystryene-water-polystryene system. In a review of the literature no theoretically or experimentally determined value for the PVT-water-PVT system was found. However, due to the similarity of PVT to polystyrene this value is a good approximation for the PVT-water-PVT system. Figure 40 presents the high and low theoretical fit to the experimental data.

It is obvious that the theory and data do not agree. However, there some very important features of this plot. The line represents the case where there is only a hard sphere and dipole interaction between the particles. As noted in Chapter II the Tonks' gas theory predicts an s dependence, where s is dependent on particle the concentration. However, in this region of

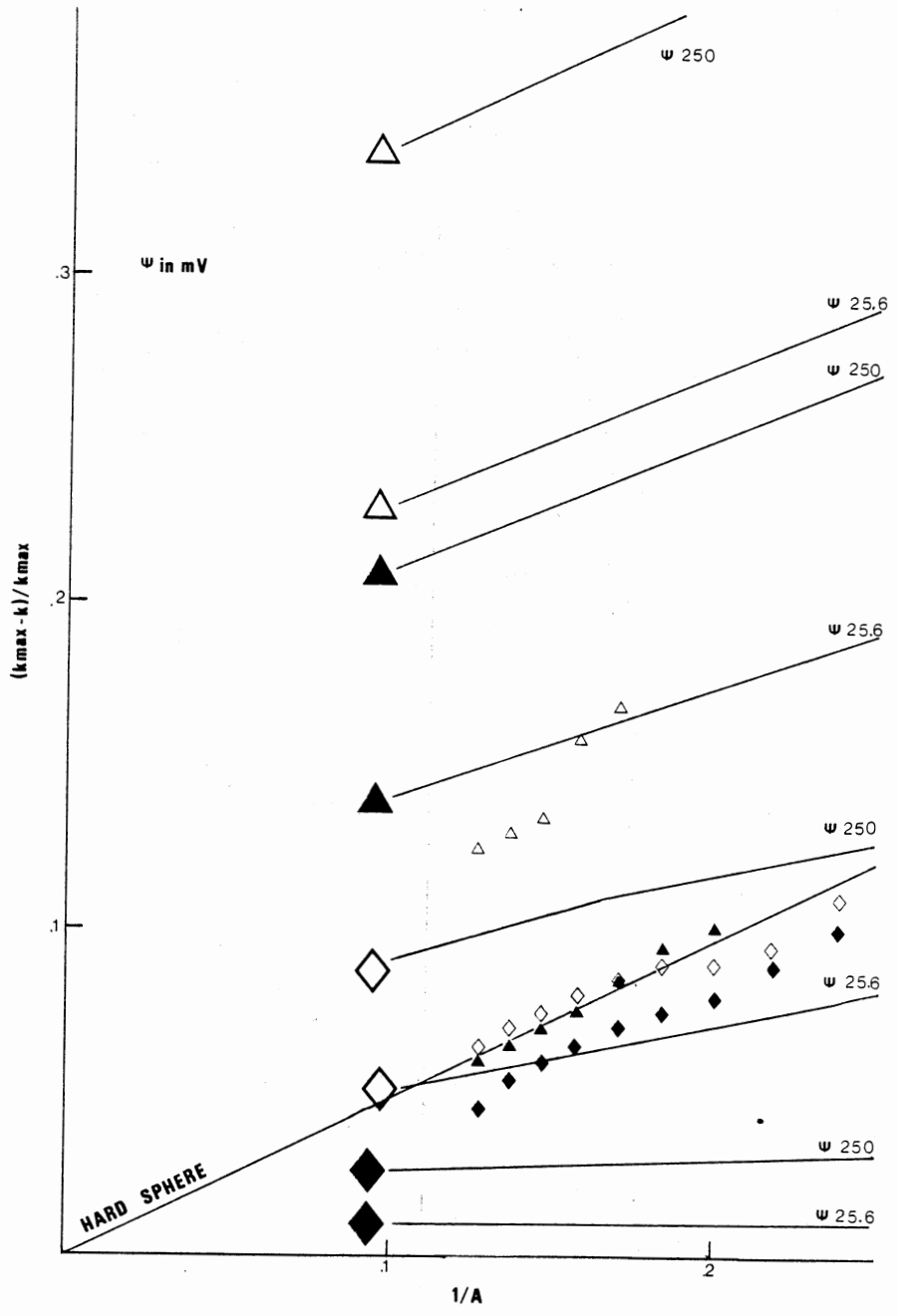

Figure 40. The initial theoretical comparison of experimental data to the Tonks' theory using the theoretically determined Hamaker constant. The open triangles correspond to 10 ul of particles in 0.0000138 M KNO_3, closed triangles in 0.000138 M KNO_3, open diamonds in 0.00138 M KNO_3 and closed diamonds in 0.0138 M KNO_3.

the applied field there is no observed, theoretical dependence on s corresponding to experimental studies.

The theoretical fits to the data represented by the closed diamonds have collapsed, i.e. the theory predicts that the particles are in the primary minimum and not the stable secondary minimum observed. Thus, the theory predicts that particles would have irreversibly aggregated. The chaining behavior is reversible implying that the particles are in a stable secondary minimum. The theory was tested as to the integration technique by changing the integral step size and location of the maximum of the barrier between the primary and secondary minimum. The location of the collapsed prediction is due to the integration step.

Qualitatively, the behavior of the fits, although they do show a linear behavior, is not in agreement with the experimental data. Thus, a modification to the pair potential used for this fit was made.

A review of the literature for experimentally determined values of the Hamaker constant showed that there is a range of values measured for a polystyrene-water-polystyrene system. A nice review of the previous experimental work as well as their own work was presented by Melik, et. al. [1985]. From this work, an experimental value of

$A = 1.7 \times 10^{-14}$ ergs

was determined through flocculation studies. Figure 41 presents a best fit of the theory to the experimental data using Ψ as the fitting parameter where the only modification in the pair potential is the value of the Hamaker constant.

In the fit, one can see that the agreement between the theory and experiment is fairly good. Figure 42 is a presentation of the DLVO potentials for the parameters obtained from the best theoretical fit of the data. Figure 43 is a presentation of the total potential experienced by the particles at the highest applied field. If the particles were to be unstable at the determined surface potentials it would be apparent in these plots. Even at the lowest ionic strength there is an observable "secondary minimum" which has a depth that is approximately 1 kT compared to the stabilization barrier, in which the particles can be trapped. It should also be pointed out that the positions of the minima in these wells are in fairly good agreement with the observed separation of the particles.

Another modification in the van der Waals theory was attempted because the region of particle separations lies between the normal van der Waals attraction and the retarded attraction, i.e. there may have been a distance dependence to the attraction. This modification follows

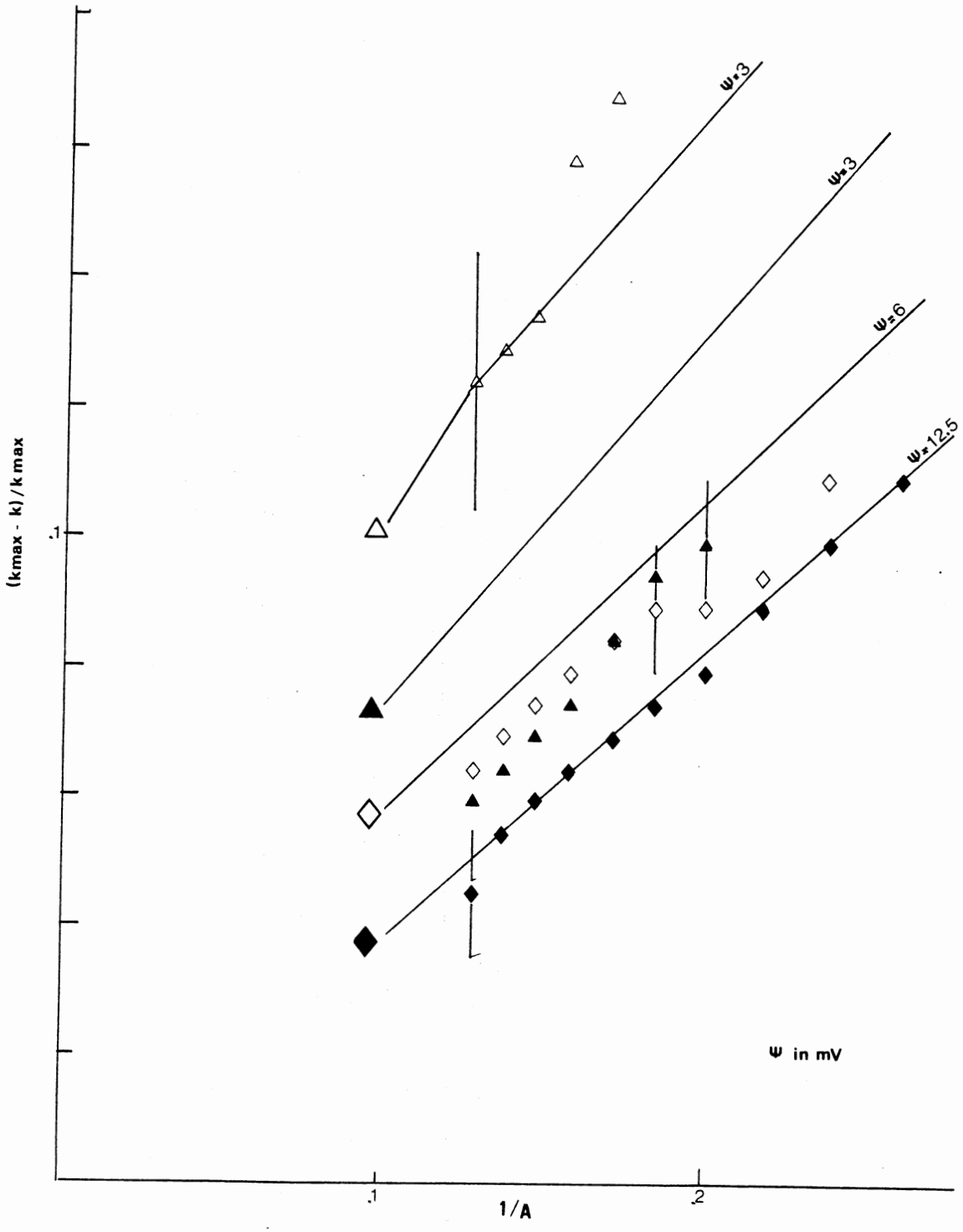

Figure 41. A comparison of the experimental data to the Tonks' theory using an experimentally determined Hamaker constant. (Symbols defined in Fig. 40)

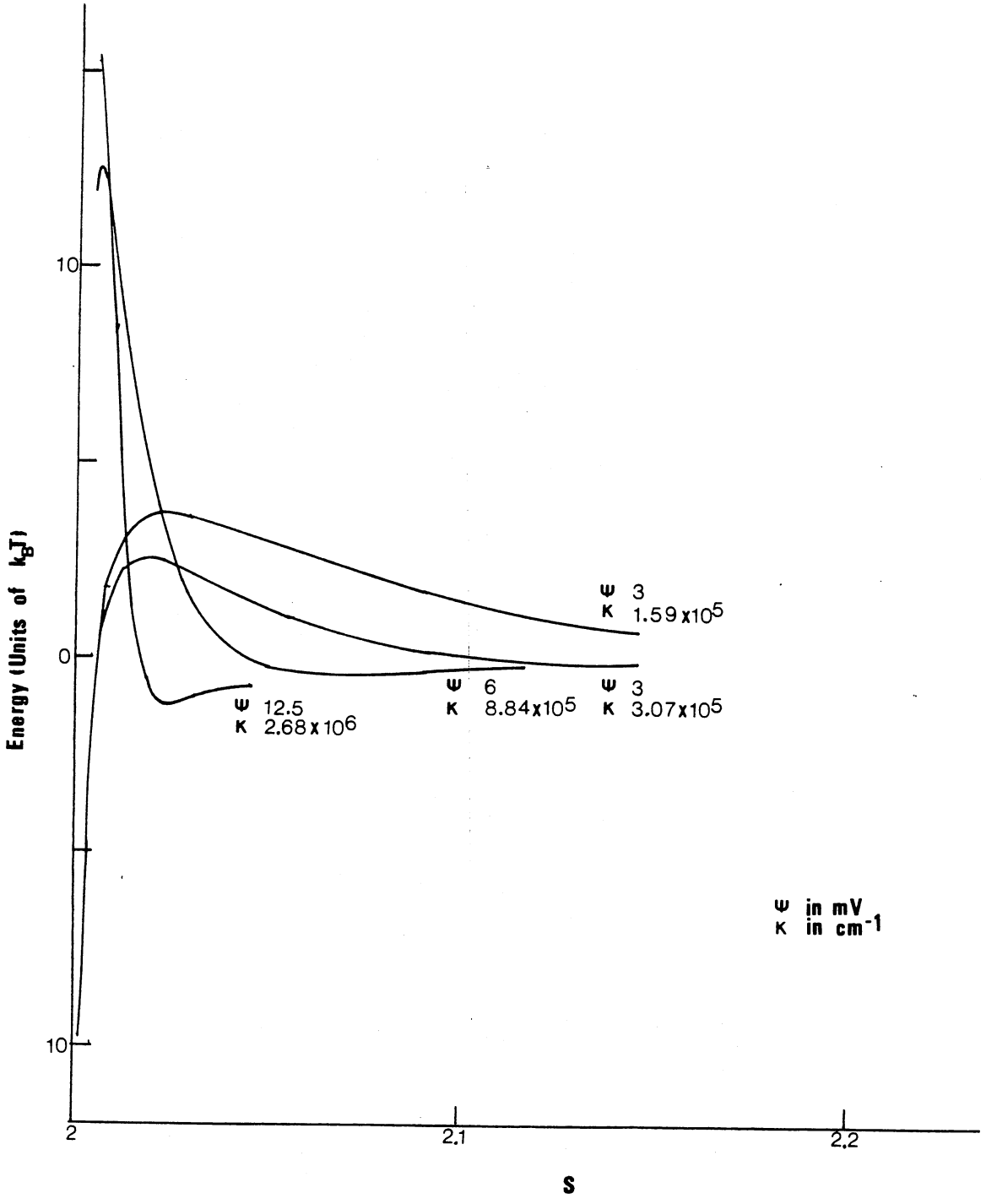

Figure 42. The DLVO potentials for the four ionic strengths used in this study for the parameters given in Figure 41.

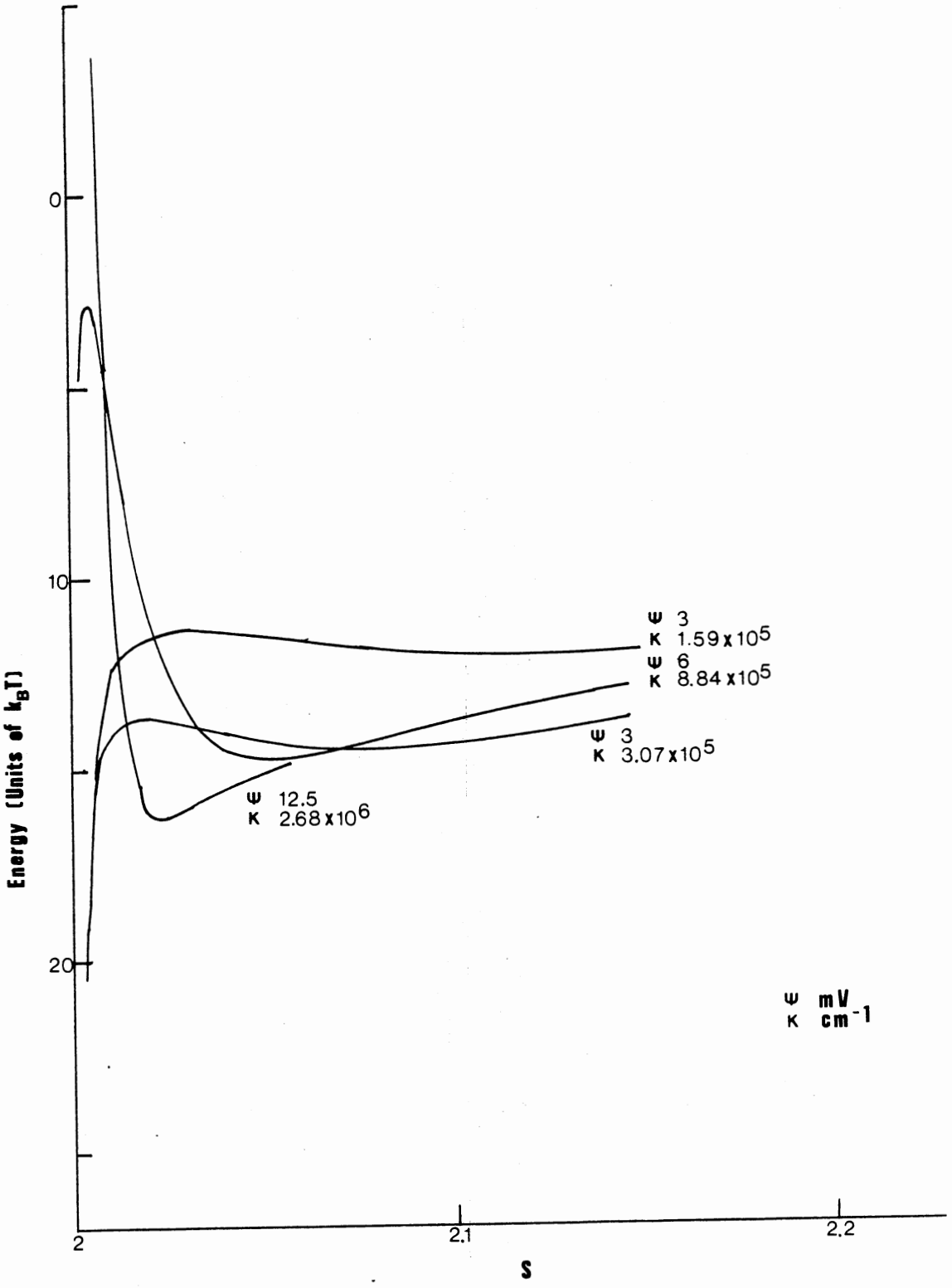

Figure 43. The total potentials for the highest applied field for the four ionic strengths used and the parameters given in Figure 41.

the method outline by Russel, et. al. [1989]. Here the attraction equation I.12 takes the dimensionless form of

$$Va = \frac{-\exp(-4\,K\,a(x-1))}{32(x-1)} - \frac{Aeff}{24(x-1)}$$

where

$$Aeff = A1\,\left(1 + (A3\,2a(x-1)^{3/2})^{-2/3}\right.$$

where

$$A1 = \frac{3\,h\,w}{16\sqrt{2}\,k^{3}\,T} \cdot \frac{(\bar{n}_o^2 - n_o^2)^2}{(\bar{n}_o^2 + n_o^2)^{3/2}}$$

and

$$A3 = \frac{n_o\,\varepsilon_w\,(\bar{n}_o^2 + n_o^2)^{1/2}}{4\sqrt{2}\,c}$$

where

$h = 1.055 \times 10^{-34}$ Js
$w = 1.88 \times 10^{16}$ 1/s
$\bar{n}_o^2 = 2.424$ polystyrene
$n_o^2 = 1.777$ water

These values are given in Russel et. al. [1989]. Figure 43 presents the best fit of the theory with the experimental data using this modification. Again the agreement is fairly good and to obtain this fit the surface potentials were higher than the previously.

Figure 45 displays the DLVO potentials given by the theoretical parameters obtained from the theoretical fit. Figure 46 is a graphic representation of the total potentials for the highest applied field. Note again here that there are stable secondary minima in the potentials. These potential plots show that the wells

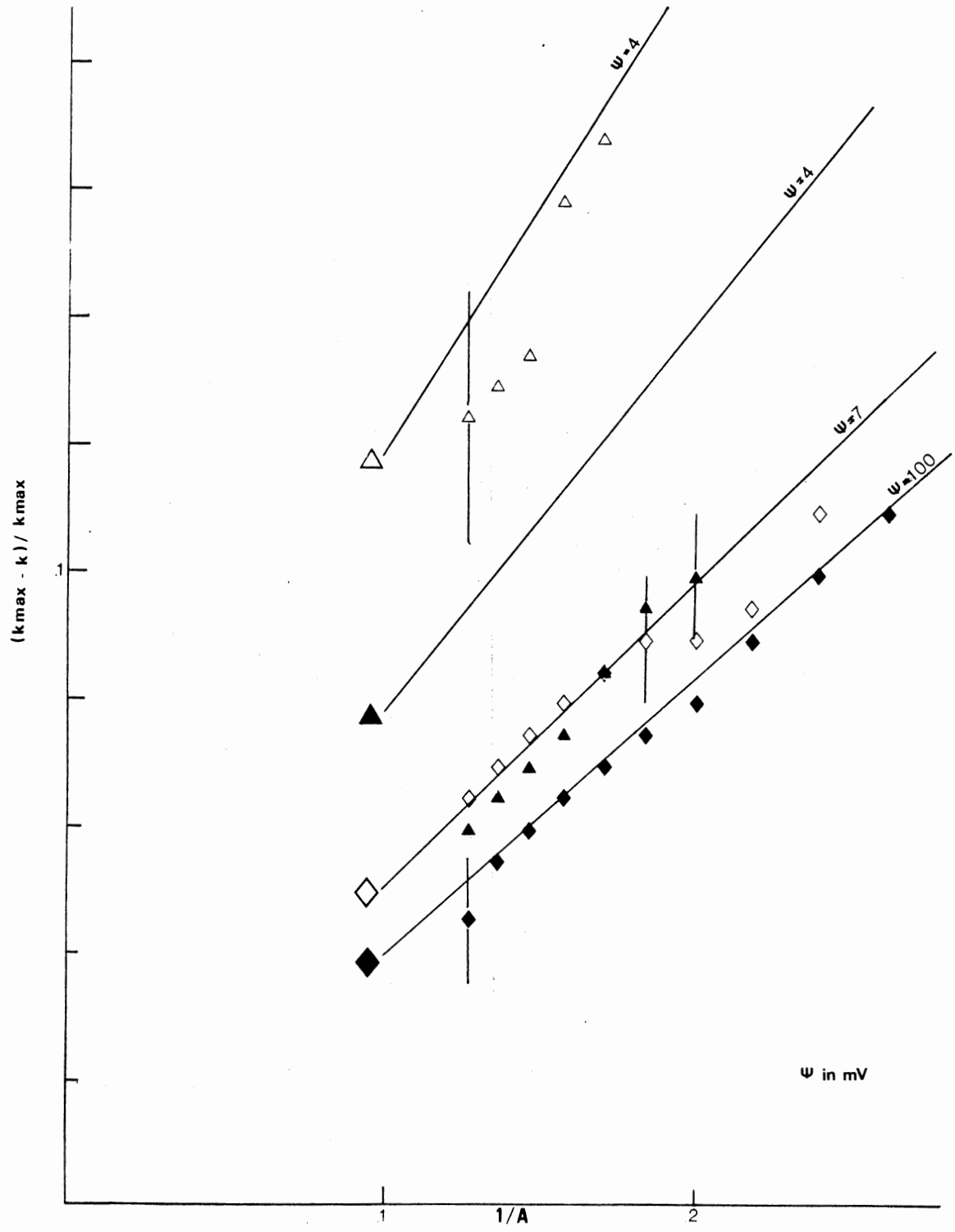

Figure 44. The comparison of experimental data to the Tonks' theory using the Russel (1989) formulation for the van der Waals attraction. (Symbols defined in Fig. 40).

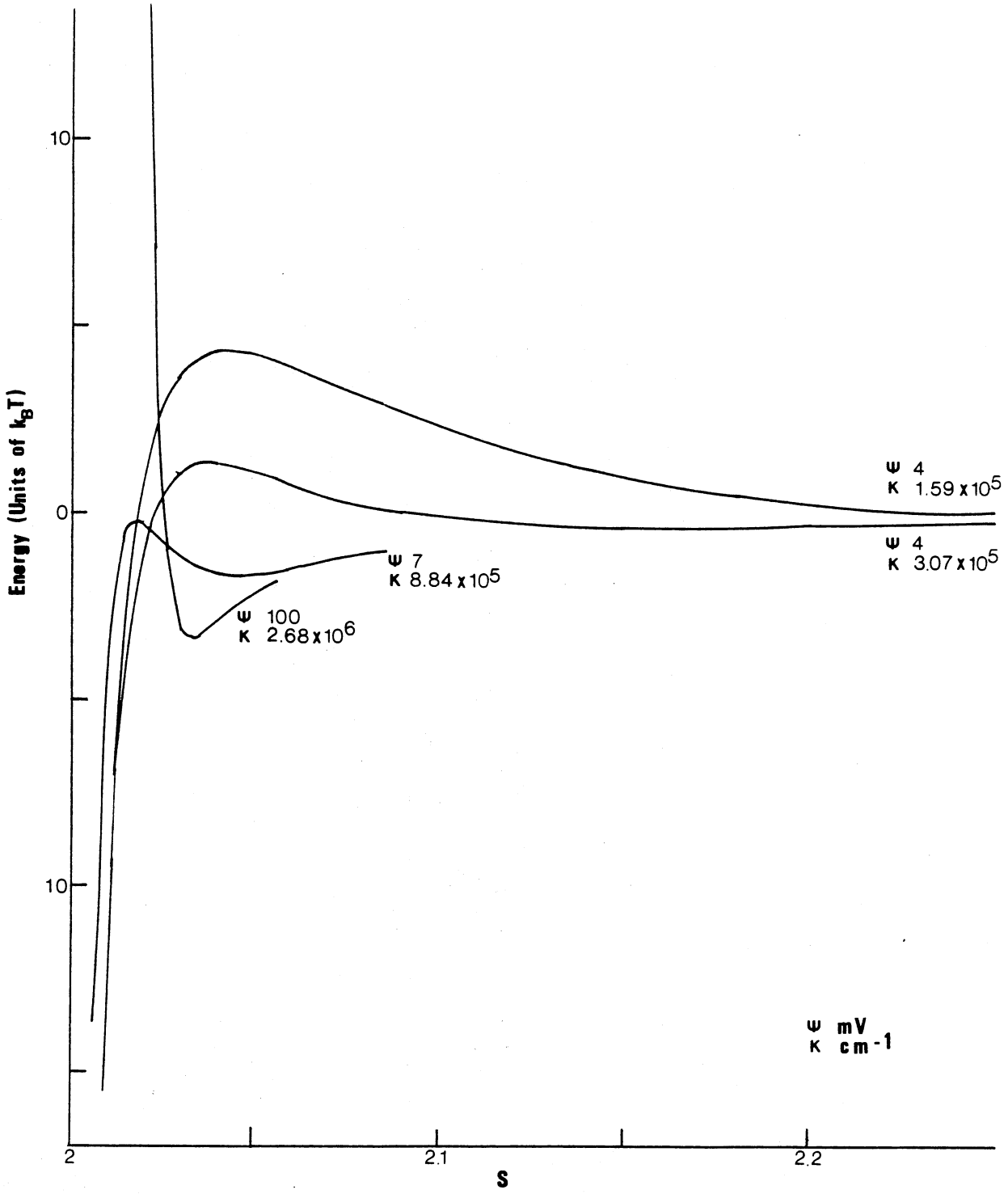

Figure 45. The DLVO potentials for the four ionic strengths used given the parameters in Figure 44.

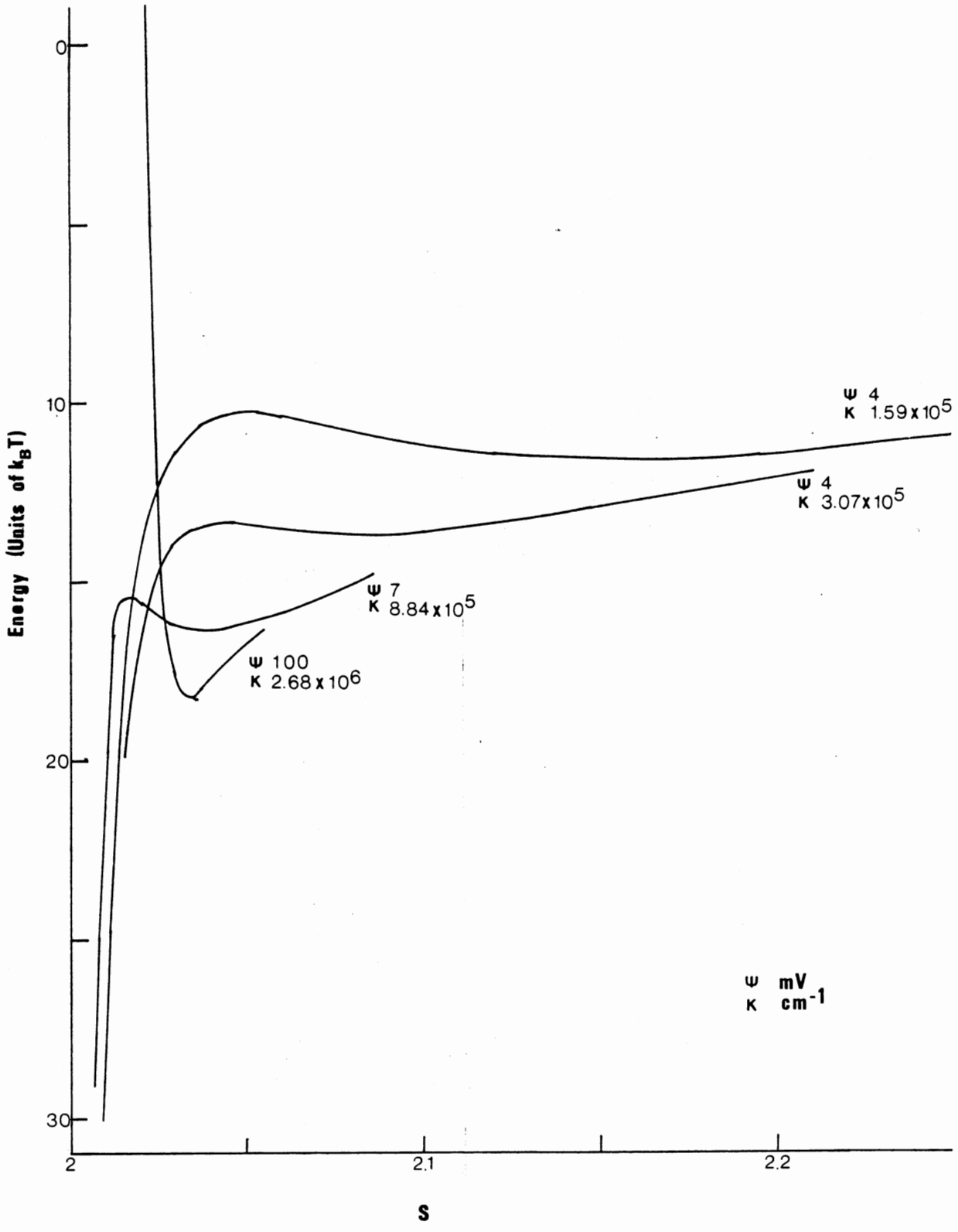

Figure 46. The total potentials for the highest applied field for the four ionic strengths used given the parameters in Figure 44.

appear to be deeper than those obtained via the fit presented earlier. Again the position of the minima are in fairly good agreement with the experimental results.

In both of these modifications, test were conducted to ensure that there were no effects related to the s dependence of the theory and to ensure that the starting point of the integration was properly chosen. Appendix C has the computer programs used for all the theoretical determinations.

Based on the results of this investigation it was determined that a particle with a measured surface potential was necessary. Hence, a 2.12 um PVT particle was ordered and the all the experiments were repeated. Figures 26 - 32 are reproductions of the surface potential measurements obtained from the manufacturer. Qualitatively all the results are the same as those obtained from the 2.02 PVT particles - there were no concentration effects, no dependence on frequency over the tested range, no time dependent effects on the position versus applied field, while there were time dependent effects on the intensity, no hystersis effects, and the average separation versus applied field decreased as the applied field was increased.

The data and the theory were compared in the same manner as before with a radius modification in the

program. First, a fit using the flocculation Hamaker constant was tried. Figure 47 shows the results of the fit provided by this modification. As one can see the fit of the data is extremely good. In fact this fit is better than those obtained from the previous study. While the surface potentials are low, they are in line with the manufacturer's measured zeta potentials.

Figure 48 displays the DLVO potentials for the values obtained via this theoretical fit. Figure 49 presents the total potentials observed for the highest electric field. Both of these display the same features noted previously.

Figure 50 is a comparison of the experimental data and the theoretical fit obtained by using the analysis according to Russel et. al. The results here are almost identical to those obtained using the experimental Hamaker constant except for the surface potential at the lowest ionic strengths. These results were checked for concentration or s dependence as before.

These plots can be compared with plots made using the surface potentials provided by the manufacturer. (See Figure 51) One can see that for the case of the higher ionic strength the surface potential determined via this experimental method agrees well with the zeta potentials determined by dielectrophersis. The zeta potential is not a true surface potential, it is based

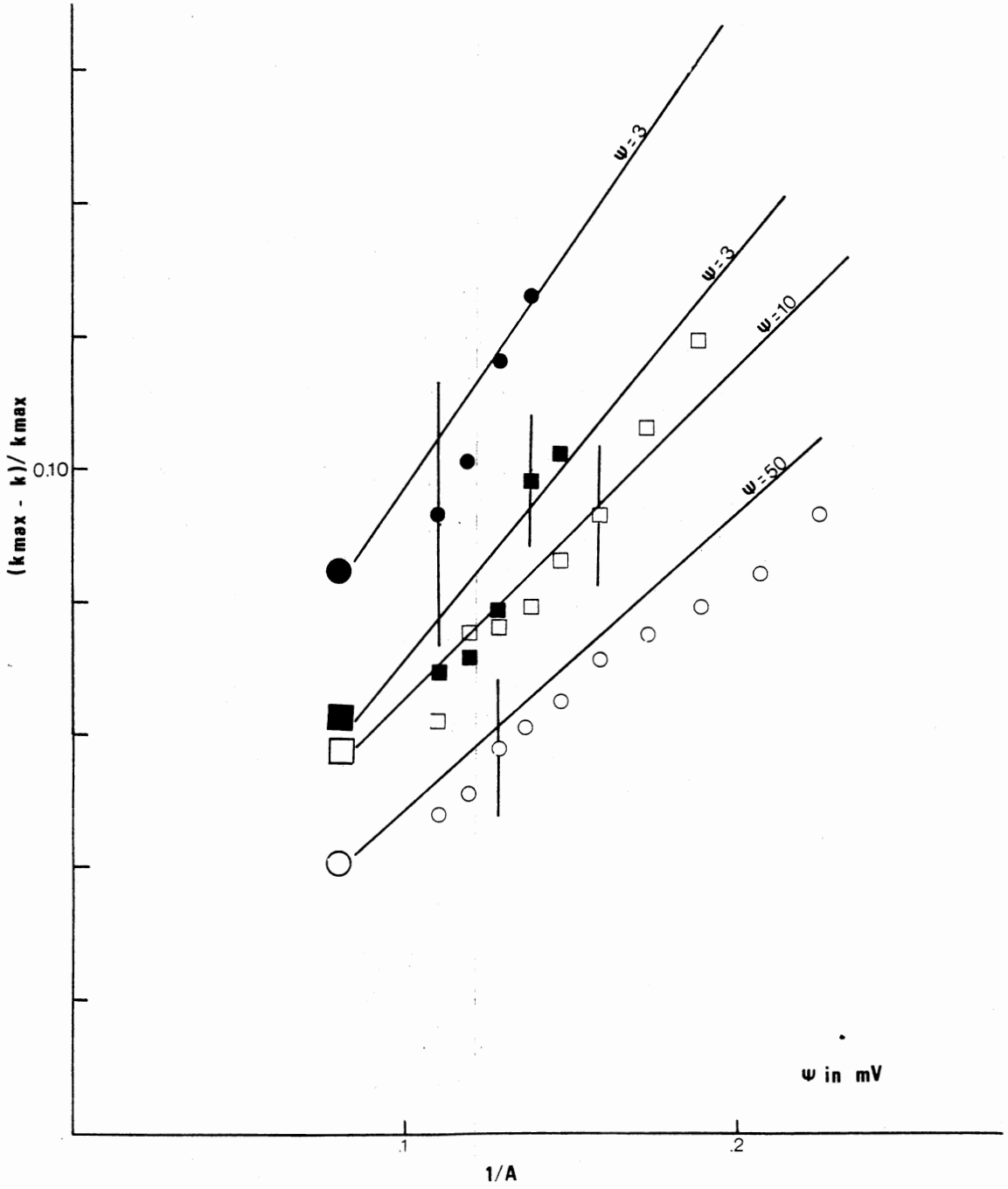

Figure 47. The comparison of the experimental data with the Tonks' theory using 2.12 um PVT particles and the experimentally determined Hamaker constant. (The open circles are 10 ul of 2.12 um PVT in 10 ul 0.0000138 M KNO_3, the open squares in 0.000138 M KNO_3, the closed squares in 0.00138 M KNO_3 and the closed circles in 0.0138 M KNO_3.)

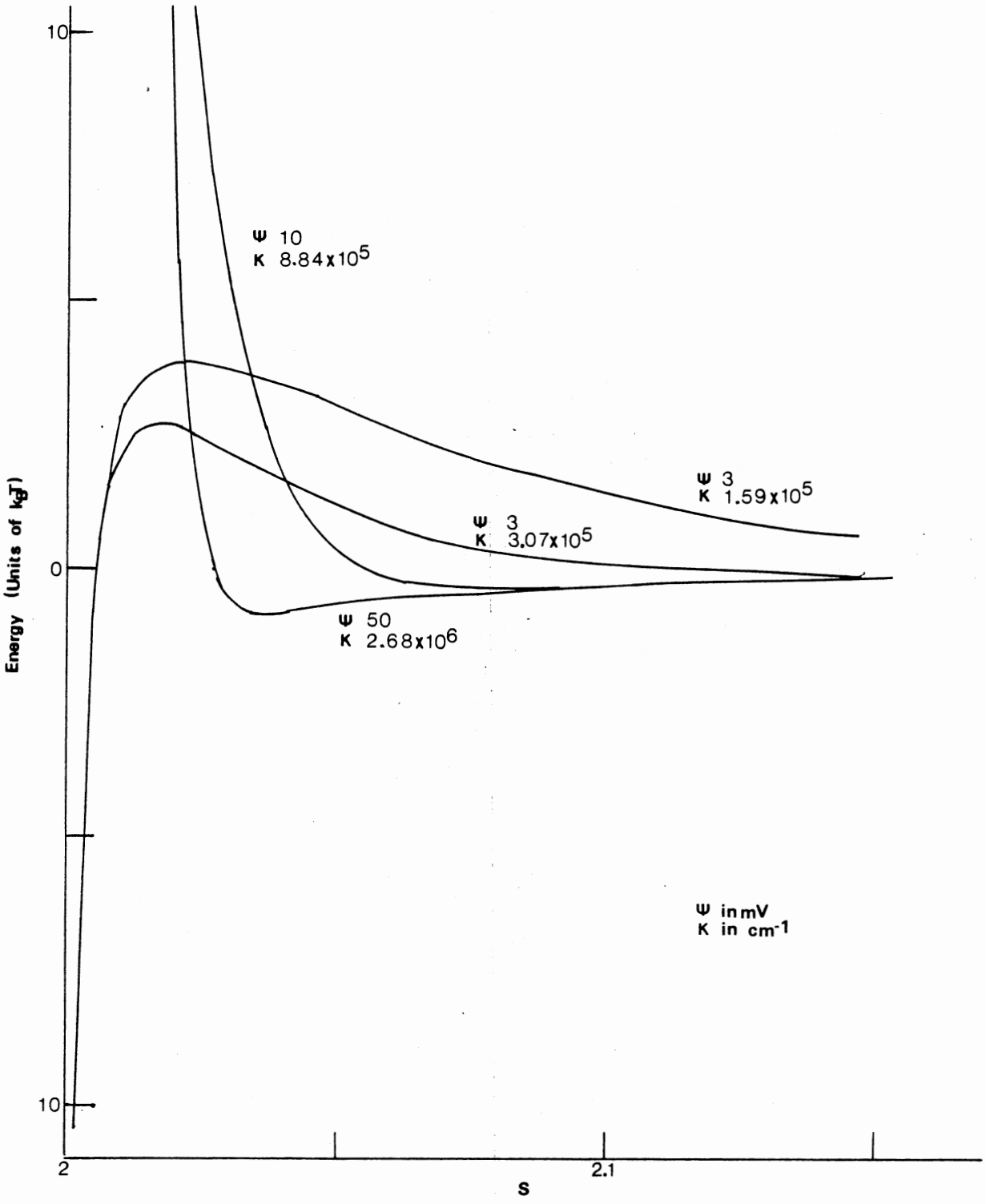

Figure 48. The DLVO potentials for the four ionic strengths used for the parameters defined in Figure 47.

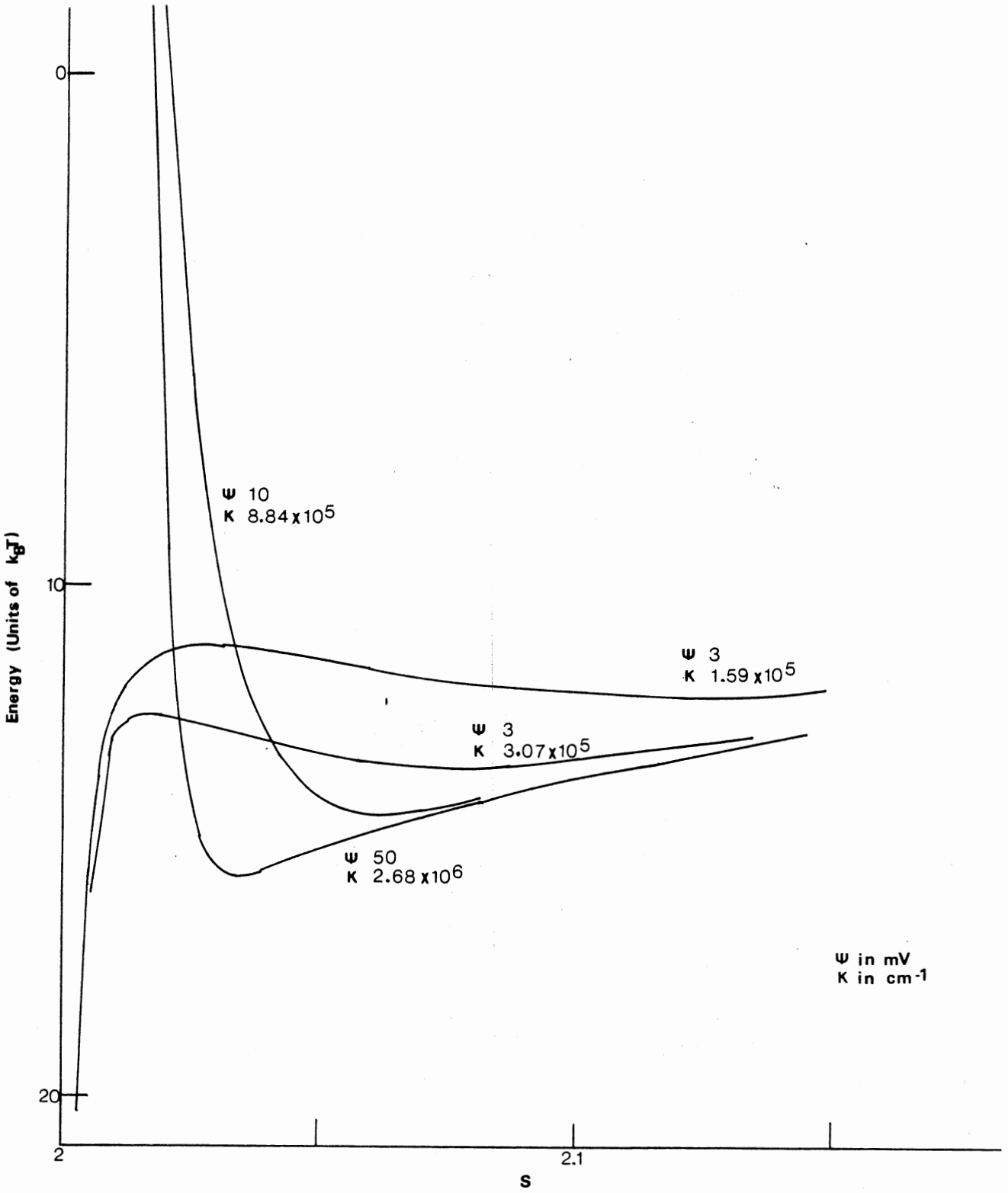

Figure 49. The total potential plots for the highest applied field for the four ionic strengths used for the parameters defined in Figure 47.

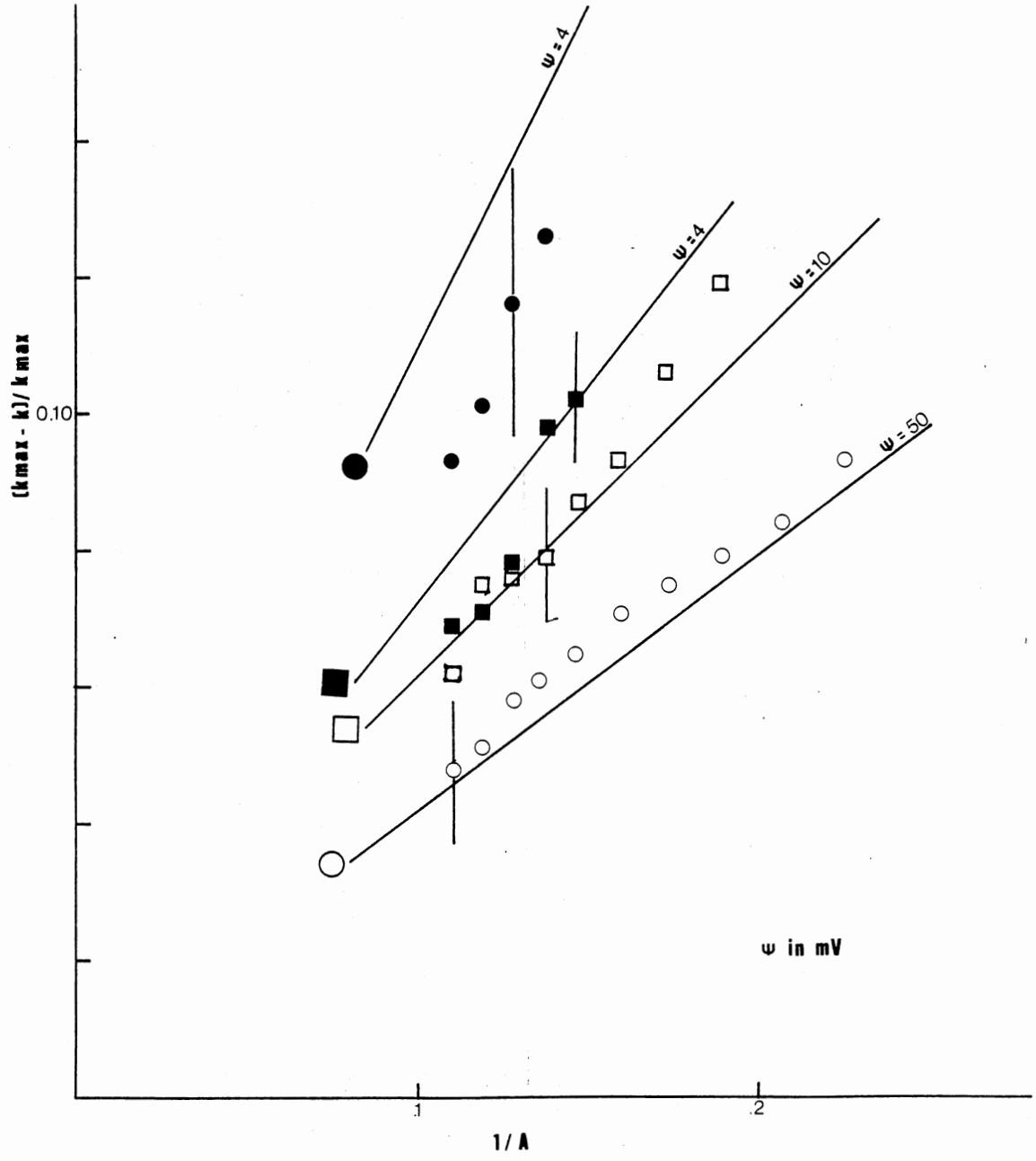

Figure 50. A comparison of the experimental data with the Tonks' theory using Russel's formulation.

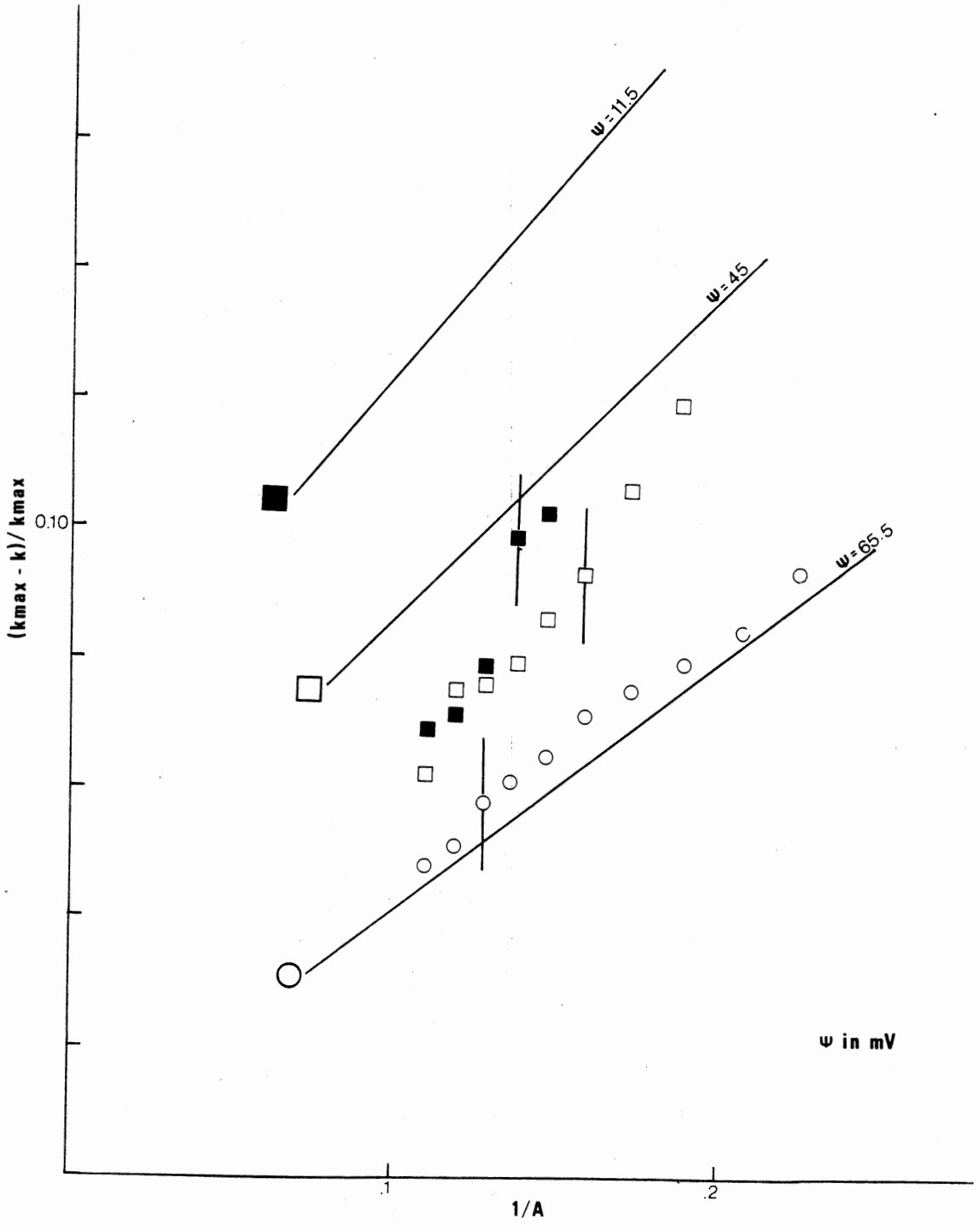

Figure 51. A comparison of the experimental data with the Tonks' theory using Russel's formulation and the experimentally determined zeta potentials.

on the mobility of a particle under going electophersis. The method here determines surface potentials which to this point have not been experimentally determined and only approximated by the zeta potential. However, at the lower ionic strength there is some discrepancy. It should be pointed out that at the lower ionic strengths the dielectrophetic measurements are very difficult. Our method at lower ionic strengths is much more sensitive to changes to the surface potential, thus the surface potentials measured are well with in acceptable agreement.

However, due to the discrepancies observed between the determined value of the surface potentials and the surface potentials provided by the manufacturer, the zeta potentials further modifications may be necessary. First since the pair potentials are based on approximations - we only tested modifications in the van der Waals attraction - one could try more exact forms for the pair potentials. Another modification made to the dipole term is possible even though the corrections to the dipole approximation appear to be small.

Conclusions

From the results obtained, it is felt that the method presented here is a viable means of investigating the interparticle forces present in a colloidal system.

It provides the means to evaluate a number of theories in comparison to the experimental data obtained. The method is extremely versatile, i.e. a variety of experimental parameters may be used to test the theories present and a variety of experimental systems may be investigated.

The technique employed here also has the potential of being an alternate technique to dielectrophersis especially at the lower ionic strengths where the dielectrophertic techniques are not as reliable. Moreover, the dielectrophertic technique is only a measure of zeta potentials - not surface potentials. The method presented here is a measure of surface potential, not zeta potential. Therefore, our method may be an improvement to the commercially available techniques.

CHAPTER V

DEVELOPMENT OF FUTURE WORK

Introduction

This thesis presents the detailed background development required for a new experimental technique. It was shown that the method was viable and allowed for a simple means of probing the interparticle forces present in a colloidal systems. It, however, presents more questions about the systems than this particular study answers. For example:

1) The ferrofluid composite systems show similar behavior, but what are the forces involved in these systems?

2) It was seen that one can selectively aggregate these colloidal systems, at higher ionic strengths, therefore, can one carefully detail the barrier between the secondary and the primary minima?

3) It was shown that the latex particles are difficult to work with in this type of experiment, i.e. the surface chemistries of the latex particles are not well defined, therefore, this study needs to be repeated with a particle that has a better defined surface chemistry. And, exactly what effect does changing the surface chemistry have on the interparticle interaction?

4) What effect does changing the pH, shape, etc. have on the interparticle interaction?

5) What effect does adding free polymer, more surfactant, etc. have on the interparticle interaction?

6) What effect does changing the medium have on the interactions?

Ferrofluid Composite Systems

The ferrofluid composite systems have been of great deal of interest [Popplewell, et. al. (1981, 1986 and 1987), Davies, et. al. (1985 and 1986), Warner, et. al. (1985), Skjeltorp (1983, 1984 and 1985)]. The systems, comprised of a ferrofluid (hydrocarbon medium in which ferrite particles on the order of 10 nm in size have been suspended) in which micron sized particles have been suspended, have been used in practical applications such as microwave polarizers. These micron sized particles exhibit the same type of behavior seen in the electric field study presented here when the field is applied in the parallel direction as discussed in Chapter I. Therefore, by using a similar technique to the one employed in the electric field studies, one may probe the stabilization forces present in this system.

A preliminary study was conducted, where a similar experimental method was employed to study the interparticle forces involved between the micron sized particles suspended in the ferrofluid. By making a

simple change at the sample platform the experimental apparatus given on page 67, one may easily obtain a separation versus applied field measurement, provided that a suitable sample maybe found.

To conduct these magnetic field experiments the electric field providing apparatus must be exchanged for the following (Figure 52):

a) a sample cell designed for the magnetic field experiment
b) a Helmholtz coil
c) a HP 6824 A DC Power Supply Amplifier.

The Helmholtz coil was specifically designed for the experiment conducted. This particular coil was made by wrapping 365 turns of copper wire designed for electric motors - 22 gauge. Figure 53 provides the actual physical dimensions of the coil employed for this investigation. Figure 54 provides a plot of the field strength in Gauss versus the applied current in Amperes through the coil.

Three types of samples were used in this preliminary investigation, PVT particles in a kerosene based ferrofluid and polymethylmethacrylate (PMMA) in both the kerosene based and in a toulene based ferrofluid. Other samples were tried as well, for example:

1) PS particles in the kerosene based fluid.

2) PVT particles in the toulene based fluid.

However, in both of these samples the hydrocarbon medium

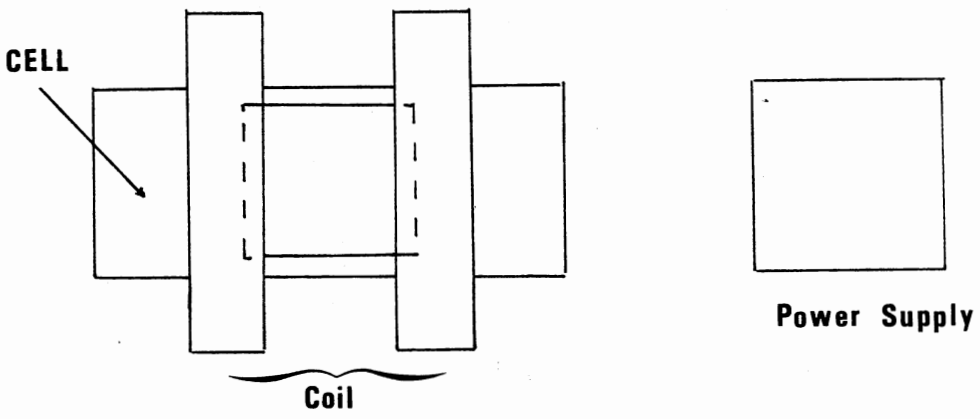

Figure 52. The magnetic field apparatus.

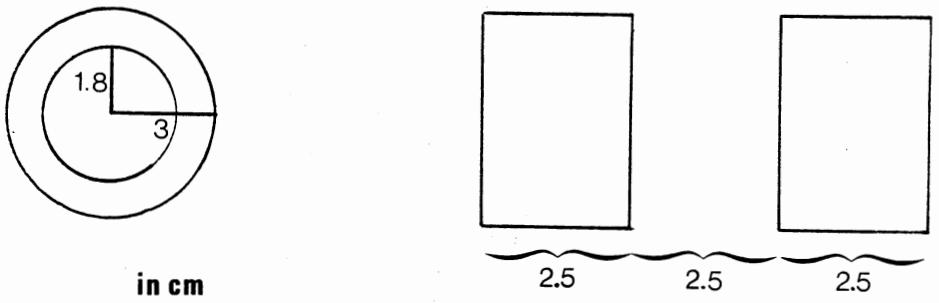

Figure 53. The physical dimensions of the Helmholtz Coil used in the magnetic field study.

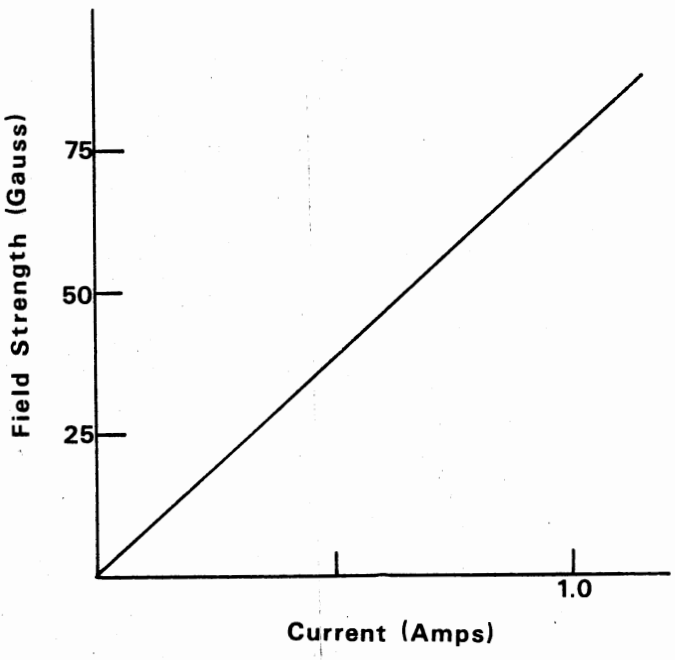

Figure 54. Field strength versus current for the Helmholtz coil used in the magnetic field study.

of the ferrofluid ultimately dissolved the colloidal particles (the PS or the PVT) suspended in them. The major difficulty preparing the samples used for this study was not the dissolving of some particles by the carrier fluid but that of suspending a particle shipped and stored in water in a hydrocarbon based fluid without water contamination. For this preliminary study, it is doubtful that the problem of water contamination was completely eliminated.

The samples were made by placing a 10 ul drop of

the selected particle on a clean microscope slide. These particles were allowed to sit until the samples appeared dry. Once dry, 10 ul of the selected ferrofluid was dropped on the particles. The particles and the ferrofluid were mixed by using a clean glass stirring rod that had been rubbed with lens paper, (thus, charging the rod). This charged rod helped to lift the particles from the glass surface. Other methods of suspending the particles were tried, however, these techniques were not as successful as the charged rod method.

Once, the particles were resuspended in the ferrofluid a microscopic cover slip was placed over the sample. The microscope slide and cover slip comprised the sample cell used for this investigation. This combination was sealed such that the same samples could be used for a variety of experimental tests.

Several methods of sealing the sample cells were tried. Some were as simple applying parafilm or silica grease to the edges of the cover slip, others required a series of parafilm wells sealed with various glues. However, the method determined to be the most successful was applying expoxy to the edges of the cover slip, once the slip was in place, thus, permanently sealing the cell. This method, although fine for this preliminary investigation, does present a major problem. One is

unable to control the thickness of the sample. The ferrofluids appear dark, thus if the samples are to thick one would be unable to conduct light scattering experiments. By not controlling the thickness of the sample, one is also unable to control the number of layers of particles. In many model experiments [Warner, et. al. (1985), Skjeltorp (1984, 1985 and 1986)], one would like to have a monolayer of the suspended particles. With this type of sample cell, control of suspended particle concentration is almost impossible. The advantage of this cell is that it allows one to keep the same sample over an extended period of time. Some of the samples are still useable three years after preparation.

The magnetic field experiments were conducted in the same manner as the applied electric field studies. The maximum field was applied, the sample was left for approximately thirty minutes to allow for a diffraction pattern to form. A run was taken which is an average of 10 scans. The form factor was divided out using the same computer program as that used in the electric field studies. Thus, particle separation versus applied field data were obtained.

Qualitatively, the results of this preliminary study compare directly with the electric field studies. The particles form chains when a parallel magnetic field

is applied. The average separation of the particles decreases as the field increases. The particles seem to be in a local equilibrium, i.e. the particles find their average separation quite rapidly, while the chain length is time dependent. Therefore, one can apply the Tonks' gas theory to this samples as was previously used in the electric field studies. Hystersis tests were conducted and no hystersis effects were observed.

However, these samples did show some significant

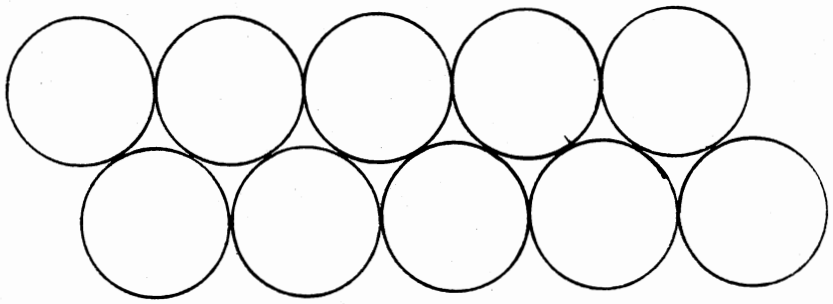

Figure 55. Double chain configuration.

differences. The particles rapidly respond to the applied field, however, the chain formation is slower than the electric field studies. This can be used to an advantage, if one were to study the aggregation kinetics of these systems. It would allow for a more detailed study of the initial steps of the aggregation. This

slowing of chain formation is most likely due to the viscosity of the ferrofluid systems.

Certain concentration effects were also noted. The double chain formation discussed earlier was observed (see Figure 55). This formation was only seen at the highest applied electric fields and in samples with a relatively high concentrations. The mechanism for this formation is not understood.

One may be able to examine "solvation" type forces in these systems. The ferrite particles are 10 nm in size, thus, as the particles approach one another particles of relatively large physical size must be excluded. There is some evidence in these ferrofluid composites that one can see this exclusion. Thus, one may be able to examine these systems in a manner similar to that used by Horn, et. al. (1980 and 1980) in his solvation studies.

In order to conduct such studies, one must eliminate certain problems. First, a better sample cell must be designed such that the samples can be keep for a long period of time where the thickness of the sample can be controlled and one can light scatter through the sample. The sample cell also must placed in a magnetic field without interfering with the field or the results. Secondly, the problems of water contamination and particle carrier fluid interactions must be eliminated.

There is some evidence that the PVT particles swell when placed in the kerosene based fluid and must be considered in further studies. Thirdly, one must account for the repulsive interaction between the particles.

The sample cell design is a fairly simple problem to overcome, however, the other problems are much more difficult to solve. The problem of water contamination as well as particle swelling may be overcome simply by finding a particle that is well characterized suspended in a medium in which a ferrofluid produced. There are several hydrocarbon media used for the ferrofluids, as well as many new water based ferrofluids. When this study was conducted, the water based ferrofluids were not very well behaved nor did they have strong interactions with the fields. There are new water based fluids in which some of these problems have been corrected. The last problem, the nature of the particle repulsion, is not as easily addressed. If the particles were suspended in a water based system, the repulsion would most likely be the double-layer interaction seen in the electric field studies. If the particles are suspended in a hydrocarbon based fluid, the problem is a little more difficult, i.e. there may be a double-layer type of repulsion or just a strict coulomb type repulsion, but these must be examined. The problem of

water contamination makes a reasonable estimate of the type of repulsion present extremely difficult, i.e. one can not estimate the parameters involved in order to make valid assessments of the data obtained.

With the knowledge gained by the electric field studies, one can attack the problems presented in these magnetic studies. Thus, these studies seem to have a great deal of potential to adding to our understanding of the interparticle interacts that are present. By using this background, one could easily extended this particular study into a meaningful and insightful investigation.

Ionic Strength Barriers

One of the qualitative observations made when investigating the effects of varying the ionic strength was that there seemed to be a region were one could selectively aggregate the colloidal systems and form permanent chains. In this region the samples of particles mixed with the ionic solution were stable until a particular applied field was reached. This selective aggregation occurred over a range of ionic strengths differing only in the strength of the field required to produce the aggregation. It is felt that this may be a means to fully characterize the barrier between the primary and secondary minima.

This permanent chaining behavior is also of great particle interest. These permanent chains may be used in some applied applications such as filters, polarizers, etc. Therefore, by carefully examining the nature of this controlled interaction, one may be able to develop useful devices.

Other Systems

As stated in the previous chapters, this study was fairly limited, it only focused on the affects of varying ionic strength. Thus, other experimental parameters can easily varied. One of the most logical parameters to vary is that of pH. By changing the pH of the solution one can effectively modify the surface chemistry of the latex particle. There are particles commercially available where the surface charge is dependent on the pH allowing one to go from a negatively charged particle to a positively charged one.

Several other particles could be used such as silica, inorganometallic, or coated particles. By varying the particles one may drastically vary the particle charge, surface chemistry, shape, and particle interactions. Therefore, one may more thoroughly test the present theories relating the particle interactions.

One may, also, investigate the effects of adding free polymer, surfactant, etc. to the solution. By understanding the nature of the interparticle interactions, one may be able to investigate the effects of these additives on the surface chemistries of a variety of particles.

Conclusions

This particular method allows for a variety of applications. The number of studies capable of investigation are countless; however, the method does have its limitations. It is a light scattering technique, and therefore, the choice of the particle must be carefully considered. It must have a very narrow particle sized distribution, and the shape of the particle must be well defined such that the particle form factor may be easily determined.

Non-aqueous samples need further investigation. The means of applying the field, either electric or magnetic, must be carefully considered. For example, one of the studies strongly suggested by the author is to attempt full characterization of the interparticle interactions responsible for the drastic results observed in electrorhelogical fluids. These fluids are comprised of silica particles suspended in a silica

based oil; therefore a high voltage DC field must be applied. Thus, this type of study may require changes in the experimental design to accommodated this type of applied field.

This author suggests that the next logical step in this investigation is to repeat the presented study here with a particle that is even better defined that the 2.12 um PVT sample. The latex particles have extremely difficult surface chemistries to characterize. They are highly dependent on the batch, the method of cleaning, the age of the sample, the conditions under which the samples are stored, etc. (This information has been verified by the manufacturer, and the laboratory which provided the dielectrophertic measurements for the manufacturer.) Thus, a well defined inorganometallic particle is suggested.

Following the previously suggested study, the next logical step would be to investigate the effects of varying pH, followed by varying the surface group of the particle, i.e. look at sterically stabilized particles and particles with surface chemistries composed of amines, proteins, carboxyl groups, etc. all of which are spherical and commercially available.

Therefore, it is the opinion of the author that a) the technique is extremely viable from an applications point of view as well as a fundamental tool of

investigation, and b) several further investigations should be conducted in order to fully understand the interparticle interaction involved over a large range of colloidal systems.

A SELECTED BIBLIOGRAPHY

Ackerson, B. J. and N. A. Clark, Phys. Rev. A, 30, 906 (1984).

Ackerson, B. J. and N. A. Clark, Phys. Rev. Lett., 46, 123 (1981).

Ackerson, B. J. and F. K. Wood, to be published 1989.

Barouch, E., E. Matijevic, T. A. Ring and J. M. Finlan, J. Coll. Int. Sci., 67, 1 (1978).

Barouch, E. and E. Matijevic, J. Coll. Int. Sci., 105, 552 (1985).

Bell, G. M., S. Levine and L. N. McCartney, J. Coll. Int. Sci., 33, 335 (1979).

Bradbury, A., S. Menear and R. W. Chantrell, J. Magn. and Magn. Mat., 54, 745 (1986).

Brooks, D., J. Goodwin, C. Hjelm, L. Marshall and C. Zukoski, Coll. and Surf., 18, 293 (1986).

Buckingham, A. D., Can. J. Physics, 63, 30 (1985).

Casmir, H. B. G. and D. Polder, Phys. Rev., 73, 360 (1948).

Casmir, H. B. G. and D. Polder, Nature, 158, 787 (1946).

Chantrell, R. W., A. Bradbury, J. Popplewell and S. W. Charles, J. Phys. D: Appl. Phys., 13, L119 (1980).

Chapman, D. L., Phil. Mag., 25, 475 (1913).

Chikazumi, S., S. Taketomi, M. Ukita, M. Mizukami, H. Miyajima, M. Setogawa, and Y. Kurihara, J. Magn. and Magn. Mat., 65, 245 (1987).

Chowdhury, A. H., B. J. Ackerson, F. Wood, M. A. Karim and A. A. S. Awwal, Mic. Opt. Tech. Lett., 1, 175 (1988).

Chowdhury, A. H., B. J. Ackerson and N. A. Clark, Phys. Rev. Lett., 55, 833 (1985).

Chowdhury, A. H., F. Wood, K. Loudiyi and B. J. Ackerson, Yamada Conference XIX - Ordering and Organization in Ionic Solutions, Ed. N. Ise and I. Sogami (World Scientific, Co. Pte. Ltd., Singapore, 1988) p. 367.

Claesson, P., R. G. Horn, and R. M. Pashley, J. Coll. Int. Sci., 100, 250 (1984).

Cowell, C., R. Li-In-On and B. Vincent, J. Chem. Soc. Faraday I, 74, 337 (1977).

Cowley, A. C., N. L. Fuller, R. P. Rand, and V. A. Parsegian, Charged Phosphilid Bilayer, 17, 3163 (1978).

Davies, P., J. Popplewell, G. Martin, A. Bradbury and R. W. Chantrell, J. Phys. D: Appl. Phys., 19, 469 (1986).

Davies, P., J. Popplewell, J. P. Llewellyn, and K. O'Grady, J. Phys. C: Solid State Phys., 18, L661 (1985).

Davies, P., J. Popplewell, and J. P. Llewellyn, IEEE Trans. Magn., MAG-22, 1131 (1986).

Donners, W. A. B., J. B. Rijnbout and A. Vrij, J. Coll. Int. Sci., 61, 249 (1977).

Duckworth, R. M. and A. Lips, J. Coll. Int. Sci., 64, 311 (1978).

Duclos, T. G., D. N. Acker and J. D. Carlson, Machine Design, 42 (1988).

Dzyaloshinskii, I. E., E. M. Lifshitz and L. P. Pitaevskii, Adv. in Phys., 10, 165 (1961).

Everett, D. H., Basic Principles of Colloid Science (Royal Society of Chemistry 1988).

Fraden, S., Reorientation Instabilites in Nematics and Electric Field Induced Association of Colloids (A Dissertation presented to Brandis University, 1987).

Fujita, T. and D. A. Huckaby, J. Stat. Phys., 38, 809 (1985).

Gruen, D. E. R., S. Marcelja and B. A. Pailthorpe, Chem. Phys. Lett., 82, 315 (1981).

Hamaker, H. C., Physica, IV, 1058 (1937).

Healy, T. W., Pure & Appl. Chem., 52, 1207 (1980).

Hesselink, F. Th., A Vrij, and J. Th. G. Overbeek, J. Phys. Chem., 75, 2094 (1971).

Hiemenz, P. C., Principles of Colloid and Surface Science, 2nd Ed. (Marcel Dekker, Inc., N. Y. 1967).

Hirschfelder, J. O., Intermolecular Forces (Interscience Pub. - John Wiley & Sons, N. Y., 1967).

Hogg, R., T. W. Healy and D. W. Fuerstenau, Trans. Faraday Soc., 62, 1638 (1966).

Horn, R. G. and J. N. Israelachvili, J. Chem. Phys., 75, 1400 (1981).

Horn, R. G. and J. N. Israelachvili, Chem. Phys. Lett., 71, 192 (1980).

Israelachvili, J. N., Adv. in Coll. Int. Sci., 16, 31 (1982).

Israelachvili, J. N., Intermolecular and Surfaces Forces - With Applications to Colloidal and Biological Systems (Academic Press, New York, 1985).

Israelachvili, J. N., Faraday Dis. Chem. Soc., 65, 20 (1978).

Israelachvili, J. N., Philosophical Mag. A, 43, 753 (1981).

Israelachvili, J. N. and G. E. Adams, J. C. S. Faraday I, 74, 975 (1978).

Israelachvili, J. N. and P. M. McGuiggan, Science, 241, 795, (1988).

Israelachvili, J. N. and B. W. Ninham, J. Coll. and Int. Sci., 58, 14 (1988).

Israelachvili, J. N. and R. M. Pashley, J. Coll. and Int. Sci., 98, 500 (1984).

Israelachvili, J. N., R. K. Tandon and L. R. White, Nature, 277, 120 (1979).

Israelachvili, J. N., M. Tirrell, J. Klien, and Y. Almog, Macromolecules, 17, 204 (1984).

Jeffrey, D. J., Proc. Roy. Soc. Lond. A, 335, 335 (1973).

Jones, T. B., J. Appl. Phys., 60, 2226 (1986).

Jones, T. B., J. Appl. Phys., 61, 2416 (1987).

Joosten, J. G. H., J. Chem. Phys., 80, 2363 (1984).

Jordan, P. C., Mol. Phys., 25, 961 (1973).

Kerker, M., The Scattering of Light (Academic Press, N. Y., 1969)

Kesavamoorthy, R., Structure and Elastic Properties of Dilute Colloids (Thesis, Univ. of Madras, Tamil Nadu, India, 1987).

Kruyt, H. R., Colloid Science - Vol. I (Elseveir Pub. Co., Amsterdam 1952).

Kruyt, H. R., Colloid Science - Vol. II (Elseveir Pub. Co., Amsterdam 1952).

Langbein, D., J. Phys. Chem. Solids, 32, 1657 (1969).

Langmuir, I., Science, 88, 430 (1938).

Lifshitz, E. M., Soviet Phys. JETP, 2, 73 (1956).

London, F., Z. Phys. Chem. B, 11, 222 (1930).

Love, J. D., J. Chem. Soc. Faraday II, 73, 669 (1977).

Lyklema, J., Pure & Appl. Chem., 52, 1221 (1980).

Lyklema, J., Pure & Appl. Chem., 53, 2199 (1981).

Lyklema, J., S. S. Dukhin, and V. N. Shilov, J. Electroanal. Chem., 143, 1 (1983).

Lyklema, J., M. M. Springer, V. N. Shilov and S. S. Dukhin, J. Electroanal. Chem., 198, 19 (1986).

Mahanty, J. and B. W. Ninham, Dipersion Forces (Academic Press, N.Y. 1976).

Maitland, G. C., M. Rigby, E. B. Brain and W. A. Wakeman, Intermolcular Forces - Their Origin and Determination (Clarendon Press, Oxford 1981).

Marcelja S. and N. Radic, Chem. Phys. Lett., 42, 129 (1976).

McLachlan, A. D., Proc. Roy. Soc. A, 271, 387, (1963).

McLachlan, A. D., Mol. Phys., 6, 423 (1963).

Melik, D. H. and H. S. Fogler, J. Coll. Int. Sci., 108, 503 (1985).

Mitchell, D. J., B. W. Ninham and B. A. Pailthorpe, Chem. Phys. Lett., 51, 257 (1977).

Mitchell, D. J. and B. W. Ninham, J. Chem. Phys., 56, 1117 (1972).

Morozov, K. I., A. F. Pshenichnikov, Yu. L. Raikher, and Shliomis, J. Magn. and Magn. Mat., 65, 269 (1987).

Munster, A., Statistical Thermodynamics, Vol. I (Springer - Verlag, Berlin 1969).

Napper, D. H., Trans. Faraday Soc., 64, 1701 (1968).

Napper, D. H., J. Coll. Int. Sci., 32, 106 (1970).

Ninham, B. W., Adv. Coll. Int. Sci., 16, 3 (1982).

Ninham, B. W., J. Phys. Chem. 384, 1423 (1980).

Ninham, B. W. and V. A. Parsegian, J. Chem. Phys., 52, 4578 (1970).

Overbeek, J. Th. G., J. Phys. Chem., 64, 1178 (1960).

Overbeek, J. Th. G., Powder Tech., 37, 195 (1984).

Overbeek, J. Th. G., J. Coll. Int. Sci., 58, 408 (1977).

Overbeek, J. Th. G., Adv. Coll. Int. Sci., 16, 17 (1982).

Overbeek, J. Th. G., Pure & Appl. Chem., 52, 1151 (1980).

Pailthorpe, B. A. and W. B. Russel, J. Coll. Int. Sci., 89, 563 (1982).

Parsegian, V. A., Adv. Coll. Int. Sci., 16, 49 (1982).

Parsegian, V. A. and B. W. Ninham, J. Coll. Int. Sci., 37, 332 (1971).

Parsegian, V. A. and B. W. Ninham, Nature (London), 224, 1197 (1969).

Parsegian, V. A. and G. H. Weiss, J. Coll. Int. Sci., 81, 285 (1981).

Parsegian, V. A., R. P. Rand and D. C. Rau, preprint, Proc. Sym. on Complex amd Supermolecular Fluids, (1987).

Pashley, R. M., J. Coll. Int. Sci., 80, 153 (1981).

Pashley, R. M., Adv. Coll. Int. Sci., 16, 57 (1982).

Pohl, H. A., Dielectrophoresis (Cambridge University Press, N. Y., 1978).

Popplewell, J., P. Davies and J. P. Llewellyn, J. Magn. and Magn. Mat., 65, 235 (1987).

Popplewell, J., P. Davies, J. P. Llewellyn, and K. O'Grady, J. Magn. and Magn. Mat., 54, 761 (1986).

Popplewell, J., P. Davies, A. Bradbury, and R. W. Chantrell, IEEE Trans. on Magn., MAG-22, 1128 (1986).

Popplewell, J., and S. W. Charles, IEEE Trans. on Magn., MAG-17, 2923 (1981).

Prieve, D. C. and M. M. J. Lin, J. Coll. Int. Sci., 86, 17 (1986).

Prieve, D. C., F. Luo and F. Lanni, Faraday Discuss. Chem. Soc., 83, 297 (1987).

Prieve, D. C. and R. Roman, J. Chem. Soc. Faraday Trans. 2, 83, 1287 (1987).

Prieve, D. C. and N. A. Frej, preprint Langmuir, (1989).

Rau, D. C., B. Lee, and V. A. Parsegian, Proc. Natl. Acad. Sci., 81, 2621 (1984).

Richetti, P., J. Prost and N. A. Clark, Physics of Complex and Supermolecular Fluids (Ed. S. A. Safran and N. A. Clark, John Wiley & Sons, N. Y., 1987) p. 387.

Rosensweig, R.E., J. Appl. Phys., 57, 4259 (1985).

Russel, W. B., Colloidal Dispersions (Cambridge University Press 1989).

Sauer, F. A., Interactions Between Electromagnetic Fields and Cells (A NATO ASI Series, Series A, Vol. 97, 1985) p. 181.

Skjeltorp, A. T., Phys. Rev. Lett., 51, 2306 (1983).

Skjeltorp, A. T., Physica, 127B, 411 (1984).

Skjeltorp, A. T., J. Appl. Phys., 55, 2587 (1984).

Skjeltorp, A. T., J. Appl. Phys., 57, 3285 (1985).

Smith, E. R., D. J. Mitchell and B. W. Ninham, J. Coll. Int. Sci., 45, 55 (1973).

Snook, I. K., W. van Megan, K. J. Gaylor, and R. O. Watts, 17, 33 (1982).

Snook, I. K. and W. van Megan, J. Chem. Phys., 72, 2907 (1980).

Stone, A. J., Proceedings of the NATO Advanced Study Institute on Molecular Liquids - Dynamics and Interactions (Ed. A. J. Barnes, W. J. Orville-Thomas and J. Yarwood, Reidel Pub. Co., Boston, 1984).

Stangroom, J. E., Phys. Technol., 14, 290 (1983).

Tabor, D., F. R. S. and R. H. S. Winterton, Proc. Roy. Soc. A, 312, 435 (1969).

Tonks, L., Phys. Rev., 50, 955 (1936).

Verwey, E. J. W. and J. Th. G. Overbeek, Theory of the Stability of Lybrobic Colloids (Elseveir Pub. Co., Inc., N.Y., 1948).

Vincent, B., P. F. Luckham, and F. A. Waite, J. Coll. Int. Sci., 73, 508 (1980).

Visser, J., Adv. Coll. Int. Sci., 3, 331 (1972).

Vold, R. D. and M. J. Vold, Colloid and Interface Chemistry (Addison-Wesley Pub. Co., Inc., 1983).

Vrij, A., Pure & Appl. Chem., 48, 471 (1976).

Warner, M. and R. M. Hornreich, J. Phys. A: Math. Gen., 18, 2325 (1985).

Wiese, G. R. and T. W. Healy, Trans. Farady Soc., 66, 490 (1970).

APPENDICES

APPENDIX A

These are the computer programs designed for use on the Apple IIe computer. The first program written by Jerry Mertz is designed to collect the data obtained from an experimental scan. The second program written by F. K. Wood is a composite program that allows one to print a hard copy of the scan, superimpose several different scans, obtain intensity measurements, and locate local maxima. The third program also written by F. K. Wood divides two scans, i.e. this program was used to divide the form factor out of the total scan.

```
100  REM !INTEGER*
110  REM

COMPILED BASIC AI13 INTE
     RFACE


120  HIMEM: 32768
122  LOMEM: 16384
125  TEXT : HOME
130 D$ =  CHR$ (4)
140  DIM A%(1001),B%(501)
150  PRINT D$"BLOAD GETAI13.TRIGG
     ER,A$8000"
155  PRINT "INPUT GAIN------"
156  INPUT GAIN
160 M = 500: REM  NUMBER OF DATA
     POINTS
170 SLOT = 5: REM    AI13 IN SLOT
      5
175  REM  DEFINE ALL VARIABLES HE
     RE FOR APPLESOFT
180 ARRYPTR = 0:FINIS = 0:X = 0:I
      = 0:LOC = 0:CHAN = 0:SET =
     0:S9 = 0:S8 = 0:Z1 = 0
185  FOR I = 1 TO 80:A$ = A$ + ".
     ": NEXT
186 C$ = " "
187 A$ = A$ +  CHR$ (13) + "."
189  FOR I = 1 TO 500:B%(I) = 0: NEXT

190  REM

***** FIND ARRAY


200 A%(0) =  - 9999: REM   SET AR
     RAY MARKER
205  REM  FOR APPLESOFT PEEK 107
     AND 108
206  REM  FOR TASC PEEK 123 AND 1
     24
210 ARRYPTR =  PEEK (123) +  PEEK
     (124) * 256
220 FINIS = ARRYPTR + 500: REM
     RANGE OF SEARCH
230  FOR I = ARRYPTR TO FINIS
240 X =  PEEK (I)
250  IF X <  > 216 THEN 280
260 X =  PEEK (I + 1)
270  IF X = 241 THEN LOC = I:I =
     FINIS: REM   GOT LOCATION
```

```
280  NEXT I
290  PRINT
300  IF LOC = 0 THEN  PRINT "NOT
     FOUND"
310  PRINT "LOCATION = "LOC
320  PRINT  PEEK (LOC)"  " PEEK (
     LOC + 1)
330  REM

***** PACK ARRAY


340 A%(0) = SLOT
350 A%(1) =  - M
370 CHAN = 0
380 SET = CHAN + 16 * GAIN
390  FOR I = 1 TO 500
392 A%(2 * I) = SET
410  NEXT I
420  REM

***** SET ARRAY LOCATION



430  POKE 8,LOC -  INT (LOC / 256
     ) * 256: POKE 9, INT (LOC /
     256)
440  REM

***** CALL AI13


480  PRINT D$"PR#1": PRINT A$: PRINT
     D$"PR#0"
490  CALL 32852
510  REM

        ******* CALCULATE SUMS


520 S9 = 32767:S8 = 0
530  FOR I = 1 TO 500
540 B%(I) = B%(I) + A%(2 * I + 1)

559  IF S9 > B%(I) THEN S9 = B%(I
     )
560  IF S8 < B%(I) THEN S8 = B%(I
     )
570  NEXT I
575 Z1 = (S8 - S9) / 160
576  IF Z1 = 0 THEN Z1 = 1
580  REM
```

```
          *******PLOT
590   HGR
600   HCOLOR= 3
610   FOR I = 1 TO 180
620 Y = (B%(2 * I) - S9) / Z1
625   IF Y < 0 OR Y > 160 THEN 635

630   HPLOT I,Y
635 Y = (B%(2 * I + 1) - S9) / Z1

636   IF Y < 0 OR Y > 160 THEN 640

637   HPLOT I,Y
640   NEXT I
660   REM

          ******* INQUERIES


665   PRINT : PRINT : PRINT : PRINT
      : PRINT : PRINT : PRINT : PRINT
      : PRINT : PRINT : PRINT : PRINT
      : PRINT
666   PRINT S8,S9
670   PRINT "ANOTHER RUN?--ENTER 1
      "
680   INPUT Z1
690   IF Z1 = 1 THEN 200
700   PRINT "SAVE DATA?--ENTER 1"
710   INPUT Z1
720   IF Z1 <  > 1 THEN 810
730   PRINT "INPUT FILE NAME--NUMB
      ER"
740   INPUT C$
750   PRINT D$"OPEN"C$
760   PRINT D$"WRITE"C$
770   FOR I = 1 TO 500
780   PRINT B%(I)
790   NEXT I
800   PRINT D$"CLOSE"
810   PRINT "KEEP GOING?--ENTER 1"

820   INPUT Z1
830   IF Z1 = 1 THEN 189
1000   END
```

```
]LISTPR#0
]LIST

1  LOMEM: 16384
2  HIMEM: 36864
10  REM  "THIS PROGRAM IS DESIGNE
D FOR PLOTTING DATA TAKEN WI
TH DR. ACKERSONS PRORAM TMPY
7"
20  REM  "THIS PROGRAM USES DATA
COMPLIED USING FIL.COMP PROG
RAM"
30  REM  "HOWEVER, DUE TO THE NAT
URE OF THIS PROGRAM ANY FILE
 SAVED USING DR. ACKERSONS P
ROGRAM TMPY7 MAY BE USED"
40 D$ =  CHR$ (4)
50 G = 10
60  DIM N(500): DIM B$(500)
65  DIM M(500)
70  REM  "THIS PROGRAM PLOTS ACTU
AL DATA AND EXPANDS THE VIEW
 REGION"
80 X1 = 0:X2 = 4000
90  PRINT "VERSION 1 - ALLOWS YOU
 TO SET DIVISION FACTOR G AN
D ALLOWS YOU THE OPTION TO S
ET MAX VALUE AND MIN VALUE"
100  INPUT "DO YOU WANT VERSION 1
 (0=NO ,1=YES)";U
110  IF U = 1 THEN  GOTO 660
120  INPUT "READ FILE?";C$
130  PRINT D$"OPEN"C$
140  PRINT D$"READ"C$
150  FOR L = 1 TO 500
160  INPUT B$(L)
170  NEXT L
180  PRINT D$"CLOSE"
190  FOR P = 1 TO 500
200 W1 =  VAL (B$(P))
210 W3 = W1 / G
220 N(P) = 1978 - W3
230  NEXT P
240  IF MC = 1 THEN 300
250  FOR L = 1 TO 500
260 X = N(L)
270  IF X1 < X THEN X1 = X
280  IF X2 > X THEN X2 = X
290  NEXT L
300  PRINT "X1 = ";X1
310  PRINT "X2 = ";X2
320  INPUT "SUPER-IMPOSE PLOT";R1
```

```
330  IF R1 = 1 THEN 360
340  HGR
350  HCOLOR= 3
360  FOR I = 50 TO 300
370 Y3 = N(I) - X2
380 Y = Y3 / (X1 - X2)
385 M(I) = Y
400 Y = 155 - (155 * Y)
410 Z = I - 50
420  HPLOT Z,Y
430  NEXT I
440  HPLOT 0,0 TO 0,155
450  HPLOT 0,155 TO 250,155
460  HPLOT 0,0 TO 5,0
470  FOR Q = 1 TO 10
480 A1 = 15.5 * Q
490 Y = A1
500  HPLOT 0,Y TO 5,Y
510 A2 = 25 * Q
520 X = A2
530  HPLOT X,150 TO X,155
540  NEXT Q
550  INPUT "DO YOU WANT A PRINT O
UT";C3
560  IF C3 = 0 THEN 625
570  PRINT  CHR$ (4);"PR#1"
580  PRINT  CHR$ (9);"GD"
590  PRINT " MAX VALUE ";X1
600  PRINT " MIN VALUE ";X2
610  PRINT C$
620  PRINT  CHR$ (4);"PR#0"
625  INPUT "DO YOU WISH TO IDENTI
FY INTENSITIES? ";R9
627  IF R9 = 1 THEN 920
630  INPUT "YOU WISH A SECOND FIL
E?";R2
640  IF R2 = 1 THEN 100
650 U = 0
660  IF U = 0 THEN  GOTO 730
670  INPUT "NO. OF DATA PTS";G
680  INPUT "DO YOU WISH TO SET MA
X AND MIN? ";MC
690  IF MC = 0 THEN  GOTO 120
700  INPUT "MAX = ";X1
710  INPUT "MIN = ";X2
720  GOTO 120
730  INPUT "DO YOU WISH TO IDENTI
FY PEAKS";R2
740  IF R2 = 0 THEN 2000
750  INPUT "BEGINING OF REGION ";
R3
```

```
760  INPUT "END OF REGION ";R4
770 L6 = 155
780  FOR Z = R3 TO R4
790 L1 = N(Z) - X2
800 L2 = L1 / (X1 - X2)
810  IF L2 > .1 THEN L2 = .1
820 L3 = 155 - (155 * 10 * L2)
830  IF L6 > L3 THEN L6 = L3
840  IF L3 = L6 THEN B1 = Z
850  NEXT Z
860  PRINT " X VALUE OF PEAK IS "
;B1
870  PRINT " RELATIVE INTENSITY *
 10 ";L6
880  INPUT "DO YOU WISH ANOTHER R
EGION";R6
890  IF R6 = 1 THEN 750
900  INPUT "YOU WISH A SECOND FIL
E? ";R2
910  IF R2 = 1 THEN 100
920  INPUT "DATA POINT? ";V1
930  INPUT "HARD COPY? ";V2
940  IF V2 = 0 THEN 1000
950  PRINT  CHR$ (4);"PR#1"
960  PRINT "DATA PT.  ";V1
970  PRINT M(V1)
980  PRINT  CHR$ (4);"PR#0"
1000  PRINT M(V1)
1010  GOTO 625
2000  END
```

```
]LIST

1  LOMEM: 16384
2  HIMEM: 36864
40 D$ =  CHR$ (4)
50 G = 10
60  DIM N(500): DIM B$(500)
70  DIM S(500): DIM A$(500)
75  DIM Q(500)
80 X1 = 0:X2 = 4000
110  IF U = 1 THEN  GOTO 660
120  INPUT "READ FILE?";C$
122 K$ = C$
125  PRINT D$"OPEN"C$
130  PRINT D$"READ"C$
135  FOR L = 1 TO 500
140  INPUT B$(L)
142  NEXT L
144  PRINT D$"CLOSE"
146  INPUT "STURCTURE FACTOR FILE
";C$
148  PRINT D$"OPEN"C$
150  PRINT D$"READ"C$
155  FOR L = 1 TO 500
160  INPUT A$(L)
165  NEXT L
180  PRINT D$"CLOSE"
190  FOR P = 1 TO 500
200 W1 =  VAL (B$(P))
205 V =  VAL (A$(P))
210 W3 = W1 / G
215 VQ = V / G
220 N(P) = 2005 - W3
225 S(P) = 2005 - VQ
230  NEXT P
250  FOR L = 1 TO 500
255 K = 1
260 X = N(L)
270  IF X1 < X THEN X1 = X
280  IF X2 > X THEN X2 = X
281  IF K = 2 THEN 290
282  IF K = 1 THEN X = S(L)
284  IF K = 1 THEN K = 2
286  GOTO 270
290  NEXT L
300  PRINT "X1 = ";X1
310  PRINT "X2 = ";X2
320 R1 = 0
330  IF R1 = 1 THEN 360
```

```
340  HGR
350  HCOLOR= 3
360  FOR I = 50 TO 300
365  IF S(I) = 0 THEN Y3 = 0
366  IF S(I) = 0 THEN  GOTO 380
370 Y3 = N(I) / S(I)
380 Y = Y3 / (X1 - X2)
385 F = Y
390  IF Y > .005 THEN Y = .005
400 Y = 155 - (155 * 200 * Y)
410 Z = I - 50
420  HPLOT Z,Y
430  NEXT I
440  HPLOT 0,0 TO 0,155
450  HPLOT 0,155 TO 250,155
460  HPLOT 0,0 TO 5,0
470  FOR Q = 1 TO 10
480 A1 = 15.5 * Q
490 Y = A1
500  HPLOT 0,Y TO 5,Y
510 A2 = 25 * Q
520 X = A2
530  HPLOT X,150 TO X,155
540  NEXT Q
570  PRINT  CHR$ (4);"PR#1"
580  PRINT  CHR$ (9);"GD"
590  PRINT " MAX VALUE ";X1
600  PRINT " MIN VALUE ";X2
610  PRINT K$
620  PRINT  CHR$ (4);"PR#0"
630  INPUT "YOU WISH A SECOND FIL
E?";R2
640  IF R2 = 1 THEN 120
920  END
```

APPENDIX B

When measuring the separation of the first order diffracted maxima from the zeroth order maxima, there is an experimental measurement error. The measurement is in error by $\pm$ 0.02 cm. We now give an example comparison of this error with respect to other errors, consider separation of 6.45 $\pm$ 0.02 cm when the screen is located 21.0 cm away from the sample. The scattering angle is determined to be 12.72 degrees. The error carried through produces an error in the angle of $\pm$ 0.04 degrees. Using this scattering angle, the average center to center separation is determined to be 2.16 $\pm$ 0.005 um, however, the data is reported to $\pm$ 0.01 um and in the lowest ionic strength measurement the data is reported to $\pm$ 0.02 um to account for the greater effects of kinking or bending at this ionic strength. This scattering angle produces a k ($k = (4\pi/\lambda) \sin 12.72$) of $(4.37 \pm 0.02) \times 10^{6}\ m^{-1}$.

APPENDIX C

These are the computer programs used to evaluate the Tonks' theory for various pair potentials. The first program contains a simple form for the potential, the dipole - hard sphere interaction. The second and third programs are slightly modified and contain the more complex forms of the potential.

This program was tested to ensure accurate results. The independence of the results on the Laplace variable s (concentration) was checked by running the program using the same parameters at different values of s; for example, .001, .01 and .1 were used for most of these tests. Integrations excluded the primary minimum region up to the maximum point in the potential barrier. This was done to ensure that the integration did not improperly weight the primary minima since we observe no coagulation for our experimental conditions, however, in most cases the integration step size solved this problem. The integration step size was also tested to ensure that the stability of the results.

```
10 ' TONKS GAS SCATTERING CALCULATION
20 ' CONCENTRATION
30 V = .35
40 FOR I9 = 1 TO 3
50 ' POTENTIAL PARAMETERS (ASSUMING HARD SPHERE AT A)
60 ' DIPOLE POT AT A TIMES KT
70 B = 16
75 FOR I8 = 1 TO 6
80 ' STEPS IN POTENTIAL INTEGRATION
90 N = 1000
100 ' INTEGRATION STEP
110 DX = 10/N
120 ' LOOP OVER K VALUES
130 PRINT " CONC     POTENTIAL AMP     K-VALUE          INTENSITY"
140 LPRINT " CONC     POTENTIAL AMP     K-VALUE          INTENSITY"
150 FOR I = 1 TO 30
160 K = 2*3.14159*(1+1/20-I/100)
170 ' LOOP FOR SPATIAL INTEGRATION
180 S0 = 0
190 S1 = 0
200 S2 = 0
210 FOR J = 1 TO N
220 X = J*DX+1
230 ' LAPLACE TRANSFORM FORM
240 T1=EXP(-V*X)
250 ' DIPOLAR ATTRACTION
260 T3=B/X/X/X
270 T2=EXP(T3)-1
280 ' PARTIAL INTEGRAND
290 T9=T1*T2*DX
300 ' PHI SUM
310 S0 = S0+T9
320 ' REAL PSI SUM
330 S1=S1+T9*COS(K*X)
340 ' IMAGINARY PSI SUM
350 S2=S2+T9*SIN(K*X)
360 NEXT J
370 ' TOTAL PHI
380 S0=S0+(EXP(-V))/V
390 ' TOTAL REAL PSI.
400 S1=S1+(EXP(-V))*(V*COS(K)-K*SIN(K))/(V*V+K*K)
410 ' TOTAL IMAGINARY PSI
420 S2=S2+(EXP(-V))*(V*SIN(V)+K*COS(K))/(V*V+K*K)
430 ' INTENSITY DENOMINATOR
440 D=S0*S0-S0*2*S1+S1*S1+S2*S2
450 ' INTENSITY
460 N1=S0*S0-S1*S1-S2*S2
470 ' INTENSITY
480 S9=N1/D
490 PRINT V,B,K,S9
500 LPRINT V,B,K,S9
510 NEXT I
520 B = B - 2
530 NEXT I8
540 V =V/10.
550 NEXT I9
1000 END
```

```
10 ' TONKS GAS SCATTERING CALCULATION
20 ' CONCENTRATION
30 V = .1
50 ' POTENTIAL PARAMETERS (ASSUMING HARD SPHERE AT A)
55 QPR = 15
60 ' DIPOLE POT AT A TIMES KT
62 'Q IS THE COEFFICENT OF THE REPULSIVE POT
63 'Q IS THE POT TIMES KT
64 I9 = 3
65 Q = .000101*80.1*(QPR*.001/300)^2/(2*4.11E-14)
66 LPRINT " si is ";QPR
67 IF I9 = 1 THEN KAPPA= 159000!
68 IF I9 = 2 THEN KAPPA = 307000!
69 IF I9 = 3 THEN KAPPA = 884000!
70 B = 16
71 IF I9 = 4 THEN KAPPA = 2680000!
72 LPRINT "kappa is ";KAPPA
75 FOR I8 = 1 TO 5
80 ' STEPS IN POTENTIAL INTEGRATION
90 N = 1000
100 ' INTEGRATION STEP
110 DX = 10/N
120 ' LOOP OVER K VALUES
130 PRINT " CONC    POTENTIAL AMP    K-VALUE        INTENSITY"
140 LPRINT " CONC    POTENTIAL AMP    K-VALUE        INTENSITY"
150 FOR I = 1 TO 65
160 K = 2*3.14159*(1+1/20-I/250)
170 ' LOOP FOR SPATIAL INTEGRATION
180 S0 = 0
190 S1 = 0
200 S2 = 0
210 FOR J = 1 TO N
220 X = J*DX+1
230 ' LAPLACE TRANSFORM FORM
240 T1=EXP(-V*X)
250 ' DIPOLAR ATTRACTION
260 T3=(B/X/X/X)
263 Z = Q*LOG(1+EXP(-KAPPA*.000212*(X-1)))
264 ZQ = EXP(-4*.000106*KAPPA*(X-1))/(32*(X-1))
265 ZQ = ZQ+(3.112*(1+(191.1*(X-1))^(3/2))^(-2/3))/(24*(X-1))
269 T3=T3-Z+ZQ
270 T2=EXP(T3)-1
280 ' PARTIAL INTEGRAND
290 T9=T1*T2*DX
300 ' PHI SUM
310 S0 = S0+T9
320 ' REAL PSI SUM
330 S1=S1+T9*COS(K*X)
340 ' IMAGINARY PSI SUM
350 S2=S2+T9*SIN(K*X)
360 NEXT J
```

```
370 ' TOTAL PHI
380 S0=S0+(EXP(-V))/V
390 ' TOTAL REAL PSI
400 S1=S1+(EXP(-V))*(V*COS(K)-K*SIN(K))/(V*V+K*K)
410 ' TOTAL IMAGINARY PSI
420 S2=S2+(EXP(-V))*(V*SIN(V)+K*COS(K))/(V*V+K*K)
430 ' INTENSITY DENOMINATOR
440 D=S0*S0-S0*2*S1+S1*S1+S2*S2
450 ' INTENSITY
460 N1=S0*S0-S1*S1-S2*S2
470 ' INTENSITY
480 S9=N1/D
490 PRINT V,B,K,S9
500 LPRINT V,B,K,S9
510 NEXT I
520 B = B - 2
530 NEXT I8
1000 END
```

```
10 ' TONKS GAS SCATTERING CALCULATION
20 ' CONCENTRATION
30 V = .1
50 ' POTENTIAL PARAMETERS (ASSUMING HARD SPHERE AT A)
55 QPR = 250
60 ' DIPOLE POT AT A TIMES KT
62 'Q IS THE COEFFICENT OF THE REPULSIVE POT
63 'Q IS THE POT TIMES KT
64 FOR I9 = 3 TO 4
65 Q = .000101*80.1*(QPR*.001/300)^2/(2*4.11E-14)
66 LPRINT " si is ";QPR
67 IF I9 = 1 THEN KAPPA= 159000!
68 IF I9 = 2 THEN KAPPA = 307000!
69 IF I9 = 3 THEN KAPPA = 884000!
70 B = 16
71 IF I9 = 4 THEN KAPPA = 2680000!
72 LPRINT "kappa is ";KAPPA
75 FOR I8 = 1 TO 7
80 ' STEPS IN POTENTIAL INTEGRATION
90 N = 1000
100 ' INTEGRATION STEP
110 DX = 10/N
120 ' LOOP OVER K VALUES
130 PRINT " CONC    POTENTIAL AMP    K-VALUE        INTENSITY"
140 LPRINT " CONC    POTENTIAL AMP    K-VALUE        INTENSITY"
150 FOR I = 1 TO 50
160 K = 2*3.14159*(1+1/20-I/250)
170 ' LOOP FOR SPATIAL INTEGRATION
180 S0 = 0
190 S1 = 0
200 S2 = 0
210 FOR J = 1 TO N
220 X = J*DX+1
230 ' LAPLACE TRANSFORM FORM
240 T1=EXP(-V*X)
250 ' DIPOLAR ATTRACTION
260 T3=(B/X/X/X)
263 Z = Q*LOG(1+EXP(-KAPPA*.000202*(X-1)))
264 ZQ=1.4E-13/(24*(X-1)*4.11E-14)
265 T3 =T3 - Z + ZQ
270 T2=EXP(T3)-1
280 ' PARTIAL INTEGRAND
290 T9=T1*T2*DX
300 ' PHI SUM
310 S0 = S0+T9
320 ' REAL PSI SUM
330 S1=S1+T9*COS(K*X)
340 ' IMAGINARY PSI SUM
350 S2=S2+T9*SIN(K*X)
360 NEXT J
370 ' TOTAL PHI
```

```
380 S0=S0+(EXP(-V))/V
390 ' TOTAL REAL PSI
400 S1=S1+(EXP(-V))*(V*COS(K)-K*SIN(K))/(V*V+K*K)
410 ' TOTAL IMAGINARY PSI
420 S2=S2+(EXP(-V))*(V*SIN(V)+K*COS(K))/(V*V+K*K)
430 ' INTENSITY DENOMINATOR
440 D=S0*S0-S0*2*S1+S1*S1+S2*S2
450 ' INTENSITY
460 N1=S0*S0-S1*S1-S2*S2
470 ' INTENSITY
480 S9=N1/D
490 PRINT V,B,K,S9
500 LPRINT V,B,K,S9
510 NEXT I
520 B = B - 2
530 NEXT I8
540 NEXT I9
1000 END
```

2

VITA

Frankie Kay Wood

Candidate for the Degree of

Doctor of Philosophy

Thesis: INTERACTIONS OF COLLOIDAL PARTICLES IN THE PRESENCE OF A PARALLEL APPLIED FIELD

Major Field: Physics

Biographical:

Personal Data: Born in Klamath Falls, Oregon, September 6, 1963. Parents are Diane F. and Timothy L. Pasquarelli.

Education: Graduated from Edmond Memorial High School, Edmond, Oklahoma, 1981; received Bachelor of Science Degree in Physics with a minor in Chemistry from Central State University in May, 1984; completed requirements for the Doctor of Philosophy degree at Oklahoma State University in May, 1989.

Professional Experience: Instructor, Department of Physics, Oklahoma State University, January, 1987 to May, 1987; Research Assistant, Department of Physics, Oklahoma State University, January, 1985 to present; Teaching Assistant, Department of Physics, Oklahoma State University, August, 1984 to present; Laboratory Improvement Coordinator, Department of Physics, Oklahoma State University, August, 1987 to May, 1988; Laboratory Assistant, Department of Physics, Central State University, August, 1983 to May, 1984; Research Assistant and Student Secretary, Department of Physics, Central State University, June, 1981 to May, 1984.